Water and Metal-Organic Frameworks
From Interaction toward Utilization

Liu, Xinlei; Wang, Xuerui; Kapteijn, Freek

DOI
10.1021/acs.chemrev.9b00746

Publication date
2020

Document Version
Final published version

Published in
Chemical Reviews

CHEMICAL REVIEWS

pubs.acs.org/CR

Review

Water and Metal–Organic Frameworks: From Interaction toward Utilization

Xinlei Liu, Xuerui Wang, and Freek Kapteijn*

Cite This: https://dx.doi.org/10.1021/acs.chemrev.9b00746

Read Online

ACCESS | Metrics & More | Article Recommendations

ABSTRACT: The steep stepwise uptake of water vapor and easy release at low relative pressures and moderate temperatures together with high working capacities make metal–organic frameworks (MOFs) attractive, promising materials for energy efficient applications in adsorption devices for humidity control (evaporation and condensation processes) and heat reallocation (heating and cooling) by utilizing water as benign sorptive and low-grade renewable or waste heat. Emerging MOF-based process applications covered are desiccation, heat pumps/chillers, water harvesting, air conditioning, and desalination. Governing parameters of the intrinsic sorption properties and stability under humid conditions and cyclic operation are identified. Transport of mass and heat in MOF structures, at least as important, is still an underexposed topic. Essential engineering elements of operation and implementation are presented. An update on stability of MOFs in water vapor and liquid systems is provided, and a suite of 18 MOFs are identified for selective use in heat pumps and chillers, while several can be used for air conditioning, water harvesting, and desalination. Most applications with MOFs are still in an exploratory state. An outlook is given for further R&D to realize these applications, providing essential kinetic parameters, performing smart engineering in the design of systems, and conceptual process designs to benchmark them against existing technologies. A concerted effort bridging chemistry, materials science, and engineering is required.

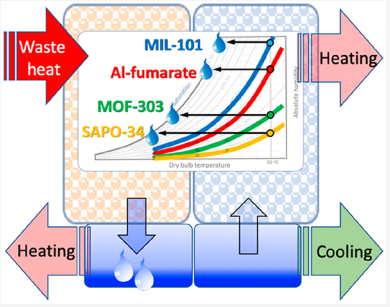

CONTENTS

1. INTRODUCTION

Life on our planet exists by virtue of the presence of water and incoming solar radiation. Water is a benign solvent and does not harm the environment, however, fresh water is unevenly

Special Issue: Porous Framework Chemistry

Received: November 18, 2019

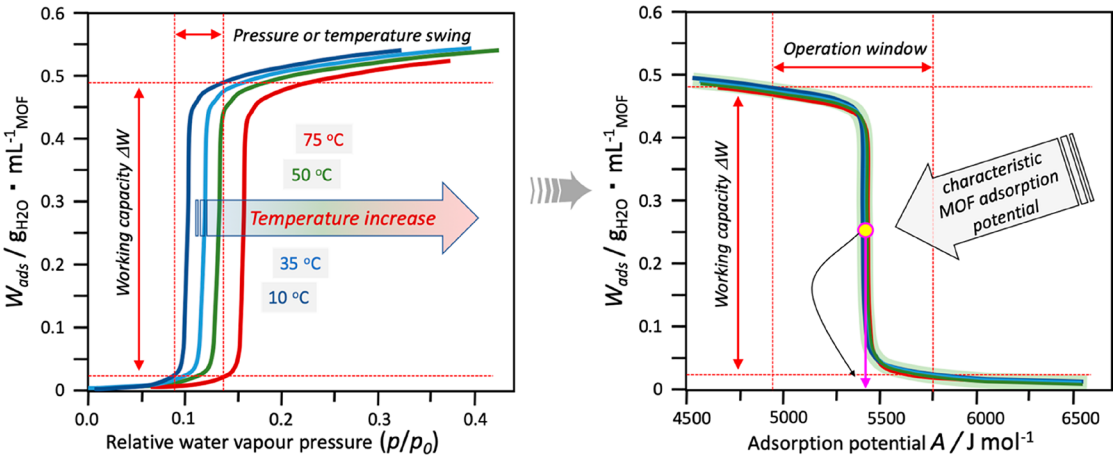

Figure 1. Characteristic example of stepwise water adsorption isotherms on a MOF. Water uptake as a function of the relative water vapor pressure at different temperatures (left), and as a function of the adsorption potential after variable transformation (right). Most MOFs exhibit some slight uptake before and after the step. Uptake given per unit volume of MOF.

available over the planet and measures are needed to secure its safe and sufficient supply. Pollution and the increase of arid areas by climate change put the supply of fresh water under pressure.

Water is used by mankind for various purposes in daily life as drinking water, in food preparation, indoor air conditioning, agriculture/farming, and in industry. In most cases, primary energy is used for the associated heating/cooling, evaporation/condensation, and transportation, generated from fossil resources. Over 70% of the global primary energy is lost, of which over 60% arise at temperatures below 100 °C as low-grade waste heat,[1] mostly released by industry, transportation, and power plants into the environment. For the USA, this was estimated (2011) at ∼33 EJ/year, of which 14.3 EJ/year could potentially be used through waste heat recovery, reducing the primary energy demand by 12%.[2] Increased CO_2 levels in the atmosphere, thermal pollution, and associated climate changes urge the increased utilization of renewable and recovered waste energy, simultaneously reducing CO_2 emissions. This heat integration can be realized in many ways,[3] one of them utilizing adsorption of water on specific sorbents.

Metal−organic frameworks (MOFs) have a role to play here, combining phase transformations in water utilization and the efficient use of renewable (solar) or waste energy. This manuscript reviews the current status of several potential applications and identifies specific MOFs that seem fit.

Why MOFs (see elsewhere in this issue)?

Unlike most porous sorbents, certain MOFs exhibit a peculiar steep water uptake, sometimes like a Heavyside step function, at or around a specific relative water vapor pressure p/p_o, much lower than 1 (Figure 1). The location of this step depends on the specific MOF and the temperature and is associated with the arrangement and interaction strength of water molecules with the MOF. A presence and magnitude of an adsorption−desorption hysteresis is also MOF dependent, and several MOFs hardly manifest any. This step implies that only a small change in relative pressure or temperature is needed to induce an uptake or release of water, resulting in an easily obtained high working capacity in comparison with other sorbents for such a small change in conditions. Following Polanyi[4] and Dubinin,[5] defining an adsorption potential $A(p/p_0, T)$ (eq 1), the temperature and relative pressure dependency of the water uptake $W(p/p_0, T)$ can conveniently be captured by only one parameter. Often, the Dubinin−Astakhov relation is used,[6] whereby all isotherms collapse onto a single characteristic curve with a step located at a MOF-specific characteristic energy of adsorption E.

$$W\left(\frac{p}{p_0}, T\right) \Rightarrow W(A) = W_{\max} \exp\left[-\left(\frac{A}{E}\right)^n\right]$$
$$A = -RT \ln\left(\frac{p}{p_0}\right) \quad (1)$$

While water adsorption on MOFs occurs around ambient temperatures, regeneration can often be realized at driving temperatures in the range of ∼55−85 °C, levels easily reached by solar panel heating or available as low-grade waste heat, opening up applications for MOFs. Although the local availability of renewable and waste energy may often not match the need, temporary thermochemical energy storage could certainly provide much opportunity.[7]

The specific water sorption and associated heat effects open up the use of MOFs in adsorption-based processes, like reallocation of heat, desiccation, water harvesting, desalination, and air conditioning. This review covers the utilization potential of MOFs in such operations. It gives a timely status update regarding earlier reviews with new developments regarding materials and applications.[7−13] In literature, most focus has been given on the development of MOFs and improvement of their intrinsic properties related to water adsorption, which, apart from stability, include the adsorption isotherm, heat of adsorption, and working capacity, all thermodynamically determined. Although essential, these properties only are not sufficient in describing their performance. Therefore, relevant engineering basics are introduced first (operation, psychrometric chart, transport phenomena), followed by the discussion and selection of MOFs based on the stability under humid conditions,[8] and their adsorption characteristics. The manuscript concludes with an evaluation regarding prospects of introduction of MOFs in these applications and needs to reach these goals.

https://dx.doi.org/10.1021/acs.chemrev.9b00746
Chem. Rev. XXXX, XXX, XXX−XXX

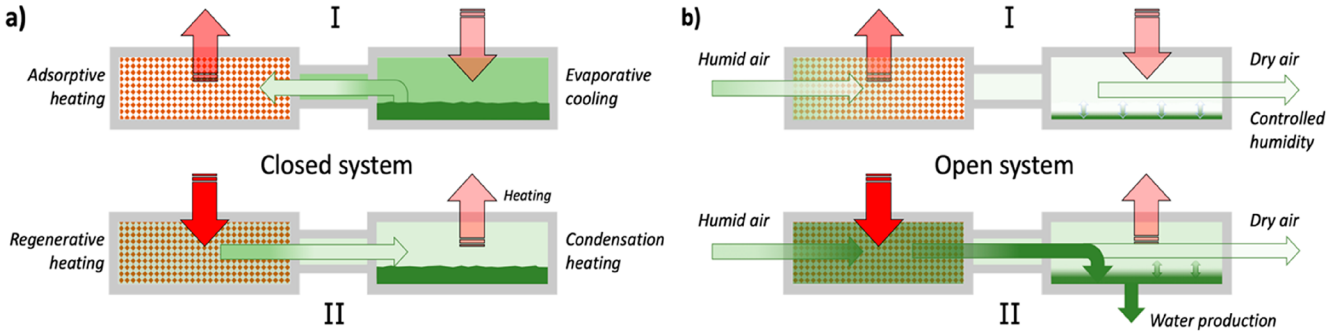

Figure 2. Schematic configuration of a "closed" (a) and an "open" (b) application in adsorption (I) and regeneration (II) mode. Key: Red arrows, energy flow; green arrows, water flow direction. Color intensities suggest temperature and concentration levels.

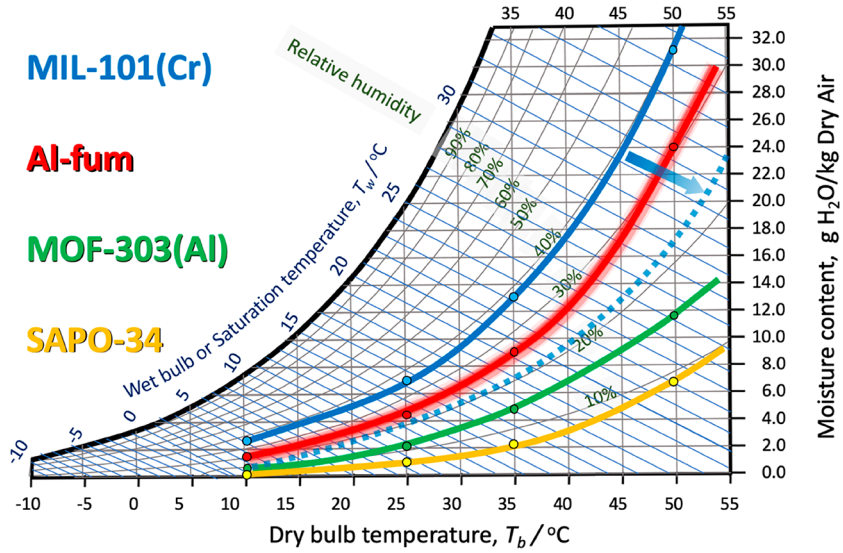

Figure 3. Psychrometric chart of the water/air system at 1 atm and superimposed for selected sorbents the loci where they exhibit a stepwise uptake of water. The dashed curve exemplifies the desorption hysteresis shift for MIL-101. Chart drawn based on literature data.[7,17,18]

2. ENGINEERING ASPECTS

2.1. Operation

The water adsorption-based applications all share a similar structure featuring two coupled basic units, a water−MOF contactor and a water processing unit, operated in a cyclic way. One distinguishes "closed" systems, where only energy exchange with the surroundings takes place, and "open" systems in which also water is supplied or removed.[14] Figure 2 shows schematically their adsorption and regeneration stages. The detailed coupling and operation modes and conditions determine the type and efficiency of application. For reallocation of heat, power density and productivity are important, while in water harvesting, rate and productivity are targeted.

In both subunits, the water vapor−liquid phase interaction dependency on partial pressure and temperature guides the operation, captured in a psychrometric chart.[15,16] Through adsorption, the presence of a MOF alters these characteristics in the water−MOF contactor. Further, in all applications, the transport of water and energy has to be considered as well. These aspects are presented first.

2.2. Psychrometric Chart

The psychrometric chart guides the design of processes in which water evaporation or condensation and humidity control, often in combination with energy management, is essential. The introduction of a MOF sorbent presents specific changes, utilized in the applications described later.

The psychrometric chart for air/water systems (Figure 3) illustrates the role of MOFs in humidity control.

The chart background is the Gibbs phase rule, specifying that for a humid air system with two components and one phase, three intensive variables (degrees of freedom) have to be specified to fix all system properties. At a pressure of one atmosphere, then a 2D graph, the psychrometric chart, can represent all intrinsic system properties. Often the absolute humidity or moisture content (kg H_2O/kg dry air) is given as a function of the temperature ("dry bulb" temperature) (Figure 3).[18] When liquid water is also present, the degrees of freedom reduce by one and one variable fixes the whole system, the saturation line where water is in equilibrium with its saturated vapor (100% relative humidity, RH). Using the relation for A for the data of a few selected MOFs and SAPO-34, their saturation step curves are included in Figure 3.[7,17] SAPO-34 is one of the few zeotype sorbents also exhibiting a step-type water uptake.[19,20] At conditions above these curves, the MOF is saturated with water, while below these curves, water is released, so small changes in temperature or humidity can trigger the MOF's state. These saturation step curves are located at lower relative humidities (RH) than the water saturation line (100% RH), so water is adsorbed before liquid

https://dx.doi.org/10.1021/acs.chemrev.9b00746
Chem. Rev. XXXX, XXX, XXX−XXX

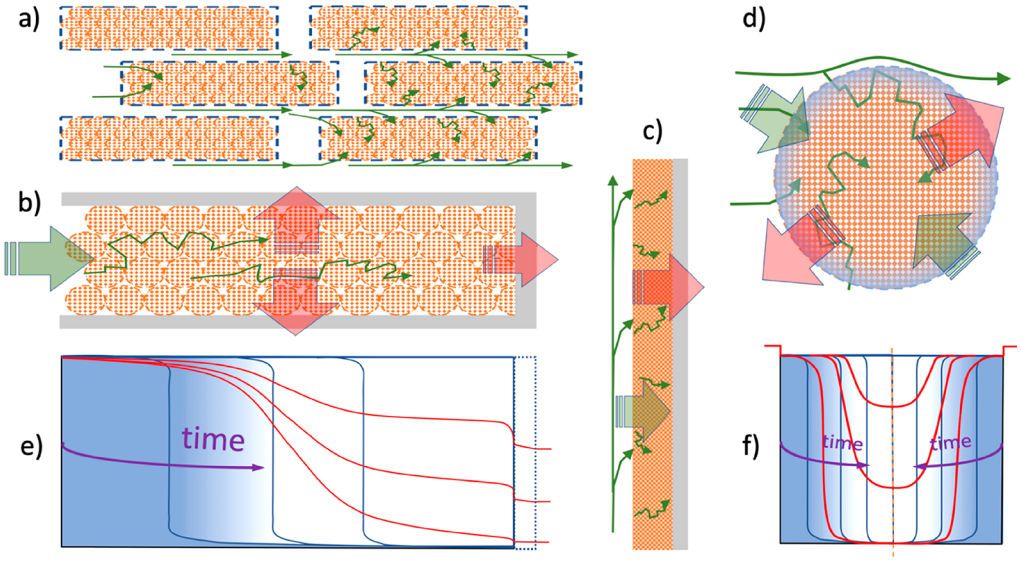

Figure 4. Contacting geometries of units for water−MOF applications, transport directions of heat (transparent red), mass (transparent green), temperature (red), and concentration (blue) profiles in the water adsorption stage. Straight green arrows indicate convective transport, segmented arrow diffusional transport. (a) Three levels of porosity structure, (b) packed bed between heat exchange fins, (c) MOF coating on heat exchange surface, (d) porous MOF particle used in packed bed, (e) temporal development (assumed, see text) of concentration (adsorbed water) and temperature in axial direction of packed bed in (b), (f) temporal development of concentration and temperature in radial direction of particle. In (e) and (f), temperature profiles outside the MOF are also sketched.

is formed at a certain temperature. The MOF saturation curve can even be considered as a phase change line, although due to some adsorption before and after the step uptake, this is fuzzier than a saturation line, as schematically indicated for Al-fumarate. When adsorption−desorption hysteresis is present, like for MIL-101(Cr), the curve shifts and higher temperatures or lower relative humidities are needed for desorption. All materials have their own characteristics, their curves run slightly steeper than the RH curves because their heats of water adsorption are ∼5−15 kJ/mol larger than the condensation heat of pure water vapor (∼40.7 kJ/mol). These heats of adsorption are generally lower than those of classical sorbents such as zeolites, contributing to the lower desorption temperatures in the range of ∼55−85 °C.

2.3. Engineering Aspects

In any application, the water has to be supplied and contacted with the MOF and the adsorption heat released removed from the MOF, all transport-related phenomena. Thermodynamics and kinetics of adsorption are scale independent phenomena, while mass (water) and energy (heat) transport are scale (size) dependent. The challenge lies in optimally balancing these in a combination ("marrying") for the purpose of an energy efficient operation. For the water−MOF contacting unit in any application, the following factors influence the performance (see Figure 4):

- Adsorption isotherms: thermodynamics control, scale independent
  (1) adsorption, desorption, equilibration
  (2) loading W as a function of the adsorption potential $A(p/p_o, T)$
- Mass transport water: kinetic control, scale dependent
  (1) convection, e.g., by fans or free-convection via spaces between sorbent packings or coatings or channels
  (2) diffusion in interparticle spaces (between particles in packed bed) and intraparticle space (coating, particles)
- Energy transport: Kinetic control, scale dependent
  (1) convection, through heat capacity of the humid air
  (2) effective conduction in packed beds or in coating layer.
  (3) transfer to/from packing or coating to heating/cooling surface
  (4) transfer from metal surface to heating/cooling fluid.

Depending on the kinetics, the slowest process will determine the adsorbed concentration and temperature profiles in the packed bed (axial and radial direction) and in the coating or particle (Figure 4). These may vary from a (preferred) uniform change in these variables during operation (adsorption rate limiting) or the development of temperature or concentration fronts (transport rate limiting, often the case), and determine the overall performance. Because of the thermal effects of ad- and desorption, concentration and temperature profiles are strongly coupled.[21] As an example, in Figure 4, the energy transport is assumed to be faster than mass transport, and the latter is slower than the adsorption uptake, resulting in steep temporal moving concentration front development. Simultaneously, the liberated water adsorption heat has to be removed sufficiently, otherwise temperature may increase such that desorption may occur.

Heat transport in a packed bed mainly occurs via the interparticle contacts and especially at the particle−heat exchange surface, the void space is even higher, resulting in poor heat transfer.[22] The good thermal conductivity of the heat exchange wall may further even out temperature gradients. Therefore, improving heat transport by particle binding or direct coating of the MOF on the heat exchange surfaces is being explored.[21,23−27] Although heat transport can be improved by 2 orders of magnitude,[28] the total MOF loading in a coated device will generally be lower than in a packed bed,

https://dx.doi.org/10.1021/acs.chemrev.9b00746
Chem. Rev. XXXX, XXX, XXX−XXX

resulting in a faster response but a lower output per adsorption cycle.[23] The specific application will dictate the choice for implementation.

To regenerate the loaded MOF temperature can be raised and/or the water partial pressure be reduced by evacuation or flushing with flowing air with a relative humidity (RH) below the step uptake in the isotherm. Transport directions in Figure 4 are then reversed.

In open system applications (harvesting, desalination, air-conditioning), depending on the humidity level, huge volumes have to be contacted with the MOF (Figure 5) by convective

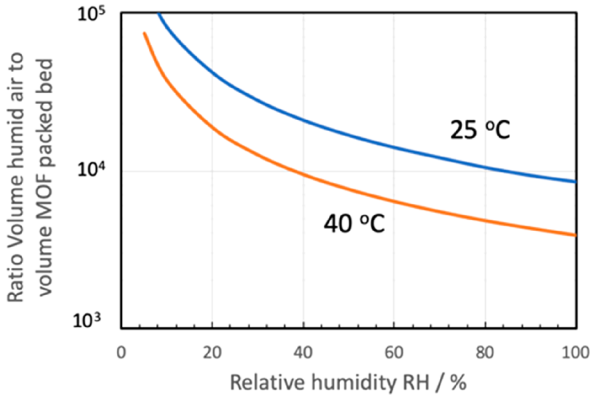

Figure 5. Ratio of the volume of humid air per volume of a packed bed of MOF particles needed to saturate the MOF as a function of the relative humidity (RH) at 25 and 40 °C to produce 1 kg H_2O. Assumed data: Atmospheric pressure, working capacity MOF 0.35 kg H_2O/kg MOF, crystal density MOF 1.2 g/mL, particle porosity 0.3, bed void 0.35, so volume packed bed 5.2 L.

transport with minimum energy penalty. Open structures are proposed with very low pressure drop[29] such as the so-called "three-levels-of-porosity"[30] reactor with regularly arranged spatially packed beds (Figure 4a) or internally finned monolithic structures[31] that may have a higher solid inventory.

Regenerative process operations like the applications dealt with here are well-known in practice and include adsorptive purification[32] and separation,[33] recovery of heat,[34,35] and combinations[36,37] thereof (e.g., chemical looping) but are basically discontinuous. Dual-bed swing operations and rotary systems allow for continuous operation. Here, segments of a rotating wheel (coated structure or packed beds) move alternating through sections that operate in the different modes of adsorption, desorption, heating, and cooling.[15,19,29,38] Rotation speed and segment sizes are adjusted to fit the application.[15,16]

3. WATER STABILITY AND ADSORPTION MECHANISMS

3.1. Stability of MOFs in Water Systems

The stability of MOFs upon exposure to a humid or aqueous liquid environment is of utmost importance for real-life application. Degradation under prolonged exposure to water is unacceptable. MOFs, since their discovery, have moved from the realm of "water sensitive" (e.g., MOF-5(Zn)[39] and HKUST-1(Cu)[40]) to "water stable" (e.g., ZIF-8(Zn)[41] and MIL-101(Cr)[42]) and now "routinely designable to withstand harsh industrial conditions" (e.g., UiO-66(Zr)[43]). In this section, the MOF stability, especially under harsh conditions in water (Table 1, 238 MOF samples), is comprehensively overviewed, aiming to recommend qualified materials for applications in water adsorption and heat transformation. Recently, a stable covalent organic framework COF-432 was also reported to exhibit a step in water uptake.[44] Although water is in its vapor phase for the applications listed in section 4, the MOF stability in liquid water environments (neutral, acidic, saline, alkaline) is also discussed here because contact with liquid water is inevitable during storage and delivery in MOF devices by overloading, mal-operation, or aerosol containing feed. Furthermore, insight in the degradation mechanism in liquid water environments provides design concepts for stable MOFs.

The stability of MOFs can be determined by multiple factors such as metal ions and their valencies, linkers, strength, and geometry of coordination bond of metal-linker, hydrophobicity of linkers, steric hindrance effect of framework, porosity, and operating environments. However, these factors can be rationalized into two classes affecting the MOF stability, namely based on thermodynamic and on kinetic aspects.[8,45] The thermodynamic stability can be quantified from the free Gibbs energy (ΔG) of the degradation reaction (Figure 6), although it is practically challenging to perform such calculations.[46,47] Beyond linkers hydrolysis in H_2O, some MOFs collapse during water activation by the intermolecular forces.[48] The kinetic inertness is related to the activation energy (E_a) to destroy the MOF structure as depicted in Figure 6. A MOF for which hydrolysis or linker exchange in water is thermodynamically favorable can be stable in a water system if it is kinetically inert.

3.1.1. Experimental Techniques Used in Assessing MOF Stability. In theory, the key criterion to determine if a MOF structure remains intact in the water stability test is through the comparison of the typical physicochemical characteristics between postexposure and pristine samples. As a rule of thumb, the powder X-ray diffraction (PXRD) pattern and gas adsorption capacity could well suggest whether the MOF loses its crystallinity or structural porosity, which were judged in Table 1. Not surprisingly, structural changes were detected by the aid of scanning electron microscopy (SEM),[49,50] Fourier-transform infrared spectroscopy (FTIR),[51,52] positronium annihilation lifetime spectroscopy (PALS),[53] nuclear magnetic resonance (NMR),[54,55] etc. Furthermore, MOF degradation can take place with partial dissolution of the material, and mass determination before and after water exposure is undoubtedly a quantified method. The release of metal ions and linkers can be confirmed by conducting ultraviolet−visible (UV−vis)[56−59] spectroscopy and inductively coupled plasma optical emission spectrometry (ICP-OES)[56,60] analysis on the spent water solutions. Additionally, an adequate amount of water solution should be used because the stability of some MOFs is concentration-dependent.[50] Furthermore, to test the acid and base stability, the pH values should be measured before and after the addition of MOFs and after filtrating MOFs to ensure accurate conclusion on the stable pH range.

3.1.2. In Neutral Water. Generally, the coordination bonds formed by the metal ions and linkers are susceptible to the attack by water molecules via linker displacement, leading to phase changes and structural decomposition. A water stable MOF structure must be strong enough to withstand the attack of water molecules on the coordination bonds, preventing the consequent losses in overall porosity and crystallinity.

https://dx.doi.org/10.1021/acs.chemrev.9b00746
Chem. Rev. XXXX, XXX, XXX−XXX

Table 1. Stability of MOFs Examined in Aqueous Solutions or under Humid Conditions[a]

MOF	hydrophilic/ hydrophobic[b]	linker	crystallinity[c]	porosity[c]	assessment condition	ref
			carboxylate linkers			
MIL-53(Cr)	hydrophilic	BDC	well-retained in all conditions	well-retained BET in all conditions	0.07 M HCl, RT, 6 h 0.07 M NaOH, RT, 6 h	88
MIL-101(Cr)	hydrophilic	BDC	well-retained in all conditions	59% increase Langmuir area 60% increase Langmuir area 55% increase Langmuir area 2% increase Langmuir area	pH = 0(HCl), RT, 3 d pH = 4(HCl), RT, 3 d pH = 12 (NaOH), RT, 3 d 5% H_2O_2, RT, 3 d	114
MIL-101(Cr)	hydrophilic	BDC	well-retained well-retained well-retained transformed MIL-53 *as*	89% increase Langmuir area 73% increase Langmuir area 38% increase Langmuir area >99% loss Langmuir area	pH = 0(HCl), RT, 2 months pH = 4(HCl), RT, 2 months pH = 12 (NaOH), RT, 2 months 5% H_2O_2, RT, 2 months	114
$Cr_3(BTC)_2$(Cr)	hydrophilic	BTC	complete degradation	96.2% BET loss	O_2/H_2O atmosphere, 1 d	131
BUT-8A(Cr)	hydrophilic	NDC-SO_3H	well-retained in all conditions		10 M H_2SO_4, 7 d conc HCl, 7 d pH = 3, 7 d pH = 9, 1 d pH = 11, 1 d	115
N_3-PCN-333(Cr)		N_3-BTB	well-retained in all conditions		1 M HCl, 24 h 10 mM NaOH, 24 h	132
MIL-53(Al)	hydrophilic	BDC	well-retained in all conditions		pH = 2, 24 h pH = 10, 24 h	113
MIL-53(Al)	hydrophilic	BDC	complete degradation well-retained well-retained partial degradation	100% loss Langmuir area 30% loss Langmuir area 95% loss Langmuir area 60% loss Langmuir area	pH = 0(HCl), RT, 3 d pH = 4(HCl), RT, 3 d pH = 12 (NaOH), RT, 3 d 5% H_2O_2, RT, 3 d	114
MIL-53(Al)	hydrophilic	BDC	complete degradation partial degradation well-retained partial degradation	100% loss Langmuir area 91% loss Langmuir area 52% loss Langmuir area 84% loss Langmuir area	pH = 0(HCl), RT, 2 months pH = 4(HCl), RT, 2 months pH = 12 (NaOH), RT, 2 months 5% H_2O_2, RT, 2 months	114
MIL-53-NH_2(Al)	hydrophilic	BDC-NH_2	partial degradation well-retained well-retained well-retained		pH = 0(HCl), RT, 3 d pH = 4(HCl), RT, 3 d pH = 12 (NaOH), RT, 3 d 5% H_2O_2, RT, 3 d	114

https://dx.doi.org/10.1021/acs.chemrev.9b00746
Chem. Rev. XXXX, XXX, XXX−XXX

Table 1. continued

MOF	hydrophilic/ hydrophobic[b]	linker	crystallinity[c]	porosity[c]	assessment condition	ref
			carboxylate linkers			
MIL-53-NH_2(Al)	hydrophilic	BDC-NH_2	complete degradation well-retained well-retained partial degradation		pH = 0(HCl), RT, 2 months pH = 4(HCl), RT, 2 months pH = 12(NaOH), RT, 2 months 5% H_2O_2, RT, 2 months	114
HP-MIL-53(Al)	hydrophilic	BDC	well-retained in all conditions		pH = 2, 24 h pH = 10, 24 h	113
MIL-53-NH_2(Al)	hydrophilic	BDC-NH_2	well-retained in all conditions		pH = 2, 24 h pH = 10, 24 h	113
HP-MIL-53-NH_2(Al)	hydrophilic	BDC-NH_2	well-retained in all conditions		pH = 2, 24 h pH = 10, 24 h	113
MIL-53(Al)	hydrophilic	BDC	partial degradation	significant loss BET	0.07 M HCl, 0.07 M NaOH, RT, 6 h	88
MIL-101-NH_2(Al)	hydrophilic	BDC-NH_2	complete degradation transformed MIL-53-NH_2 transformed MIL-53-NH_2 transformed MIL-53-NH_2	100% loss Langmuir area 91% loss Langmuir area 91% loss Langmuir area 79% loss Langmuir area	pH = 0(HCl), RT, 3 d pH = 4(HCl), RT, 3 d pH = 12 (NaOH), RT, 3 d 5% H_2O_2, RT, 3 d	114
MIL-101-NH_2(Al)	hydrophilic	BDC-NH_2	complete degradation transformed MIL-53-NH_2 transformed MIL-53-NH_2 transformed MIL-53-NH_2	100% loss Langmuir area 91% loss Langmuir area 91% loss Langmuir area 81% loss Langmuir area	pH = 0(HCl), RT, 2 months pH = 4(HCl), RT, 2 months pH = 12 (NaOH), RT, 2 months 5% H_2O_2, RT, 2 months	114
PDMVBA-MIL-121(Al)	hydrophilic	BTEC	well-retained after 1 ads cycle of NaCl	10−20% loss of salt adsorption capacitiy in the first 3 ads cycles, and steady in the next 7 adsorption cycles for all conditions	0.1 g MOF in 10000 ppm salt (LiCl) solution (20 mL) 0.1 g MOF in 10000 ppm salt (NaCl) solution (20 mL) 0.1 g MOF in 10000 ppm salt ($MgCl_2$) solution (20 mL) 0.1 g MOF in 10000 ppm salt ($CaCl_2$) solution (20 mL)	108
CAU-1(Al)	hydrophilic	BDC-NH_2	well-retained in all conditions		pH = 4, RT, 3 d pH = 9, RT, 3 d	133
BIT-72(Al)	hydrophilic	BDC-OH	well-retained in all conditions		pH = 4, RT, 3 d pH = 9, RT, 3 d	133

https://dx.doi.org/10.1021/acs.chemrev.9b00746
Chem. Rev. XXXX, XXX, XXX−XXX

Table 1. continued

MOF	hydrophilic/ hydrophobic[b]	linker	crystallinity[c]	porosity[c]	assessment condition	ref
			carboxylate linkers			
BIT-73(Al)	hydrophilic	BDC-CH_3	well-retained in all conditions		pH = 4, RT, 3 d pH = 9, RT, 3 d	133
BIT-74(Al)	hydrophilic	BDC-$(CH_3)_2$	well-retained in all conditions		pH = 4, RT, 3 d pH = 9, RT, 3 d	133
AITCS-1(Al)		TCS	well-retained in all conditions		pH = 1, 24 h pH = 5, 24 h pH = 11, 24 h aqua regia, 24 h	134
AITCS-2(Al)		TCS	well-retained in all conditions		pH = 1, 24 h pH = 5, 24 h pH = 11, 24 h	134
AITCS-2(Al)		TCS	complete degradation		aqua regia, 24 h	134
DUT-5(Al)	hydrophilic	BPDC	well-retained in all conditions		pH = 2, 24 h pH = 11, 24 h	113
HP-DUT-5(Al)	hydrophilic	BPDC	well-retained in all conditions		pH = 2, 24 h pH = 11, 24 h	113
MOF-467(Al)		BTTB	well-retained in all conditions		pH = 1∼11, HCl/NaOH, 36 h 30% H_2O_2, 24 h	135
PCN-333(Al)	hydrophilic	TATB	well-retained in all conditions	well-retained in all conditions	pH = 3 pH = 9	136
DUT-5-o-2CF_3(Al)	hydrophobic	BPDC-o-2CF_3	well-retained in all conditions	well-retained in all conditions	80 mg MOF in 8 mL solution, 1 M HCl, 1 d 80 mg MOF in 8 mL solution, 10 mM NaOH (pH = 12), 1 d	90
Al-TPDC-o- 2CF_3(Al)	hydrophobic	TPDC-o- 2CF_3	well-retained	well-retained	80 mg MOF in 8 mL solution, 1 M HCl, 1 d 80 mg MOF in 8 mL solution, 10 mM NaOH (pH = 12), 1 d	90
PCN-250(Fe_2Co)		L22	well-retained in all conditions	partial BET loss in all conditions	pH = 1∼12, 24 h	137
PCN-333(Fe)	hydrophilic	TATB	well-retained in all conditions	well-retained in all conditions	pH = 3 pH = 9	136

https://dx.doi.org/10.1021/acs.chemrev.9b00746
Chem. Rev. XXXX, XXX, XXX−XXX

Table 1. continued

MOF	hydrophilic/ hydrophobic[b]	linker	crystallinity[c]	porosity[c]	assessment condition	ref
			carboxylate linkers			
MUV-2(Fe)	hydrophilic	TTFTB	well-retained in all conditions	ca. 25% loss on CO_2 uptake in all conditions	5 mg MOF in 5 mL solution, pH = 2 5 mg MOF in 5 mL solution, pH = 11	138
N_3-PCN-333(Fe)		N_3-BTB	complete degradation in all conditions		1 M HCl, 24 h 10 mM NaOH, 24 h	132
Eu_2(BPDC)$(BDC)_2$	hydrophilic	BPDC, BDC	well-retained in all conditions		NaX (X = F^-, Cl^-, Br^-, I^-) solutions (10^{-2} M), 48 h	139
Tb_2(BPDC)$(BDC)_2$	hydrophilic	BPDC, BDC	well-retained in all conditions		NaX (X = F^-, Cl^-, Br^-, I^-) solutions (10^{-2} M), 48 h	139
AUBM-1(In)		BTC	well-retained in all conditions		pH = 1−12	116
DUT-101(Tb)		BPDC	partial degradation		UO_2^{2+} aqueous solution	140
BUT-70B(In)		TTTA	well-retained		pH = 4 (HCl) RT, 24 h	117
MIL-68-NH_2(In)		BDC-NH_2	well-retained in all conditions	3% BET loss 1% BET loss	MOF/solution weight ratio 0.04:100, pH = 3 (HCl), RT, 2 h MOF/solution weight ratio 0.04:100, pH = 5 (HCl), RT, 2 h	118
MIL-68-NH_2(In)		BDC-NH_2	complete degradation in all conditions	92% BET loss 99% BET loss	MOF/solution weight ratio 0.04:100, pH = 1 (HCl), RT, 2 h MOF/solution weight ratio 0.04:100, pH = 2 (HCl), RT, 2 h	118
MIL-68(In)		BDC	well-retained in all conditions	partial BET loss in all conditions	MOF/solution weight ratio 0.04:100, pH = 3 (HCl), RT, 2 h MOF/solution weight ratio 0.04:100, pH = 5 (HCl), RT, 2 h	118
MIL-68(In)		BDC	complete degradation in all conditions	significant BET loss in all conditions	MOF/solution weight ratio 0.04:100, pH = 1 (HCl), RT, 2 h MOF/solution weight ratio 0.04:100, pH = 2 (HCl), RT, 2 h	118
SUMOF-7I(La)		TCTPA	well-retained in all conditions		pH = 2, RT, 24 h pH = 3, RT, 24 h pH = 11, RT, 24 h	141

https://dx.doi.org/10.1021/acs.chemrev.9b00746
Chem. Rev. XXXX, XXX, XXX−XXX

Table 1. continued

MOF	hydrophilic/ hydrophobic[b]	linker	crystallinity[c]	porosity[c]	assessment condition	ref
			carboxylate linkers			
LaBTB(La)	hydrophobic	BTB	well-retained in all conditions		pH = 2 (HCl), 333 K, 3 d pH = 14 (NaOH), 373 K, 3 d	130
LaBTN(La)	hydrophilic	BTN	well-retained in all conditions	65% loss CO_2 uptake 23% loss CO_2 uptake	pH = 2(HCl), 373 K, 24 h pH = 12(NaOH), 373 K, 24 h	142
$Eu_6(\mu 3\text{-}OH)_8(1,4\text{-}NDC)_6(Eu)$	hydrophilic	NDC	well-retained in all conditions	well-retained well-retained 20% loss N_2 uptake 20% loss N_2 uptake	pH = 3.5(HCl), RT, 24 h pH = 10(NaOH), RT, 24 h pH = 3.5(HCl), 373K, 24 h pH = 10(NaOH), 373K, 24 h	143
MIL-53(V)		BDC	complete degradation in all conditions	complete loss BET in all conditions	0.07 M HCl, RT, 6 h 0.07 M NaOH, RT, 6 h	88
Sm(BTB)(Sm)	hydrophobic	BTB	well-retained in all conditions		pH = 2−12, 48 h	119
UiO-66(Zr)	hydrophilic	BDC	well-retained		HCl, pH = 1, 2 h	144
UiO-66(Zr)	hydrophilic	BDC	partial degradation		NaOH, pH = 14, 2 h	144
UiO-66(Zr)	hydrophilic	BDC	well-retained complete degradation	4% BET loss 90% BET loss	pH = 1.5 (HCl), RT, 2 d pH = 12.5 (NaOH), RT, 2 d	56
UiO-66(Zr)	hydrophilic	BDC	well-retained in all conditions	3% BET loss after treatment of $MgCl_2$ solution	0.06g MOF in five saline water solutions (KCl, NaCl, $CaCl_2$, $MgCl_2$ or $AlCl_3$) (0.20 wt %, 100 mL each), 323 K, 100 d	107
UiO-66(Zr)	hydrophilic	BDC	complete degradation in all conditions		0.01g MOF in 20 mL HCl (12 M) 0.01g MOF in 20 mL H_2SO_4 (18M) 0.01g MOF in 20 mL HF (40%) 0.01g MOF in 20 mL NaOH (14 M) 0.01g MOF in 20 mL chromic acid solution (0.1 M $K_2Cr_2O_7$ in concentrate H_2SO_4)	145
UiO-66(Zr)	hydrophilic	BDC	partial degradation in all conditions		0.5 M NaCl, 7 d 0.5 M Na_2SO_4, 7 d	146
UiO-66(Zr)	hydrophilic	BDC	well-retained in all conditions		concentrated HCl, 24 h pH = 12, 24 h	113

https://dx.doi.org/10.1021/acs.chemrev.9b00746
Chem. Rev. XXXX, XXX, XXX−XXX

Table 1. continued

MOF	hydrophilic/ hydrophobic[b]	linker	crystallinity[c]	porosity[c]	assessment condition	ref
			carboxylate linkers			
UiO-66(Zr)	hydrophilic	BDC	well-retained in all conditions	46% loss Langmuir area	pH = 0(HCl), RT, 3 d	114
				5% increase Langmuir area	pH = 4(HCl), RT, 3 d	
				4% increase Langmuir area	pH = 12(NaOH), RT, 3 d	
				3% loss Langmuir area	5% H_2O_2, RT, 3 d	
UiO-66(Zr)	hydrophilic	BDC	well-retained in all conditions	47% loss Langmuir area	pH = 0(HCl), RT, 2 months	114
				3% loss Langmuir area	pH = 4(HCl), RT, 2 months	
				14% loss Langmuir area	pH = 12(NaOH), RT, 2 months	
				13% increase Langmuir area	5% H_2O_2, RT, 2 months	
UiO-66(Zr)	hydrophilic	BDC	well-retained		25 mg MOF in 5 mL solutions, 0.1 M HCl, RT, 24 h	147
			complete degradation		25 mg MOF in 5 mL solutions, 0.1 M NaOH, RT, 24 h	
HP-UiO-66(Zr)	hydrophilic	BDC	well-retained in all conditions		concentrated HCl, 24 h, pH = 12, 24 h	113
UiO-66-NH_2(Zr)	hydrophilic	BDC-NH_2	well-retained		25 mg MOF in 5 mL solutions, 0.1 M HCl, RT, 24 h	147
			complete degradation		25 mg MOF in 5 mL solutions, 0.1 M NaOH, RT, 24 h	
UiO-66-NH_2(Zr)	hydrophilic	BDC-NH_2	well-retained		pH = 1(HCl), 2 h	144
UiO-66-NH_2(Zr)	hydrophilic	BDC-NH_2	complete degradation		pH = 14(NaOH), 2 h	144
UiO-66-NH_2(Zr)	hydrophilic	BDC-NH_2	well-retained in all conditions	20% loss Langmuir area	pH = 0(HCl), RT, 3 d	114
				12% increase Langmuir area	pH = 4(HCl), RT, 3 d	
				33% loss Langmuir area	pH = 12(NaOH), RT, 3 d	
				22% loss Langmuir area	5% H_2O_2, RT, 3 d	
UiO-66-NH_2(Zr)	hydrophilic	BDC-NH_2	well-retained in all conditions	33% loss Langmuir area	pH = 0(HCl), RT, 2 months	114
				18% loss Langmuir area	pH = 4(HCl), RT, 2 months	
				27% loss Langmuir area	pH = 12(NaOH), RT, 2 months	
				45% loss Langmuir area	5% H_2O_2, RT, 2 months	
UiO-66-NH_2(Zr)	hydrophilic	BDC-NH_2	well-retained in all conditions		concentrated HCl, 24 h pH = 12, 24 h	113
HP-UiO-66-NH_2(Zr)	hydrophilic	BDC-NH_2	well-retained in all conditions		concentrated HCl, 24 h pH = 12, 24 h	113

https://dx.doi.org/10.1021/acs.chemrev.9b00746
Chem. Rev. XXXX, XXX, XXX−XXX

Table 1. continued

MOF	hydrophilic/ hydrophobic[b]	linker	crystallinity[c]	porosity[c]	assessment condition	ref
			carboxylate linkers			
UiO-66-NO_2(Zr)	hydrophilic	BDC-NO_2	well-retained		pH = 1 (HCl), 2 h	144
UiO-66-NO_2(Zr)	hydrophilic	BDC-NO_2	well-retained		pH = 14 (NaOH), 2 h	144
UiO-66-NO_2(Zr)	hydrophilic	BDC-NO_2	well-retained complete degradation	1% BET loss after pH = 1.5 (HCl)	pH = 1.5 (HCl) RT, 2 d pH = 12.5 (NaOH), RT, 2 d	56
UiO-66-NO_2(Zr)	hydrophilic	BDC-NO_2	well-retained in all conditions		concentrated HCl, 24 h pH = 12, 24 h	113
HP-UiO-66-NO_2(Zr)	hydrophilic	BDC-NO_2	well-retained in all conditions		concentrated HCl, 24 h pH = 12, 24 h	113
UiO-66-Br(Zr)	hydrophilic	BDC-Br	well-retained		pH = 1 (HCl), 2 h	144
UiO-66-Br(Zr)	hydrophilic	BDC-Br	partial degradation		pH = 14 (NaOH), 2 h	144
UiO-66-ox-Cu(Zr)	hydrophilic	BDC, OX	complete degradation	71% loss in BET area	1431 ppm NH_3 and 80% RH, RT breakthrough 1 cycle	148
UiO-66-$(COOCu)_2$(Zr)	hydrophilic	BTC 1,2,4,5-benzene- tetracarboxylate	well-retained		1431 ppm NH_3 and 80% RH, RT breakthrough 1 cycle	148
UiO-66-COOCu(Zr)	hydrophilic	BTC 1,2,4-benzene- tricarboxylic	well-retained		1431 ppm NH_3 and 80% RH, RT breakthrough 1 cycle	148
UiO-66⊃Cu(Zr)	hydrophilic	BDC	well-retained		1431 ppm NH_3 and 80% RH, RT breakthrough 1 cycle	148
UiO-66-ox(Zr)	hydrophilic	BDC, OX	well-retained		1431 ppm NH_3 and 80% RH, RT breakthrough 1 cycle	148
UiO-66-$(CH_3)_2$	hydrophilic	BDC-$(CH_3)_2$	well-retained		pH = 1 (HCl), 2 h	149
UiO-66-$(CH_3)_2$	hydrophilic	BDC-$(CH_3)_2$	well-retained		pH = 14 (NaOH), 2 h	149
OPA-UiO-66-SO_3H(Zr)	hydrophobic	BDC-SO_3H	well-retained	1% BET increase	pH = 11, 7 d	146
OPA-UiO-66-SO_3H(Zr)	hydrophobic	BDC-SO_3H	well-retained in all conditions		0.5 M NaCl, 7 d 0.5 M Na_2SO_4, 7 d	146
UiO-66-SO_3H(Zr)	hydrophilic	BDC-SO_3H	partial degradation	53% BET loss	pH = 11, 2 d	146

https://dx.doi.org/10.1021/acs.chemrev.9b00746
Chem. Rev. XXXX, XXX, XXX−XXX

Table 1. continued

MOF	hydrophilic/ hydrophobic[b]	linker	crystallinity[c]	porosity[c]	assessment condition	ref
			carboxylate linkers			
UiO-66-SO_3H(Zr)	hydrophilic	BDC-SO_3H	complete degradation in all conditions		0.5 M NaCl, 7 d 0.5 M Na_2SO_4, 7 d	146
OPA-UiO-66(Zr)	hydrophobic	BDC	well-retained in all conditions		0.5 M NaCl, 7 d 0.5 M Na_2SO_4, 7 d	146
UiO-66-$(OH)_2$(Zr)	hydrophilic	DOBDC	well-retained in all conditions	partial BET loss in all conditions	pH = 2, 7 d pH = 12, 1 d	150
UiO-66-$(OH)_2$(Zr)	hydrophilic	DOBDC	partial degradation	significant BET loss	pH = 12, 2 day	150
UiO-67(Zr)	hydrophilic	BPDC	complete degradation well-retained well-retained complete degradation	99% loss Langmuir area 9% loss Langmuir area 42% loss Langmuir area 99% loss Langmuir area	pH = 0(HCl), RT, 3 d pH = 4(HCl), RT, 3 d pH = 12(NaOH), RT, 3 d 5% H_2O_2, RT, 3 d	114
UiO-67(Zr)	hydrophilic	BPDC	complete degradation partial degradation well-retained complete degradation	99% loss Langmuir area 99% loss Langmuir area 15% loss Langmuir area 97% loss Langmuir area	pH = 0(HCl), RT, 2 months pH = 4(HCl), RT, 2 months pH = 12(NaOH), RT, 2 months 5% H_2O_2, RT, 2 months	114
UiO-67(Zr)	hydrophilic	BPDC	partial degradation in all conditions		concentrated HCl, 24 h pH = 12, 24 h	113
UiO-67(Zr)	hydrophilic	BPDC	complete degradation in all conditions		25 mg MOF in 5 mL solutions, 0.1 M HCl, RT, 24 h 25 mg MOF in 5 mL solutions, 0.1 M NaOH, RT, 24 h	147
UiO-67(Zr)	hydrophilic	BPDC	complete degradation in all conditions		80 mg MOF in 8 mL solution, 1 M HCl, 1 d 80 mg MOF in 8 mL solution, 10 mM NaOH (pH = 12), 1 d	90
UiO-67-o-$2CF_3$(Zr)	hydrophobic	BPDC-o-$2CF_3$	well-retained in all conditions	2% increase BET 2% increase BET 2% increase BET	80 mg MOF in 8 mL solution, 1 M HCl, 1 d 80 mg MOF in 8 mL solution, 4 M HCl, 1 d 80 mg MOF in 8 mL solution, 8 M HCl, 1 d 80 mg MOF in 8 mL solution, 10 mM NaOH (pH = 12), 1 d	90

https://dx.doi.org/10.1021/acs.chemrev.9b00746
Chem. Rev. XXXX, XXX, XXX−XXX

Table 1. continued

MOF	hydrophilic/ hydrophobic[b]	linker	crystallinity[c]	porosity[c]	assessment condition	ref
			carboxylate linkers			
				2% loss BET 3% loss BET	80 mg MOF in 8 mL solution, 50 ppm NaF, 1 d	
UiO-67-m-2CF_3(Zr)	hydrophobic	BPDC-m-2CF_3	well-retained in all conditions	1% loss BET	80 mg MOF in 8 mL solution, 1 M HCl, 1 d	90
				2% increase BET	80 mg MOF in 8 mL solution, 10 mM NaOH (pH = 12), 1 d	
UiO-67-m-2CF_3(Zr)	hydrophobic	BPDC-m-2CF_3	complete degradation in all conditions	65% loss BET	80 mg MOF in 8 mL solution, 4 M HCl, 1 d	90
				70% loss BET	80 mg MOF in 8 mL solution, 8 M HCl, 1 d	
				86% loss BET	80 mg MOF in 8 mL solution, 50 ppm NaF, 1 d	
UiO-67-BIPY(Zr)	hydrophilic	BIPY	complete degradation in all conditions		25 mg MOF in 5 mL solutions, 0.1 M HCl, RT, 24 h	147
					25 mg MOF in 5 mL solutions, 0.1 M NaOH, RT, 24 h	
HP-UiO-67(Zr)	hydrophilic	BPDC	partial degradation in all conditions		concentrated HCl, 24 h	113
					pH = 12, 24 h	
UiO-67-BN	hydrophilic	BPDC-BN	well-retained in all conditions		50 mg MOF in 10 mL pH = 1−12 (HCl, NaOH), 30 min	151
UiO-67-BN	hydrophilic	BPDC-BN	complete degradation in all conditions		50 mg MOF in 10 mL pH = 13 (NaOH), 30 min	151
					50 mg MOF in 10 mL pH = 14 (NaOH), 30 min	
PCN-202(Ni)-Hf(Zr,Ni,Hf)	hydrophilic	TCPP DCDPS HDPDCS	well-retained in all conditions		pH = 1, 24 h pH = 7, 24 h pH = 12, 24 h	152
PCN-202(Ni)-Zr(Zr, Ni)	hydrophilic	TCPP DCDPS HDPDCS	well-retained in all conditions	well-retained in all conditions	pH = 1, 24 h pH = 7, 24 h pH = 12, 24 h	152
PCN-222(Zr)	hydrophilic	TCPP	well-retained in all conditions	BET loss as a function of increased H_2SO_4 concentration	50 mg MOF in 5 mL solution, 0.005 M H_2SO_4, 24 h	153
					50 mg MOF in 5 mL solution, 0.01 M H_2SO_4, 24 h	
					50 mg MOF in 5 mL solution, 0.1 M H_2SO_4, 24 h	

https://dx.doi.org/10.1021/acs.chemrev.9b00746
Chem. Rev. XXXX, XXX, XXX−XXX

Table 1. continued

MOF	hydrophilic/ hydrophobic[b]	linker	crystallinity[c]	porosity[c]	assessment condition	ref
			carboxylate linkers			
OPA-PCN-222(Zr)	hydrophobic	TCPP	well-retained	6% BET increase	pH = 11, 7 d	146
PCN-222(Zr)	hydrophilic	TCPP	complete degradation		pH = 11, 2 d	146
PCN-222(Fe)(Zr,Fe)		TCPP	well-retained in all conditions	2% loss BET	100 mg MOF in 15 mL solution, 2 M HCl, 24 h	70
				1% loss BET	100 mg MOF in 15 mL solution, 4 M HCl, 24 h	
				2% increase BET	100 mg MOF in 15 mL solution, 8 M HCl, 24 h	
				1% loss BET	100 mg MOF in 15 mL solution, concentrated HCl, 24 h	
PCN-223(Zr)	hydrophilic	TCPP	well-retained in all conditions	partial loss at pH = 10	1 M HCl pH = 10	154
PCN-225(Zr)	hydrophilic	TCPP	well-retained	well-retained	pH = 1−11, 12 h	155
PCN-225(Zr)	hydrophilic	TCPP	well-retained in all conditions	significant BET loss in all conditions	pH = 0, 12 h pH = 12, 12 h	155
PCN-229(Zr)	hydrophilic	TCP-2	well-retained in all conditions		1 M HCl, 24 h pH = 12 (NaOH), 24 h	156
PCN-230(Zr)	hydrophilic	TCP-3	well-retained	partial loss of N_2 uptake	pH = 0−12 (HCl, NaOH), 24 h	156
PCN-777(Zr)	hydrophilic	TATB	well-retained in all conditions		pH = 3, 12 h pH = 11, 12 h	157
MOF-808(Zr)	hydrophilic	BTC	well-retained in all conditions		concentrated HCl pH = 11	113
HP-MOF-808(Zr)	hydrophilic	BTC	well-retained in all conditions		concentrated HCl pH = 11	113
MOF-808P(Zr)	hydrophilic	BTC	well-retained in all conditions	well-retained BET in all conditions	0.5 g MOF in 50 mL solution, 0.005 M H_2SO_4, 24 h 0.5 g MOF in 50 mL solution, 0.01 M H_2SO_4, 24 h 0.5 g MOF in 50 mL solution, 0.1 M H_2SO_4, 24 h	126
DUT-67(Zr)	hydrophilic	TDC	well-retained		concentrated HCl, 3 days	121
DUT-68(Zr)	hydrophilic	TDC	well-retained		concentrated HCl, 3 days	121

https://dx.doi.org/10.1021/acs.chemrev.9b00746
Chem. Rev. XXXX, XXX, XXX−XXX

Table 1. continued

MOF	hydrophilic/ hydrophobic[b]	linker	crystallinity[c]	porosity[c]	assessment condition	ref
			carboxylate linkers			
DUT-69(Zr)	hydrophilic	TDC	well-retained		HCl (1 mol/L), 1 day	121
BUT-12(Zr)	amphiphilic	CTTA	well-retained in all conditions		2 M HCl, RT, 24 h 6 M HCl, RT, 24 h concentrated HCl, RT, 24 h pH = 10 (NaOH), RT, 24 h	122
BUT-13(Zr)	amphiphilic	TTNA	well-retained in all conditions		2 M HCl, RT, 24 h 6 M HCl, RT, 24 h concentrated HCl, RT, 24 h pH = 10 (NaOH), RT, 24 h	122
BUT-39(Zr)	hydrophilic	BTBA	well-retained in all conditions	partial BET loss in all conditions	2 M HCl, 24 h pH = 12 NaOH, 24 h	158
BUT-46A(Zr)	hydrophilic	TPHB CH3COO	well-retained in all conditions	partial BET loss, no linkers leaching confirmed by UV−vis	100 mg MOF in 20 mL solution, pH = 1 (HCl), RT, 24 h 100 mg MOF in 20 mL solution, pH = 10 (NaOH), RT, 24 h	58
BUT-46W(Zr)	hydrophilic	TPHB	well-retained in all conditions	partial BET loss, no linkers leaching confirmed by UV−vis	100 mg MOF in 20 mL solution, pH = 1 (HCl), RT, 24 h 100 mg MOF in 20 mL solution, pH = 10 (NaOH), RT, 24 h	58
BUT-46B(Zr)	hydrophilic	TPHB, PhCOO, HCOO	well-retained in all conditions	partial BET loss, no linkers leaching confirmed by UV−vis	100 mg MOF in 20 mL solution, pH = 1 (HCl), RT, 24 h 100 mg MOF in 20 mL solution, pH = 10 (NaOH), RT, 24 h	58
BUT-46F(Zr)	hydrophilic	TPHB, HCOO	well-retained in all conditions	partial BET loss, no linkers leaching confirmed by UV−vis	100 mg MOF in 20 mL solution, pH = 1 (HCl), RT, 24 h 100 mg MOF in 20 mL solution, pH = 10 (NaOH), RT, 24 h	58
NUS-6(Zr)	hydrophilic	BDC-SO_3Na	well-retained partial degradation	porosity well-retained at pH = 1	pH = 1, RT, 24 h pH = 12, RT, 24 h	159
FJI-H6(Zr)	hydrophilic	TBPP	well-retained	1% BET increase	100 mg MOF in 1.5 mL 8 M HCl + 10 mL DMF, 358 K, 12 h	160
BUT-66(Zr)	hydrophilic	BDB	well-retained in all conditions		pH = 3 (HCl), 30 d pH = 10(NaOH), 30 d	104

https://dx.doi.org/10.1021/acs.chemrev.9b00746
Chem. Rev. XXXX, XXX, XXX−XXX

Table 1. continued

MOF	hydrophilic/ hydrophobic[b]	linker	crystallinity[c]	porosity[c]	assessment condition	ref
			carboxylate linkers			
BUT-67(Zr)	hydrophilic	NDB	well-retained in all conditions		pH = 3 (HCl), 2 d pH = 10(NaOH), 2 d	104
MIP-200(Zr)	hydrophilic	MDIP	well-retained in all conditions	8% increase BET	100 mg MOF in 20 mL solution, 9 M H_2SO_4, RT, 3 d	123
				12% loss BET	100 mg MOF in 20 mL solution, pH = 12 (KCl, NaOH), RT, 3 d	
MIP-200(Zr)	hydrophilic	MDIP	well-retained in all conditions	40% increase BET	100 mg MOF in 20 mL solution, 15 M HNO_3, RT, 3 d	123
				12% loss BET	100 mg MOF in 20 mL solution, 6 M H_3PO_4, RT, 3 d	
				47% increase BET	100 mg MOF in 20 mL solution, aqua regia, RT, 3 d	
MIP-200(Zr)	hydrophilic	MDIP	well-retained in all conditions	1% increase BET	100 mg MOF to NH_4OH vapor, RT, 3 d	123
				12% increase BET	500 mg MOF in 12 M HCl, RT, 3 d	
spiro-1(Zr)	hydrophilic	L1 for spiro-1	well-retained in all conditions	well-retained N_2 uptake in all conditions	concentrated HCl, RT, 7 d 0.01 M NaOH, RT, 7 d	124
spiro-2(Zr)	hydrophilic	L2 for spiro-2	well-retained in all conditions	partial increase CO_2 uptake partial loss CO_2 uptake	concentrated HCl, RT, 7 d 0.01 M NaOH, RT, 7 d	124
MIL-125-NH_2(Ti)	hydrophilic	BDC-NH_2	well-retained in all conditions		pH = 4 (HCl), 1 d, 298 K pH = 4 (HCl), 5 d, 298 K pH = 9 (NaOH), 5 d, 298 K	161
MIL-125-NH_2(Ti)	hydrophilic	BDC-NH_2	significant degradation in all conditions		pH = 4 (HCl), 20 d, 298 K pH = 9 (NaOH), 10 d, 298 K pH = 9 (NaOH), 15 d, 298 K	161
MIL-125-NHCyp(Ti)	hydrophobic	BDC-NHCyp	well-retained in all conditions		pH = 4 (HCl), 1 d, 298 K pH = 4 (HCl), 5 d, 298 K pH = 9 (NaOH), 5 d, 298 K pH = 9 (NaOH), 10 d, 298 K pH = 9 (NaOH), 15 d, 298 K	161
MIL-125-NHCyp(Ti)	hydrophobic	BDC-NHCyp	partial degradation		pH = 4 (HCl), 298 K, 20 d	161
MIL-177-LT(Ti)		MDIP	well-retained in all conditions	8% BET increase	aqua regia, RT	125

https://dx.doi.org/10.1021/acs.chemrev.9b00746
Chem. Rev. XXXX, XXX, XXX−XXX

Table 1. continued

MOF	hydrophilic/ hydrophobic[b]	linker	crystallinity[c]	porosity[c]	assessment condition	ref
			carboxylate linkers			
				2.5% BET loss	37% HCl, RT	
				2.5% BET loss	65% HNO_3, RT	
				4% BET loss	98% H_2SO_4, RT	
				22% BET loss	6 M H_3PO_4, RT	
NUS-6(Hf)	hydrophilic	BDC-SO_3Na	well-retained partial degradation	porosity well-retained at pH = 1	pH = 1, RT, 24 h	159
					pH = 12, RT, 24 h	
UO_2(DCPBA)(U)		DCPBA	well-retained in all conditions		pH = 3−12(HNO_3/NaOH), 3 d	82
NU-1300(U)		TBAPy	well-retained in all conditions		pH = 1−10, 7 d	81
MOF-5(Zn)	hydrophilic	BDC	complete degradation in all conditions		0.01 g MOF in 20 mL HCl (12 M)	145
					0.01 g MOF in 20 mL H_2SO_4 (18M)	
					0.01 g MOF in 20 mL HF (40%)	
					0.01 g MOF in 20 mL NaOH (14 M)	
					0.01 g MOF in 20 mL chromic acid solution (0.1 M $K_2Cr_2O_7$ in concentrate H_2SO_4)	
MOF-5(Zn)	hydrophilic	BDC	significant degradation	complete loss	water saturated CO_2, 318 K, 4 h	127
MOF-5-VF(Zn)	hydrophobic	BDC-VF	well-retained	well-retained	water saturated CO_2, 318 K, 168 h	127
MOF-5-VF(Zn)	hydrophobic	BDC-VF	well-retained in all conditions		acid (0.001−10 M H^+) and base (0.001−0.01 M OH^-) solutions, 7 d	127
JXNU-4(Zn)		BPDC	well-retained in all conditions		pH = 4−11, HCl, NaOH, 24 h	162
NENU-500(Zn)	hydrophilic	BTB	well-retained in all conditions		pH = 1−12, RT, 24 h	101
NENU-500(Zn)	hydrophilic	BTB	partial degradation		0.5 M H_2SO_4, 6 h	101
NENU-501(Zn)		BPT	well-retained in all conditions		pH = 1−12, RT 24 h	101
NENU-501(Zn)		BPT	partial degradation		0.5 M H_2SO_4, 6 h	101
NENU-522(Zn)		CDC	well-retained in all conditions		pH = 4−12, HCl/NaOH, 2 h	163
Zn_3IPA_3(Zn)		IPA	well-retained in all conditions		pH = 3, 24 h	164
					pH = 4, 24 h	

https://dx.doi.org/10.1021/acs.chemrev.9b00746
Chem. Rev. XXXX, XXX, XXX−XXX

Table 1. continued

MOF	hydrophilic/ hydrophobic[b]	linker	crystallinity[c]	porosity[c]	assessment condition	ref
			carboxylate linkers			
					pH = 6, 24 h	
					pH = 8, 24 h	
					pH = 10, 24 h	
HKUST-1(Cu)	hydrophilic	BTC	complete degradation in all conditions		pH = 1.5 (HCl), RT, 2 d	56
					pH = 12.5 (NaOH), RT, 2 d	
HKUST-1(Cu)	hydrophilic	BTC	complete degradation in all conditions		0.01 g MOF in 20 mL HCl (12 M)	145
					0.01 g MOF in 20 mL H_2SO_4 (18 M)	
					0.01 g MOF in 20 mL HF (40%)	
					0.01 g MOF in 20 mL NaOH (14 M)	
					0.01 g MOF in 20 mL chromic acid solution (0.1 M $K_2Cr_2O_7$ in concentrate H_2SO_4)	
HKUST-1(Cu)	hydrophilic	BTC	complete degradation	100% loss Langmuir area	pH = 0(HCl), RT, 3 d	114
			partial degradation	30% increase Langmuir area	pH = 4(HCl), RT, 3 d	
			complete degradation	82% loss Langmuir area	pH = 12 (NaOH), RT, 3 d	
			well-retained	52% loss Langmuir area	5% H_2O_2, RT, 3 d	
HKUST-1(Cu)	hydrophilic	BTC	complete degradation	100% loss Langmuir area	pH = 0(HCl), RT, 2 months	114
			partial degradation	69% loss Langmuir area	pH = 4(HCl), RT, 2 months	
			complete degradation	66% loss Langmuir area	pH = 12(NaOH), RT, 2 months	
			complete degradation	95% loss Langmuir area	5% H_2O_2, RT, 2 months	
JUC-1000(Cu)	hydrophilic	BTPO	well-retained, no Cu^{2+} released in all conditions	5% loss BET	pH = 1.5 (HCl), RT, 2 d	56
				1% loss BET	pH = 12.5 (NaOH), RT, 2 d	
ZJNU-51(Cu)		TPADPA	well-retained in all conditions		pH = 2−11, HCl/NaOH, 36 h	165
ZJNU-51(Cu)		TPADPA	complete degradation in all conditions		pH = 1 (HCl), 36 h	165
					pH = 12 (NaOH), 36 h	
HKUST-1(Cu)	hydrophilic	BTC	partial degradation in all conditions	14.1% BET loss	O_2/H_2O atmosphere, 1 d	131
				19.2% BET loss	O_2/H_2O atmosphere, 3 d	
				23.3% BET loss	O_2/H_2O atmosphere, 5 d	
BUT-155(Cu)	hydrophilic	TDHB	partial degradation in all conditions	22% BET loss	15 mg in 20 mL HCl (pH = 4), RT, 24 h	57
				11% BET loss	15 mg in 20 mL NaOH (pH = 10), RT, 24 h	

https://dx.doi.org/10.1021/acs.chemrev.9b00746
Chem. Rev. XXXX, XXX, XXX−XXX

Table 1. continued

MOF	hydrophilic/ hydrophobic[b]	linker	crystallinity[c]	porosity[c]	assessment condition	ref
			carboxylate linkers			
Cd-EDDA(Cd)	hydrophilic	EDDA	well-retained in all conditions		pH = 2.0 pH = 4.2 pH = 10.3 pH = 12.2	166
			Azolate Linkers			
ZIF-8(Zn)	hydrophobic	MIM	well-retained in all conditions		0.1 M NaOH, 373 K, 24 h 8 M NaOH, 373 K, 24 h	41
ZIF-8(Zn)	hydrophobic	MIM	complete degradation well-retained	0.5% BET loss after pH = 12.5	pH = 1.5(HCl), RT, 2 d pH = 12.5(NaOH), RT, 2 d	56
ZIF-8(Zn)	hydrophobic	MIM	complete degradation in all conditions		0.01 g MOF in 20 mL HCl (12 M) 0.01 g MOF in 20 mL H_2SO_4 (18 M) 0.01 g MOF in 20 mL HF (40%) 0.01 g MOF in 20 mL NaOH (14 M) 0.01 g MOF in 20 mL chromic acid solution (0.1 M $K_2Cr_2O_7$ in concentrate H_2SO_4)	145
ZIF-8(Zn)	hydrophobic	MIM	complete degradation well-retained well-retained partial degradation	100% loss Langmuir area 13% loss Langmuir area 16% loss Langmuir area 35% loss Langmuir area	pH = 0(HCl), RT, 3 d pH = 4(HCl), RT, 3 d pH = 12(NaOH), RT, 3 d 5% H_2O_2, RT, 3 d	114
ZIF-8(Zn)	hydrophobic	MIM	complete degradation partial degradation partial degradation complete degradation	100% loss Langmuir area 79% loss Langmuir area 82% loss Langmuir area 86% loss Langmuir area	pH = 0(HCl), RT, 2 months pH = 4(HCl), RT, 2 months pH = 12(NaOH), RT, 2 months 5% H_2O_2, RT, 2 months	114
ZIF-8(Zn)	hydrophobic	MIM	well-retained		0.06 wt % MOF in 0.45% MIM water	50
ZIF-8(Zn)	hydrophobic	MIM	well-retained	partial BET loss	LiCl, RT, 24 h, molar ratio of salt to ZIF-8 is 0.5	167
ZIF-8(Zn)	hydrophobic	MIM	partial degradation in all conditions	partial BET loss in all conditions	$LiNO_3$, RT, 24 h, molar ratio of salt to ZIF-8 is 0.5 NaCl, RT, 24 h, molar ratio of salt to ZIF-8 is 0.5 $NaNO_3$, RT, 24 h, molar ratio of salt to ZIF-8 is 0.5	167
ZIF-8(Zn)	hydrophobic	MIM	complete degradation in all conditions	significant BET loss in all conditions	$NiCl_2$, RT, 24 h, molar ratio of salt to ZIF-8 is 0.5	167

https://dx.doi.org/10.1021/acs.chemrev.9b00746
Chem. Rev. XXXX, XXX, XXX−XXX

Table 1. continued

MOF	hydrophilic/ hydrophobic[b]	linker	crystallinity[c]	porosity[c]	assessment condition	ref
			Azolate Linkers			
					$Ni(NO_3)_2$, RT, 24h, molar ratio of salt to ZIF-8 is 0.5 $CoCl_2$, RT, 24 h, molar ratio of salt to ZIF-8 is 0.5 $Co(NO_3)_2$, RT, 24 h, molar ratio of salt to ZIF-8 is 0.5 $CuCl_2$, RT, 24 h, molar ratio of salt to ZIF-8 is 0.5 $Cu(NO_3)_2$, RT, 24 h, molar ratio of salt to ZIF-8 is 0.5 $AlCl_3$, RT, 24 h, molar ratio of salt to ZIF-8 is 0.5 $Al(NO_3)_3$, RT, 24 h, molar ratio of salt to ZIF-8 is 0.5 $InCl_3$, RT, 24 h, molar ratio of salt to ZIF-8 is 0.5 $In(NO_3)_3$, RT, 24 h, molar ratio of salt to ZIF-8 is 0.5	
ZIF-8(Zn)	hydrophobic	MIM	significant degradation	61% BET loss	water saturated CO_2 at 318 K for 240 h	127
ZIF-8-VF(Zn)	hydrophobic	MIM-VF	well-retained	6% BET loss	water saturated CO_2 at 318 K for 720 h	127
ZIF-8-VF(Zn)	hydrophobic	MIM-VF	well-retained in all conditions		acid (0.001−0.01 M H^+) and base (0.001−10 M OH^-) solutions, 7 d	127
MAF-X27-Cl(Co)		BTTA	well-retained in all conditions		0.001 M HCl, KOH, 7 d 1.0 M KOH, 7 d	86
PCN-601(Ni)		TPP	well-retained in all conditions		5 mg MOF in 3.5 mL solutions, 0.01 mM, RT, 24 h 5 mg MOF in 3.5 mL solutions, 0.1 mM HCl, RT, 24 h 5 mg MOF in 3.5 mL solutions, s-NaOH, RT, 24 h 5 mg MOF in 3.5 mL solutions, 1 M NaOH, 373 K, 24 h 5 mg MOF in 3.5 mL solutions, 10 M NaOH, 373 K, 24 h 5 mg MOF in 3.5 mL solutions, s-NaOH, 373 K, 24 h	59
PCN-601(Ni)		TPP		slight higher porosity in all conditions	100 mg MOF in 35 mL solutions of 0.1 mM HCl, RT, 24 h 100 mg MOF in 35 mL solutions of s-NaOH, 373K, 24 h	59

https://dx.doi.org/10.1021/acs.chemrev.9b00746
Chem. Rev. XXXX, XXX, XXX−XXX

Table 1. continued

MOF	hydrophilic/ hydrophobic[b]	linker	crystallinity[c]	porosity[c]	assessment condition	ref
			Azolate Linkers			
PCN-601(Ni)		TPP		no linkers released confirmed by UV−vis	5 mg MOF in 3.5 mL solutions of 0.1 mM HCl, RT, 24 h 5 mg MOF in 3.5 mL solutions of s-NaOH, 373 K, 24 h	59
PCN-602(Ni)	hydrophilic	TPPP	well-retained in all conditions	well-retained in all conditions	100 mg MOF in 35 mL of 0.1 mM HCl (pH = 4), RT, 24 h 100 mg MOF in 35 mL of 1 M NaOH (pH = 14), RT, 24 h 100 mg MOF in 35 mL of 1 M KF, RT, 24 h 100 mg MOF in 35 mL of 1 M Na_2CO_3, RT, 24 h 100 mg MOF in 35 mL of 1 M K_3PO_4, RT, 24 h	109
$Ni_3(BTP)_2$(Ni)		BTP	well-retained in all conditions	6% loss increase Langmuir area 7% loss increase Langmuir area 1% increase Langmuir area	pH = 2 (HCl), 373 K, 14 d pH = 2 (HNO_3), 373 K, 14 d pH = 14 (NaOH), 373 K, 14 d	85
$Cu_3(BTP)_2$(Ni)		BTP	complete degradation in all conditions	complete loss porosity in all conditions	pH = 3 (HCl), RT, 1 d pH = 14 (NaOH), RT, 1 d	85
$Zn_3(BTP)_2$(Ni)	hydrophobic	BTP	well-retained complete degradation	complete loss porosity at pH = 14	pH = 3 (HCl), 373 K, 7 d pH = 14 (NaOH), RT, 1 h	85
Zn(1,3-BDP)(Zn)	hydrophobic	BDP	well-retained		pH = 3 aqueous solution, 363 K, 30 min	105
kag-MOF-1(Zn)	hydrophilic	TZE	well-retained in all conditions	CO_2 uptake well preserved after adsorbing humid (75%) CO_2	pH = 4 pH = 10	168
BUT-83(Co)	hydrophilic	DCDPP	well-retained		concentrated HCl, 24 h	128
IPM-MOF-201(Ni)	hydrophilic	IPA	partial degradation for all conditions and Ni^{2+} (1.85 ppm) released at pH = 4	slightly shifted on CO_2 uptake in all conditions	50 mg MOF in 5 mL solution (pH = 4), RT, 24 h 50 mg MOF in 5 mL solution (p H = 10), RT, 24 h 50 mg MOF in 5 mL solution (pH = 12), RT, 24 h 50 mg MOF in 5 mL solution (pH = 14), RT, 24 h	60

https://dx.doi.org/10.1021/acs.chemrev.9b00746
Chem. Rev. XXXX, XXX, XXX−XXX

Table 1. continued

MOF	hydrophilic/ hydrophobic[b]	linker	crystallinity[c]	porosity[c]	assessment condition	ref
			Azolate Linkers			
$Cu_4(SiW_{12}O_{40})(L)(Cu)$		RABL	well-retained in all conditions		pH = 2−14	169
MCIF(Cu)	hydrophobic	DCI	well-retained in all conditions		pH = 2−13, 1 d	170
$Cu_6(Trz)_{10}(Cu)$	hydrophilic	TRZ	well-retained in all conditions		pH = 2, 353 K, 24 h pH = 11, 353 K, 24 h pH = 12, 353 K, 24 h	171
$Ag(ABTA)_2$		ABTA	well-retained in all conditions		pH = 2.4 pH = 10.8 pH = McIlvaine	172
$Ag_3(ABTA)_3$		ABTA	well-retained in all conditions		pH = 2.2 pH = 7.5 pH = McIlvaine	172
			Bifunctional Linkers (Carboxylate, Azolate)			
MOS-1(Co)	hydrophilic	IDC, PDA	well-retained after 3 ads cycles	2% loss in NH_3 uptake after 3 ads cycles	steam of 4% ammonia solution, 298 K	173
MOS-2(Co)	hydrophilic	IDC, PHEN	well-retained after 3 ads cycles	3% loss in NH_3 uptake after 3 ads cycles	steam of 4% ammonia solution, 298 K	173
MOS-3(Co)	hydrophilic	IDC, BPY	well-retained after 3 ads cycles	6% loss in NH_3 uptake after 3 ads cycles	steam of 4% ammonia solution, 298 K	173
FJI-H14(Cu)		BTTA	well-retained in all conditions		pH = 2−12, 373 K, 24 h	174
$Cd_2(sdb)_2(pcih)_2$ (Cd)	hydrophilic	SDB PCIH	well-retained		pH = 3(HCl) pH = 5(HCl)	175
$Cd_2(sdb)_2(pcih)_2$ (Cd)	hydrophilic	SDB PCIH	complete degradation partial degradation		pH = 1(HCl) pH = 9(NaOH)	175
PCN-124-stu(Cu)		PDAD	well-retained in all conditions		pH = 2−12 (HCl, NaOH), 7 d	176
PCN-124-stu(Cu)		PDAD	complete degradation in all conditions		pH = 1(HCl), 7 d pH = 13(NaOH), 7 d pH = 14(NaOH), 7 d	176
NENU-601(Zn)		BDC, BIM	well-retained in all conditions		pH = 1(HCl), 24 h	177

https://dx.doi.org/10.1021/acs.chemrev.9b00746
Chem. Rev. XXXX, XXX, XXX−XXX

Table 1. continued

MOF	hydrophilic/ hydrophobic[b]	linker	crystallinity[c]	porosity[c]	assessment condition	ref
			Bifunctional Linkers (Carboxylate, Azolate)			
					pH = 3(HCl), 24 h pH = 5(HCl), 24 h pH = 9(NaOH), 24 h pH = 11(NaOH), 24 h pH = 12(NaOH), 24 h electrolyte 12 h	
Co_2(TCS)(BPY)(Co)		TCS, BPY	well-retained in all conditions		pH = 5−11	178
Ni_2(TCS)(BPY)(Ni)		TCS, BPY	well-retained in all conditions		pH = 2−11	178
Cu_2(TCS)(BPY)(Cu)		TCS, BPY	well-retained in all conditions		pH = 3−11	178
$Cd_{1.5}$(TPO)$(bipy)_{1.5}$(Cd)		TPO, BIPY	well-retained in all conditions		pH = 2−10, HCl, NaOH, 24 h	179
IISERP-MOF2(Ni)		PCY	well-retained	no loss of CO_2 uptake	humid CO_2, 24 h	103
$Co_6L_4(TPT)_2(\mu3\text{-}OH)_2$(Co)		TPT, TCYM	well-retained in all conditions		pH = 2, 24 h pH = 9, 24 h	180
$Cd_2(tib)_2(bda)_2$(Cd)		TIB, BDA	well-retained in all conditions		pH = 3 (HCl), 12 h pH = 4 (HCl), 12 h pH = 10 (NaOH), 12 h pH = 11(NaOH), 12 h	181
USTC-7(Zn)		TZBPDC	well-retained in all conditions		pH = 2, 12 h pH = 12, 12 h	182
Zn(NO_2-BDC)$(dmbpy)_{0.5}$	hydrophilic	BDC-NO_2, DMBPY	well-retained in all conditions		pH = 5−6, RT, 3 d pH = 8−9, RT, 3 d pH = 7.4 (phosphate buffer), RT, 3 d	183
rht-MOF-tri(Cu)		TAIP	well-retained	2% BET loss	pH = 2.5(HCl), RT, 24 h	184
rht-MOF-tri(Cu)		TAIP	complete degradation in all conditions		pH = 1(HCl), 6 h pH = 2.5(HCl), 48 h	184
rht-MOF-pyr(Cu)		PAIP	well-retained	4% BET loss	pH = 2.5(HCl), RT, 7 d	184
rht-MOF-pyr(Cu)		PAIP	well-retained		pH = 1(HCl), 6 h	184

https://dx.doi.org/10.1021/acs.chemrev.9b00746
Chem. Rev. XXXX, XXX, XXX−XXX

Table 1. continued

MOF	hydrophilic/ hydrophobic[b]	linker	crystallinity[c]	porosity[c]	assessment condition	ref
			Bifunctional Linkers (Carboxylate, Azolate)			
NUM-5(Zn)		BPANTH, OBA	well-retained in all conditions		pH = 3−11, 1 d	185
NUM-5(Zn)		BPANTH, OBA	complete degradation in all conditions		pH = 2, 1 d pH = 12, 1 d	185
			Bifunctional Linkers (Carboxylate, Aldehyde)			
H_2Q-HK(Cu)		BTC, Q	well-retained		pH = 3, 7 d	186
H_2Q-HK(Cu)		BTC, Q	partial degradation		pH = 5, 7 d	186
H_2Q-HK(Cu)		BTC, Q	well-retained		pH = 9, 7 d	186
			Bifunctional Linkers (Carboxylate, Phosphonate)			
1-Cr(Cr)	hydrophobic	CPP	well-retained in all conditions	16% BET loss 20% BET loss	pH = 4(HCl), 7 d pH = 9(NaOH), 7 d	187
1-Mg(Mg)	hydrophobic	CPP	well-retained in all conditions	6% BET loss 10% BET loss	pH = 4(HCl), 7 d pH = 9(NaOH), 7 d	187
1-Mn(Mn)	hydrophobic	CPP	well-retained in all conditions	2% BET loss 4% BET loss	pH = 4(HCl), 7 d pH = 9(NaOH), 7 d	187
1-Zr(Zr)	hydrophobic	CPP	well-retained in all conditions	3% BET loss 3% BET loss	pH = 4(HCl), 7 d pH = 9(NaOH), 7 d	187
Mn_2L_1(Mn)		FCP1	well-retained partial degradation	10% BET loss 24% BET loss	pH = 4(HCl), 24 h pH = 11(NaOH), 24 h	91
Mn_2L_2(Mn)		MCP	complete degradation in all conditions		pH = 4(HCl), 24 h pH = 11(NaOH), 24 h	91
Mn_2L_3(Mn)		FCP3	complete degradation in all conditions		pH = 4(HCl), 24 h pH = 11(NaOH), 24 h	91
			Bifunctional Linkers (Carboxylate, Hydroxyl)			
MOF-74(Mg)	hydrophilic	DOBDC	complete degradation partial degradation	69% BET loss after pH = 12.5(NaOH)	pH = 1.5(HCl), RT, 2 d pH = 12.5(NaOH), RT, 2 d	56
MOF-74(Mg)	hydrophilic	DOBDC	phosphonate linkers	66% loss of CO_2 uptake	humid CO_2, 313 K, 15 breakthrough cycles	188

https://dx.doi.org/10.1021/acs.chemrev.9b00746
Chem. Rev. XXXX, XXX, XXX−XXX

Table 1. continued

MOF	hydrophilic/ hydrophobic[b]	linker	crystallinity[c]	porosity[c]	assessment condition	ref
			Bifunctional Linkers (Carboxylate, Hydroxyl)			
SZ-1(Zr)		TPPM	well-retained in all conditions		pH = 1−11(HNO_3, NaOH), 1 d 3 M H_2SO_4, 1 d	129
SZ-1(Zr)		TPPM	well-retained in all conditions	95% BET loss and mass maintained after aqua regia treatment	aqua regia, RT, 12 h oleum, RT, 12 h concentrated HNO_3, RT, 12 h concentrated HCl, RT, 12 h	129
SZ-1(Zr)		TPPM	complete degradation in all conditions		pH = 13(NaOH), 1 d pH = 14(NaOH), 1 d	129
SZ-2(Zr)		TPPM	well-retained in all conditions		pH = 1−11(HNO_3, NaOH), 1 d	129
SZ-2(Zr)		TPPM	complete degradation in all conditions	80% BET loss after aqua regia treatment	pH = 13(NaOH), 1 d pH = 14 (NaOH), 1 d	129
SZ-3(Zr)		TPPA	well-retained in all conditions		pH = 1−11(HNO_3, NaOH), 1 d 3 M H_2SO_4, 1 d	129
SZ-3(Zr)		TPPA	well-retained in all conditions	4% BET increase after aqua regia treatment	aqua regia, RT, 12 h concentrated HNO_3, RT, 12 h concentrated HCl, RT, 12 h	129
SZ-3(Zr)		TPPA	complete degradation in all conditions		pH = 13(NaOH), 1 d oleum, 12 h	129
JUC-200(Zn)		PA	well-retained in all conditions		pH = 2∼5 (HCl), 7 d	189

[a]Pure water systems are not considered, some are included in Table 2. Common name, metal, hydrophilic/hydrophobic property of the MOFs, linker, integrity of crystallinity and porosity, and the assessment conditions are provided where available. [b]Interior property, amphiphilic MOFs are noted as hydrophilic materials. [c]The integrity of crystallinity/porosity is in the (subjective) order of "well-retained" > "partial degradation/loss" > "significant degradation/loss" > "complete degradation/loss".

https://dx.doi.org/10.1021/acs.chemrev.9b00746
Chem. Rev. XXXX, XXX, XXX−XXX

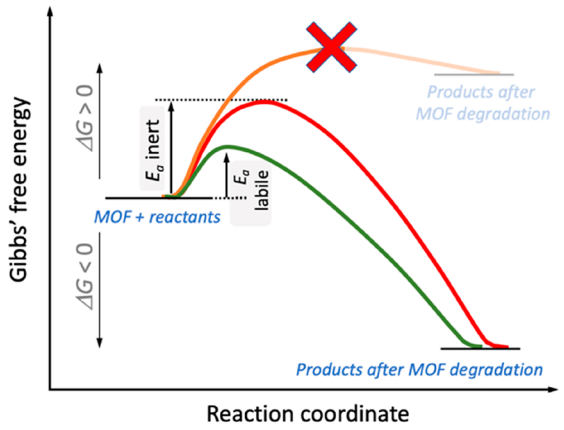

Figure 6. Reaction coordinate diagram illustrating the degradation of MOFs in a water system. The thermodynamic stability is predicted by the Gibbs' free energy (ΔG). The cross symbol on the topmost curve indicates that this route is unfeasible. The kinetic stability depends on the activation energy (E_a) required to reach the transition state. The figure is plotted referring to ref 8.

From the thermodynamic side, the strength of metal−linker bond is the decisive factor. Pearson's hard/soft acid/base (HSAB) principle[61] provides some guidelines on designing strong metal−linker bonds. The carboxylate-linkers can be regarded as hard bases, while high-valent metal ions (Cr(III), Fe(III), Al(III), Zr(IV), Ti(IV), etc.) are hard acids. Pioneering work on high-valent metal based MOFs was established by Férey and co-workers,[62−64] who developed MIL-53(Cr) (in 2002),[65] MIL-100(Cr),[66] and MIL-101-(Cr),[42] which are prototypical trivalent metal based MOFs. Subsequently, CAU MOFs (e.g., CAU-1(Al)[67] and CAU-10(Al)[68]) were reported. In 2008, Lillerud et al.[43] unveiled the earliest Zr(IV)-MOFs including the well-known UiO-66(Zr). Given by their outstanding stability, the field of Zr(IV)-MOFs has been flourishing in the last 10 years.[9,69] Examples like PCN-222(Zr),[70] NU-1000(Zr),[71] MIL-140(Zr),[72] MOF-801-(Zr),[73−76] and MOF-808(Zr)[75,77] have been extensively studied. The first Ti(IV)-carboxylate MOF MIL-125[78] was reported in 2009, one year after the discovery of Zr(IV)-MOFs, although Ti(IV)-phosphonate MOFs were reported earlier.[79,80]

Consistent with the HSAB principle, the metal−linker bond strengths with a given linker are negatively correlated to the ionic radius and positively correlated to charges of the metal cations. The effects of radius and charge can be combined into the concept of charge density. When the linkers and the coordination environment remain identical, high-valent metal ions with high charge densities can form stronger coordination bonds and thus a stronger framework. Recently, highly charged U(VI) was successfully employed to construct MOFs[81−83] that exhibited good water stability. Future improvements are expected, discovering robust MOFs via engineering metal-linker bonds with novel high-valent cations (e.g., V(V), Mo(VI), and W(VI)).

According to the HSAB principle, soft azolate linkers (such as imidazolates, pyrazolates, triazolates, and tetrazolates) and soft divalent metal ions (such as Zn(II), Cu(II), Ni(II), Co(II), and Mn(II)) can also yield stable MOFs. The most studied examples are the zeolitic imidazolate frameworks (ZIFs) reported by Yaghi et al.[41] Besides, Long and co-workers developed triazole-based Cu-BTTri[84] and pyrazolate-based MOFs $Ni_3(BTP)_2$,[85] while Zhou's group developed PCN-601(Ni).[59] Stable Co-azolate frameworks (e.g., MAF-X27(Co)-Cl[86] and $Co_2Cl_2(BTDD)$[87]) were unveiled by Chen's and Dincă's teams.

From a kinetic aspect, inert metal ions, hydrophobic and bulky linkers, high connectivity of secondary building units (SBUs), and penetration of frameworks could prevent the metal−linker coordination bonds from water attack.

A comparative study of the MIL-53(Al, Cr) and MIL-47(V) structures revealed that the relative chemical stability of these frameworks (Cr > Al > V) increases with the inertness of the metal ions instead of the average metal−oxygen bond strength.[88] The exceptionally high stability of MIL-53(Cr) originates from a large energy difference in the frontier orbitals of chromium and water,[8] which lowers the linker exchange rate.[47] As predicted by this concept, Rh-based MOFs[89] were reported with exceptionally high chemical stabilities.

The access of water to the coordination bonds can be blocked by appending linkers with hydrophobic fluorinated or alkyl functional groups. Trifluoromethyl groups were incorporated into UiO-67(Zr)[90] and $Mn_2L1(Mn)$[91] to improve their water stability. The robustness of ZIF-302(Zn),[92] MAF-69(Mo, W),[93] MAF-6(Zn),[94] and CALF-25(Ba)[95] in a water system was confirmed by decorating phenyl, ethyl, ethyl and ethyl ester groups on their linkers, respectively. Besides, many ZIFs such as ZIF-8(Zn)[96] and ZIF-412(Zn)[97] display strong hydrophobicity assigned to the combination of the small pore opening and the lack of polar centers. It is worth noting that incorporating hydrophobic linkers into MOFs will compromise their capability for water adsorption, especially negative for water adsorption at relative low pressures.

A prominent example of MOFs with high connectivity is UiO-66(Zr),[43] constructed from 12-connected $Zr_6O_4(OH)_4$ secondary building units (SBUs) stitched together by carboxylate linkers, forming a framework with cubic close packed structure. The high connectivity provides for steric shielding of the SBU and renders UiO-66(Zr) with high stability toward water. MIL-125(Ti)[78] is another example with 12-connected SBUs. MOFs built from infinite, rod-like SBUs, like MIL-53(Cr),[65] CAU-10(Al),[68] Al-fumarate,[98] CAU-23-(Al),[99] MIL-160(Al),[100] and MOF-303(Al),[74] are often water stable, relying on the steric shielding from the binding groups.

Framework interpenetration is beneficial for boosting water stability when steric hindrance against water is favorable. NENU-500(Zn)[101] has a 2-fold interpenetrated *ctn* topology which could stabilize its framework in water conditions. MOFs with similar interpenetrated structures were described with satisfying performance in water systems, including SIFSIX-2-Cu-i(Cu),[102] IISERP-MOF2(Ni),[103] BUT-66(Zr),[104] and Zn(1,3-BDP).[105]

3.1.3. In Saline Water. The metal ions or linkers from MOFs will be replaced if cations or anions with a stronger affinity are present in the aqueous solution, which is a principle used in obtaining mixed metal or linker MOFs.[106] To overcome the issues of decomposition, the metal ions and linkers for constructing MOFs should form stronger coordinating bonds than the competing species. The concept has been exemplified by UiO-66(Zr),[107] MIL-121(Al),[108] and PCN-602(Ni)[109] (Table 1). Both the crystalline structure and the porosity of UiO-66(Zr) were maintained after immersion in 0.2 wt % NaCl, $CaCl_2$, $MgCl_2$, and $AlCl_3$ solutions for 100 days, as the tetravalent Zr has a stronger affinity with carboxylate linkers than lower valent metal ions (Na^+, Ca^{2+},

https://dx.doi.org/10.1021/acs.chemrev.9b00746
Chem. Rev. XXXX, XXX, XXX−XXX

Table 2. Water Adsorption Properties of MOFs[a]

Material	Linker	α [-][b]	q_{max} [g g^{-1}][c]	$-\Delta_{ads}H$ [kJ mol^{-1}][d]	V_p [cm^3 g^{-1}][e]	Stability	REF
Cr-soc-MOF-1	TCPT	0.69	1.95	-	2.1	No loss in Δq over 100 ads. cycles / with significant hysteresis	194
MIL-101(Cr)	BDC	0.4	1.73	75-36	-	-	7, 196
MIL-101(Cr)	BDC	0.4	1.7 (303K)	80-45	1.7	No loss in Δq over 10 ads. cycles	210
MIL-101(Cr)	BDC	0.33	1.66	-	1.77	8% loss in q_{max} over 5 ads. cycles / with hysteresis	233
MIL-101(Cr)	BDC	0.51	1.5	-	-	No loss in q_{max} over 10 ads. cycles / with hysteresis	211
L_A^2-Zr_6^8-csq	L_A^2	0.77	1.5	-	2.0	89% loss in q_{max} over 5 ads. cycle	234
MIL-101(Cr)	BDC	0.44	1.43	-	-	-	235
MIL-101(Cr)	BDC	0.48	1.4	70-35	1.58	-	213
MIL-101(Cr)	BDC	0.47	1.35	-	-	No loss in q_{max} over 5 ads. cycles / with hysteresis	212
MIL-101(Cr)	BDC	0.45	1.3	-	1.6	With hysteresis	236
MIL-101(Cr)	BDC	0.46	1.3	52-40	1.6	-	197
L_B^2-Zr_6^8-csq	L_B^2	0.60	1.14	-	1.41	91% loss in q_{max} over 5 ads. cycle	234
NU-1000(Zr)	TBAPy	0.75	1.14	-	1.46	73% loss in q_{max} over 3 ads. cycles / with significant hysteresis	217
$Ni_8(L5)_6$	L5	0.7	1.12	-	1.25	No loss in q_{max} over 3 ads. cycles / with hysteresis	237
Zn_2Co_3(MFU-4l)	BTDD	0.40	1.11	-	-	Crystallinity was retained with slight loss in porosity after water ads. / with hysteresis	238
MIL-101(Cr)-NH_2	NH_2-BDC	0.42	1.05 (293K)	43	1.6	6.3% loss in S_{BET} after 40 ads. cycles	239
Zn_5(MFU-4l)	BTDD	0.65	1.04	-	-	Porosity and crystallinity were retained after water ads. / with hysteresis	238
MIL-101(Cr)-*p*COOH	BDC-*p*COOH	0.39	1.02	-	1.26	No loss in q_{max} over 3 ads. cycles	236
MIL-101(Cr)-pNH_2	(NH_2)-BDC	0.41	1 (293K)	43	1.3	6.3% loss in S_{BET} after 40 ads. cycles	239
MIL-101(Cr)	BDC	0.44	1	-	1.1	3.2% loss in q_{max} after 40 ads. cycles	240
NU-1000(Zr)	TBAPy	0.75	1.0	-	1.4	-	241
SALI-BA(Zr)	TBAPy, BA	0.82	1.0	-	1.21	55% loss in q_{max} over 3 ads. cycles / With significant hysteresis	217

https://dx.doi.org/10.1021/acs.chemrev.9b00746
Chem. Rev. XXXX, XXX, XXX−XXX

Table 2. continued

Material	Linker	α [-][b]	q_{max} [g g^{-1}][c]	$-\Delta_{ads}H$ [kJ mol^{-1}][d]	V_p [cm^3 g^{-1}][e]	Stability	REF
$Ni_8(L3)_6$	L3	0.4	0.99	-	1.21	No loss in q_{max} over 3 ads. cycles / with hysteresis	237
Co_2Cl_2(BTDD)	BTDD	0.29	0.97	55-41	-	6.3% loss in Δq over 30 ads. cycles	203
MIL-101(Cr)-SO_3H	SO_3H-BDC	0.28	0.95	60-35	0.94	-	213
MIL-101(Cr)-NH_2	NH_2-BDC	0.42	0.95	75-38	1.27	-	213
Zn_3Co_2(MFU-4l)	BTDD	0.44	0.95	-	-	Crystallinity was retained with slight loss in porosity after water ads. / with hysteresis	238
MIL-101(Cr)-NH_2	NH_2-BDC	0.35	0.9	-	0.97	-	202
$Ni_8(L4)_6$	L4	0.45	0.9	-	0.97	No loss in q_{max} over 3 ads. cycles / with hysteresis	237
MOF-74(Ni)-TPP	TPP	0.5	0.9	60-41	1.14	-	242
NU-1000(Zr)-SALI-1	CF_3-TBAPy	0.80	0.9	-	1	Structure was maintained after 1 ads. cycle	241
MIL-100(Fe)	BTC	0.38	0.87 (303K)	80-45	0.92	No loss in Δq over 10 ads. cycles	210
MIL-101(Cr)	BDC	0.47	0.87	-	1.22	-	202
$Ni_8(L5\text{-}(CF_3)_2)_6$	L5-$(CF_3)_2$	0.85	0.86	-	-	-	237
MOF-74(Ni)-BPP	BPP	0.23	0.81	62-44	0.88	-	242
MIL-101(Cr)-NH_2	BDC-NH_2	0.37	0.81	-	1.5	With hysteresis	236
MIL-100(Cr) (X=F)	BTC	0.3	0.88	48	0.93	5% loss in q_{max} after 2000 ads. cycles	214
MIL-100(Fe)	BTC	0.35	0.79	65-40	0.82	-	197
SALI-9'(Zr)	TBAPy, $C_5H_{19}COO$	0.81	0.78	-	0.87	13% loss in q_{max} over 20 ads. cycles	217
Ni_2Cl_2(BTDD)	BTDD	0.32	0.77	-	-	Crystallinity and porosity were retained after 1 ads. cycle	203
MIL-100(Fe)	BTC	0.29	0.75	90-50	0.85	6.4% loss in Δq over 40 ads. cycles	215
$ZnCo_4$(MFU-4l)	BTDD	0.30	0.75	-	-	Unstable after water ads. / with hysteresis	238
L_B^3-Zr_6^8-flu	L_B^3	0.44	0.74	-	0.90	No loss in q_{max} over 5 ads. cycles	234
L_A^2-Zr_6^{12}-shp	L_A^2	0.61	0.73	-	0.89	81% loss in q_{max} over 5 ads. cycles	234

https://dx.doi.org/10.1021/acs.chemrev.9b00746
Chem. Rev. XXXX, XXX, XXX−XXX

Table 2. continued

Material	Linker	α [-][b]	q_{max} [g g^{-1}][c]	$-\Delta_{ads}H$ [kJ mol^{-1}][d]	V_p [cm^3 g^{-1}][e]	Stability	REF
SALI-5(Zr)	TBAPy, $C_9F_{11}COO$	0.81	0.72	-	0.85	No loss in q_{max} over 20 ads. cycles	217
MIL-100(Fe)	BTC	0.35	0.72	-	0.96	No loss in q_{max} over 6 ads. cycles	221
HKUST-1(Cu)	BTC	0.5	0.72	-	-	Unstable when contacted with H_2O	243
L_A^3-Zr_6^8-flu	L_A^3	0.63	0.72	-	1.01	No loss in q_{max} over 5 ads. cycles	234
MIL-101(Cr)-*p*Mal	BDC-*p*Mal	0.40	0.71	-	0.89	With hysteresis	236
L_B^2-Zr_6^8-scu	L_B^2	0.60	0.71	-	0.96	94% loss in q_{max} over 5 ads. cycles	234
MIL-101(Cr)-*p*3SO$_3$H	BDC-*p*3SO$_3$H	0.36	0.70	-	0.71	With hysteresis	236
MIL-101(Cr)-NO_2	NO_2-BDC	0.45	0.7	-	0.95	-	202
Ni_8(L5-$(CH_3)_2)_6$	L5-$(CH_3)_2$	0.72	0.70	-	-	-	237
NU-1000(Zr)-SALI-3	$CF_3(CF_2)_2$-TBAPy	0.80	0.7	-	0.8	Structure was maintained after 1 ads. cycle	241
MIL-125(Ti)-NH_2	BDC-NH_2	0.23	0.68 (308K)	-	0.64	No loss in Δq over 10 ads. cycles	225
PIZOF-2(Zr)	$(OMe)_2$-PEDB	0.75	0.68	-	0.67	Unstable/with hysteresis	75
MIL-100(Cr)	BTC	0.36	0.67	-	-	15% loss in q_{max} after 1 ads. cycle, no loss in q_{max} over 2-5 ads. cycles	212
HKUST-1(Cu)	BTC	0.16	0.65	-	-	42% loss in q_{max} over 10 ads. cycles	211
MIL-101(Cr)-NO_2	NO_2-BDC	0.48	0.65	38-20	1.19	-	213
UiO-66(Zr)-$NH^{3+}Cl^-$	BDC-$NH^{3+}Cl^-$	0.16	0.64	-	0.35	7% loss in Δq over 10 ads. cycles	222
MOF-74(Mg)	$(OH)_2$-BDC	0.02	0.63	-	0.65	83% loss in S_{BET} after 1 cycle	244
Ni_8(L2)$_6$	L2	0.8	0.63	-	0.52	Mild degradation after H_2O ads.	237
Basolite™ C300 (HKUST-1)(Cu)	BTC	0.12	0.62	-	-	49% loss in q_{max} over 4 ads. cycles	245
HKUST-1(Cu)	BTC	0.11	0.61	-	0.61	-	246
MIL-100(Fe)	BTC	0.3	0.61	-	-	48% loss in q_{max} over 1-2 ads. cycles, no loss in q_{max} over 2-5 ads. cycles	212
MIL-100(Al)	BTC	0.33	0.61	-	-	14% loss in q_{max} over 1-2 ads. cycles, no loss in q_{max} over 2-5 ads. cycles	212

https://dx.doi.org/10.1021/acs.chemrev.9b00746
Chem. Rev. XXXX, XXX, XXX−XXX

Table 2. continued

Material	Linker	α [-][b]	q_{max} [g g^{-1}][c]	$-\Delta_{ads}H$ [kJ mol^{-1}][d]	V_p [cm^3 g^{-1}][e]	Stability	REF
MOF-74(Mg)	$(OH)_2$-BDC	0.05	0.60	-	0.53	49% loss in q_{max} over 1-2 ads. cycles, no loss in q_{max} over 2-5 ads. cycles/ strong H_2O ads	75
Basolite™ C300 (HKUST-1)(Cu)	BTC	0.16	0.6	46.6	-	-	235
MIL-100(Cr) (X=SO_4)	BTC	0.25	0.6	48-49	0.70	-	214
MIL-100(Cr) (X=Cl)	BTC	0.31	0.6	48-49	0.70	-	214
BIT-72(Al)	BDC-OH	0.47	0.6	-	0.59	-	133
MIL-101(Cr)-pNO_2	(NO_2)-BDC	0.48	0.6 (293K)	48	1.0	20% loss in S_{BET} after 40 ads. cycles	239
MIL-125(Ti)-$NH^{3+}Cl^-$	BDC-$NH^{3+}Cl^-$	0.19	0.59 (293K)	-	0.50	No loss in Δq over 10 ads. cycles	222
MOF-808(Zr)	BTC	0.3	0.59	-	0.84	Unstable/strong H_2O ads.	75
Ni-MOF-74	DOBDC	0.07	0.58	-	-	-	247
BUT-46W(Zr)	TPHB	0.33	0.58	-	0.71	5% loss in q_{max} over 2 ads. cycles	58
$Ni_{75}Zn_{25}$-MOF-74	DOBDC	0.13	0.57	-	-	-	247
HKUST-1(Cu)	BTC	0.19	0.55	16.3-9.8	0.73	-	248
UiO-66(Zr)	BDC	0.36	0.55	-	-	13% loss in q_{max} over 1-2 ads. cycles, no loss in q_{max} over 2-10 ads. cycles	211
CAU-1(Al)	NH_2-BDC	0.38	0.55		0.64	-	249
MIL-101(Cr)-*p*UR2	BDC-*p*UR2	0.50	0.55	-	0.64	With hysteresis	236
DUT-51(Zr)	DTTDC	0.63	0.55	-	1.08	23% reduction in q_{N2} after 12 h in liq.	250
MOF-74(Ni)	$(OH)_2$-BDC	0.02	0.54	-	-	Little loss in q_{CO2} after H_2O ads.	243
$Ni_{50}Zn_{50}$-MOF-74	DOBDC	0.09	0.54	-	-	5% loss in Δq after 8 ads. cycles	247
HKUST-1(Cu)	BTC	0.15	0.54	-	-	-	251
MIL-125(Ti)	BDC	0.35	0.54 (293K)	-	0.56	8% loss in Δq over 10 ads. cycles	222
BUT-46F(Zr)	TPHB, HCOO	0.42	0.54	-	0.71	No loss in q_{max} over 5 ads. cycles	58
MIL-125(Ti)-NH_2	BDC-NH_2	0.21	0.53 (293K)	-	0.53	3% loss in Δq over 10 ads. cycles	222

https://dx.doi.org/10.1021/acs.chemrev.9b00746
Chem. Rev. XXXX, XXX, XXX−XXX

Table 2. continued

Material	Linker	α [-][b]	q_{max} [g g^{-1}][c]	$-\Delta_{ads}H$ [kJ mol^{-1}][d]	V_p [cm^3 g^{-1}][e]	Stability	REF
Al-fumarate	FA	0.27	0.53	-	-	11% loss in Δq over 1-4 ads. cycles, no loss in Δq over 4-10 ads. cycles / With hysteresis	252
$Ni_{25}Zn_{75}$-MOF-74	DOBDC	0.12	0.52	-	-	-	247
MIL-125(Ti)-NH_2	NH_2-BDC	0.2	0.52	-	0.67	Stable in aqueous solution (48hrs)	253
DUT-4(Al)	2,6-NDC	0.65	0.52	-	0.79	Unstable during first ads. cycle	197
MOF-74(Ni)	$(OH)_2$-BDC	0.05	0.51	-	0.49	51% loss in q_{max} over 1-2 ads. cycle, no loss in q_{max} over 2-5 ads. cycles/ strong H_2O ads	75
MOF-841(Zr)	MTB	0.22	0.51	58-42	0.53	7% loss in q_{max} after 5 ads. cycles	75
BIT-73(Al)	BDC-CH_3	0.52	0.51	-	0.56	-	133
CAU-3(Al)	BDC	0.63	0.51	-	0.64	-	254
HKUST-1(Cu)	BTC	0.1	0.5 (293K)	-	0.83	26% loss in S_{BET} after 1 cycle	255
HKUST-1(Cu)	BTC	0.1	0.5	-	0.72	-	197
DUT-67(Zr)	TDC	0.22	0.50	-	0.60	Unstable/strong H_2O ads.	75
UiO-66(Zr)	BDC	0.25	0.5	45-20	0.77	-	227
MIL-100(Al)	BTC	0.28	0.5	80-42	0.8	6.6% loss in Δq after 40 ads. cycles	215
Al-fumarate	FA	0.30	0.50	-	-	No loss in q_{max} over 100 ads. cycles / with hysteresis	211
MIL-101(Cr)+POM	BDC	0.42	0.5	-	-	-	11
UiO-67(Zr)-BN	BNDCA	0.53	0.50	-	0.55	With hysteresis	151
CAU-3(Al)-NH_2	NH_2-BDC	0.67	0.50	-	0.53	-	254
$Zn_4O(bfbpdc)_3(bpy)_{0.5}$	bfbpdc/bpy	0.92	0.50	-	0.59	Stable upon exposure to water (vapour)	256
MOF-74(Co)	$(OH)_2$-BDC	0.05	0.49	-	0.46	37% loss in q_{max} over 1-2 ads. cycles, no loss in q_{max} over 2-5 ads. cycles/ strong H_2O ads.	75
Al-fumarate	FA	0.27	0.48	-	0.44	-	257
Y-shp-MOF-5	BTEB	0.63	0.48	-	0.63	9% loss in q_{max} after 1000 ads. cycles / with significant hysteresis	195

https://dx.doi.org/10.1021/acs.chemrev.9b00746
Chem. Rev. XXXX, XXX, XXX−XXX

Table 2. continued

Material	Linker	α [-][b]	q_{max} [g g^{-1}][c]	$-\Delta_{ads}H$ [kJ mol^{-1}][d]	V_p [cm^3 g^{-1}][e]	Stability	REF
MOF-74(Ni)	DOBDC	0.03	0.47	-	-	No loss in Δq over 50 ads. cycles	258
Ni-MOF-74	DOBDA	0.03	0.47	-	-	No loss in Δq over 10 ads. cycles	252
BUT-46A(Zr)	TPHB, CH_3COO	0.47	0.47	-	0.69	No loss in q_{max} over 5 ads. cycles	58
MOF-74(Ni)	DOBDC	0.05	0.46	62-51	0.49	-	242
Zn-MOF-74	DOBDC	0.13	0.46	-	-	-	247
BIT-74(Al)	BDC-$(CH_3)_2$	0.39	0.46	-	0.51	-	133
BUT-46B(Zr)	TPHB, PhCOO, HCOO	0.53	0.46	-	0.65	No loss in q_{max} over 5 ads. cycles	58
MOF-303(Al)	PDC	0.13	0.45	50-40	0.54	No loss in q_{max} over 5 ads. cycles	74
MOF-303(Al)	PDC	0.13	0.45	55.4-40.9 (52 aver.)	0.58	-	17
UiO-66(Zr)-NH_2	NH_2-BDC	0.15	0.45	120-60	0.70	~38% loss in q_{max} after 40 ads. cycles	227
MIL-125(Ti)-NH_2	NH_2-BDC	0.2	0.45	-	0.51	-	202
UiO-66(Zr)	BDC	0.25	0.45	-	0.52	2% loss in S_{BET} after 1 ads. cycle	244
UiO-66(Zr)	BDC	0.26	0.45	-	0.55	-	259
Al-fumarate	FA	0.27	0.45	50-42	0.48	No loss in Δq over 4500 ads. cycles	199
MIL-53(Al)-SO_3H	SO_3H-BDC	0.45	0.45	-	-	Stable over 3 ads. cycles	260
Zn(NDI-H)	NDI-H	0.45	0.45 (293K)	-	0.65	Survives liq. water (24 hr.)	261
MIL-101(Cr)-NO_2	NO_2-BDC	0.5	0.45 (293K)	46	0.6	25% loss in S_{BET} after 40 ads. cycles	239
NU-1000(Zr)-SALI-7	$CF_3(CF_2)_6$-TBAPy	0.85	0.45	-	0.6	Structure was maintained after 1 ads. cycle	241
Zn_4O(dmcapz)$_3$	dmcapz	0.85	0.45	-	0.43	8% in q_{max} after 1 ads. cycle	262
Ni_8(L1)$_6$	L1	0.9	0.45	-	0.52	Stable over 3 ads. cycles	237
MIP-200(Zr)	MDIP	0.18	0.45 (303K)	70-45	0.40	6% loss in Δq over 1-10 ads. cycles and no loss in Δq over 10-40 ads. Cycles	123
SALI-9(Zr)	TBAPy, FDA	0.82	0.44	-	0.63	No loss in q_{max} over 20 ads. cycles	217
Cr_3(BTC)$_2$	BTC	0.17	0.44	-	-	Gradual loss in porosity after exposing to water vapour atmosphere	131

https://dx.doi.org/10.1021/acs.chemrev.9b00746
Chem. Rev. XXXX, XXX, XXX−XXX

Table 2. continued

Material	Linker	α [-][b]	q_{max} [g g^{-1}][c]	$-\Delta_{ads}H$ [kJ mol^{-1}][d]	V_p [cm^3 g^{-1}][e]	Stability	REF
MIL-53(Al)-TDC	TDC	0.37	0.44	46.8	0.48	3.7% loss in q_{max} after 20 ads. cycles / with slight hysteresis	263
Co_2Cl_2BBTA	BBTA	0.02	0.43	-	-	Significant loss of porosity after 1 H_2O ads. cycle	264
Al-fumarate	FA	0.26	0.43	50-49	0.43	-	265
BUT-155(Cu)	TDHB	0.26	0.43	-	0.82	11% loss in q_{max} over 1-3 ads. cycles, no loss in q_{max} over 3-5 ads. cycles / With hysteresis	57
DMOF-TM2(Zn)	TMBDC/DABCO	0.26	0.43	-	0.51	Stable over 3 ads. cycles	266
MAF-7(Zn)	MTZ	0.27	0.43	-	0.65	-	267
UiO-66(Zr)	BDC	0.34	0.43	-	0.49	8% loss in q_{max} over 1-2 ads. cycles, no loss in q_{max} over 2-5 ads. cycles/ with hysteresis	75
UiO-66(Zr)	BDC	0.35	0.43	-	-	With hysteresis	212
Ni-MOF	BDP	0.35	0.43	-	0.71	-	268
MIL-101(Al)-NH_2	NH_2-BDC	0.35	0.43	-	1.67	Rapidly degrades upon exposure to vapour	269
MIL-100(Cr)-EG	BTC	0.35	0.43 (293K)	-	0.47	-	270
MAF-4$_{.23}$-7$_{.77}$	mIm/mTz	0.37	0.43	-	0.64	-	267
CAU-1(Al)	BDC-NH_2	0.38	0.43	-	-	-	133
UiO-66(Zr)	BDC	0.46	0.43	-	-	-	271
MAF-4$_{.49}$-7$_{.51}$	mIm/mTz	0.62	0.43	-	0.65	-	267
MIL-125(Ti)-NH_2	BDC-NH_2	-	>0.42	54.9-49.7	0.56	7% loss in Δq over 1-2 ads. cycles, no loss in Δq over 2-10 ads. cycles	226
Al-Fumarate	FA	0.27	0.42 (303K)	51.3-40.7	0.57	-	17
Ni_2Cl_2BBTA	BBTA	0.03	0.42 (296K)	56-43	-	8% loss in Δq over 9 ads. cycles	264
HKUST-1(Cu)	BTC	0.1	0.42	50.7	-	-	235
UiO-66(Zr)-2,5-$(OMe)_2$	$(OMe)_2$-BDC	0.2	0.42	-	0.38	No loss in crystallinity after ads.	259
CAU-23(Al)	TDC	0.27	0.42	48.2	0.48	No loss in Δq over 5000 ads. cycles	99
MIL-100(Cr)-DEG	BTC	0.35	0.42 (293K)	-	0.50	-	270

https://dx.doi.org/10.1021/acs.chemrev.9b00746
Chem. Rev. XXXX, XXX, XXX−XXX

Table 2. continued

Material	Linker	α [-][b]	q_{max} [g g^{-1}][c]	$-\Delta_{ads}H$ [kJ mol^{-1}][d]	V_p [cm^3 g^{-1}][e]	Stability	REF
DMOF-TM(Cu)	TMBDC/DABCO	0.55	0.42	-	0.46	4.9% loss in S_{BET} after 1 cycle	272
MIL-53(Al)-(OH)$_2$	(OH)$_2$-BDC	0.65	0.42	-	0.07	-	273
MOF-801(Zr)	FA	0.10	0.41	55[274]	-	14% loss in Δq over 1-2 ads. cycles, no loss in Δq over 2-80 ads. cycles	73
MOF-303(Al) (Scaled-up)	PDC	0.17	0.41	50-41	0.37	No loss in Δq over 150 ads. cycles / with hysteresis	74
DUT-67(Zr)	TDC	0.35	0.41	-	0.44	Survives HCl sol. (1 mol L^{-1}), 3 days	121
CAU-6(Al)	NH$_2$-BDC	0.09	0.40	-	0.25	-	275
MFU-4(Zn)	BBTA	0.25	0.4	-	-	No loss in q_{max} after 1 ads. cycle	276
DMOF-TM(Co)	TMBDC/DABCO	0.35	0.40	-	0.49	3.4% loss in S_{BET} after 1 cycle	272
MIL-100(Cr)	BTC	0.36	0.4 (293K)	-	0.77	-	270
MIL-101(Cr)	BDC	0.45	0.4	-	-	-	11
DMOF-TM(Ni)	TMBDC/DABCO	0.45	0.40	-	0.48	2.5% loss in S_{BET} after 1 cycle	272
CAU-1(Al)-NHCH$_3$	NHCH$_3$-BDC	0.48	0.40		0.53	-	249
MIL-53(Al)-OH	OH-BDC	0.75	0.40	-	-	-	198
MAF-4$_{.76}$-7$_{.24}$	mIm/mTz	0.85	0.4	-	0.64	-	267
MOF-801(Zr)	FA	0.14	0.39	55	0.34	No loss in q_{max} after 5 water harvesting cycles	76
Mn$_2$Cl$_2$(BTDD)	BTDD	0.27	0.39	-	-	Crystallinity and porosity were completely lost after 1 ads. cycle	203
Basolite™ F300 (Fe)	BTC	0.28	0.39	-	-	-	245
Mn$_2$(Gd-H-DOTA-4AmP)(H$_2$O)$_7$	Gd-H-DOTA-4AmP	0.53	0.39	-	-	Switched between closed and open pores	277
MIL-160(Al)	FDC	0.09	0.38 (303K)	64-43	0.40	No loss in Δq over 10 ads. cycles	100
CAU-10(Al)-H	1,3-BDC	0.18	0.38	54[278]	0.28	Survives liq. water (18 hr.)	68
L$_C^2$-Zr$_6^{12}$-fcu	L$_C^2$	0.36	0.38	-	0.61	9% loss in q_{max} over 5 ads. cycles	234
UiO-66(Zr)	BDC	0.41	0.38	-	0.37	4% loss in q_{max} over 1-2 ads. cycles, no loss in q_{max} over 2-6 ads. cycles/ with hysteresis	221
L$_A^1$-Zr$_6^8$-csq	L$_A^1$	0.60	0.38	-	2.18	87% loss in q_{max} over 2 ads. cycles	234

https://dx.doi.org/10.1021/acs.chemrev.9b00746
Chem. Rev. XXXX, XXX, XXX−XXX

Table 2. continued

Material	Linker	α [-][b]	q_{max} [g g^{-1}][c]	$-\Delta_{ads}H$ [kJ mol^{-1}][d]	V_p [cm^3 g^{-1}][e]	Stability	REF
[Cd(L'1)(Cl)](H$_2$O)	L'1	0.9	0.38	-	-	-	279
CAU-10(Al)-H	1,3-BDC	0.16	0.37	53.5	-	No loss in Δq over 9 ads. cycles	200
CAU-10(Al)-H	1,3-BDC	0.17	0.37	49	0.28	Crystallinity and porosity were retained after boiling water treatment for 1d	100
CAU-10(Al)-H	1,3-BDC	0.18	0.37	62-59	-	Crystallinity was well retained after 20 ads. cycles	280
UiO-66(Zr)-NO$_2$	NO$_2$-BDC	0.18	0.37	-	0.42	No loss in crystallinity after ads.	259
MIL-125(Ti)-NH$_2$	BDC-NH$_2$	0.22	0.37 (308K)	-	-	4% loss in S_{BET} after 1 ads. cycle	161
UiO-66(Zr)-NH$_2$	BDC-NH$_2$	0.22	0.37	-	0.39	14% loss in Δq over 10 ads. cycles	222
Mg-CUK-1	PDC	0.25	0.37 (303K)	38-48	0.28	No loss in Δq over 50 ads. cycles	205
UiO-66(Zr)	BDC	0.31	0.37 (303K)	-	0.35	No loss in q_{max} over 5 ads. cycles	201
UiO-66(Zr)	BDC	0.31	0.37	-	0.35	No loss in q_{max} over 2 ads. cycles	201
CAU-10(Al)-H	1,3-BDC	0.32	0.37	56-50	0.26	No loss in Δq over 10000 ads. cycles	219
UiO-66(Zr)-NO$_2$	BDC-NO$_2$	0.35	0.37	-	0.43	No loss in q_{max} over 2 ads. cycles / with hysteresis	281
MIL-100(Cr)-EN	BTC	0.35	0.37 (293K)	-	0.42	~2% loss in q_{max} after 20 ads. cycles	270
UiO-66(Zr)	BDC	0.35	0.37	-	0.52	-	282
MOF-801(Zr)	FA	0.09	0.36	62-47	0.45	Stable over 5 ads. cycles	75
UiO-66(Zr)-NH$_2$	NH$_2$-BDC	0.15	0.36	-	0.35	-	202
UiO-66(Zr)-NH$_2$	NH$_2$-BDC	0.16	0.36	-	0.57	No loss in S_{BET} after 1 ads. cycle	244
MIL-125(Ti)	BDC	0.25	0.36	-	0.47	-	202
UiO-66(Zr)	BDC	0.33	0.36	-	0.38	7% loss in Δq over 10 ads. cycles	222
UiO-66(Zr)	BDC	0.33	0.36	-	0.41	-	202
MIL-101(Al)-URPh	URPh-BDC	0.40	0.36	-	0.83	Slowly degrades upon exposure to vapour	269
MIL-53(Al)-(OH)$_{.68}$(NH$_2$)$_{.32}$	NH$_2$-/OH-BDC	0.80	0.36	-	-	-	283
CAU-10(Al)-H	1,3-BDC	0.18	0.35	54[278]	0.27	Stable over 700 ads. cycles	284

https://dx.doi.org/10.1021/acs.chemrev.9b00746
Chem. Rev. XXXX, XXX, XXX−XXX

Table 2. continued

Material	Linker	α [-][b]	q_{max} [g g^{-1}][c]	$-\Delta_{ads}H$ [kJ mol^{-1}][d]	V_p [cm^3 g^{-1}][e]	Stability	REF
MIL-125(Ti)-NH$_2$	NH$_2$-BDC	0.19	0.35	95-45	0.45	17% loss in q_{max} and no loss in Δq after 40 ads. cycles	227
CAU-1 (Al)	BDC-NH$_2$	0.46	0.35	-	0.61	-	278
NU-1000(Zr)-SALI-9	CF$_3$(CF$_2$)$_8$-TBAPy	0.85	0.35	-	0.6	Structure was maintained after 1 ads. cycle	241
Cu$_2$Cl$_2$BBTA	BBTA	0.03	0.34	-	-	Complete loss of porosity after 1 H$_2$O ads. cycle	264
MOF-806(Zr)	(OH)$_2$-BPDC	0.1	0.34	-	0.85	Unstable/strong H$_2$O ads.	75
UiO-66(Zr)-NH$_2$	NH$_2$-BDC	0.16	0.34	-	0.52	-	259
MIL-160(Al)	FDC	>0.30	>0.34	56	0.46	Crystallinity and porosity were retained after 10 ads. cycles	285
DUT-68(Zr)	TDC	0.40	0.34	-	0.41	Survives HCl sol. (1 mol L^{-1}), 3 days	121
L$_A^1$-Zr$_6^{12}$-shp	L$_A^1$	0.59	0.34	-	0.94	82% loss in q_{max} over 2 ads. cycles	234
MOF-801(Zr)	FA	0.16	0.33	53-43	0.28	With hysteresis	74
MOF-805(Zr)	(OH)$_2$-NDC	0.31	0.33	-	0.48	Unstable/strong H$_2$O ads.	75
MIL-100(Cr)-TEG	BTC	0.35	0.33 (293K)	-	0.53	-	270
MIL-68(In)-NH$_2$	NH$_2$-BDC	0.44	0.33	-	0.30	-	202
UiO-66D(Zr)	ABDC	0.7	0.33	-	-	-	271
MOS-1(Co)	IDC, PDA	0.1	0.32	-	-	-	173
UiO-66(Zr)-(OH)$_2$	BDC-(OH)$_2$	0.12	0.32 (273K)	-	0.56	8% loss in Δq over 10 ads. cycles	150
Ni-CUK-1	PDC	0.13	0.32 (303K)	38-62	0.26	No loss in Δq over 10 ads. cycles	205
CAU-1(Al)-(OH)$_2$	BDC-(OH)$_2$	0.35	0.32	-	0.50	-	278
ZIF-90(Zn)	Ica	0.35	0.32	-	0.49	-	286
L$_C^1$-Zr$_6^{12}$-fcu	L$_C^1$	0.48	0.32	-	0.92	79% loss in q_{max} over 5 ads. cycles	234
HKUST-1(Cu)	BTC	0.15	0.31	-	-	Gradual loss in porosity after exposing to water vapour atmosphere	131
MIL-125(Ti)-NHMe	BDC-NHMe	0.27	0.31 (308K)	-	-	4% loss in BET after 1 ads. cycle	161
UiO-66(Zr)-CH$_3$	CH$_3$-BDC	0.29	0.31	-	0.51	Stable after 1 ads. cycle	282

https://dx.doi.org/10.1021/acs.chemrev.9b00746
Chem. Rev. XXXX, XXX, XXX−XXX

Table 2. continued

Material	Linker	α [-][b]	q_{max} [g g^{-1}][c]	$-\Delta_{ads}H$ [kJ mol^{-1}][d]	V_p [cm^3 g^{-1}][e]	Stability	REF
UiO-66(Hf)-(OH)$_2$	BDC-(OH)$_2$	0.05	0.3 (273K)	-	0.4	-	150
Co-CUK-1	PDC	0.12	0.30 (303K)	45-60	0.26	No loss in Δq over 50 ads. cycles	205
CAU-10(Al)-H	1,3-BDC	0.16	0.30	-	0.26	No loss in q_{max} over 5 ads. cycles	75
CAU-10(Al)-OH	1,3-BDC-OH	0.16	0.30	-	-	Survives liq. water (18 hr.)	68
[La$_3$L$_4$(H$_2$O)6]-Cl	TAPP	0.25	0.3	-	-	15% loss in q_{max} over 1-2 ads. cycles, no loss in q_{max} over 2-3 ads. cycles / with hysteresis	287
Zn(NDI-SOEt)	NDI-SOEt	0.26	0.30 (293K)	-	0.38	-	261
Basolite™ F300	-	0.31	0.3	47.6	-	-	235
MIL-125(Ti)	BDC	0.35	0.30	-	0.60	Unstable during H$_2$O adsorption	253
MIL-68(In)	BDC	0.58	0.30	-	0.42	-	202
Cu$_2$(pzdc)$_2$bpe	Pzdc/bpe	0.08	0.29 (303K)	-	-	-	288
CAU-10(Al)-H	1,3-BDC	0.16	0.29	54	0.25	No loss of q_{max} over 5 ads. cycles	278
DUT-67(Hf)	TDC	0.35	0.29	-	0.33	Survives HCl sol. (1 mol L^{-1}), 3 days	121
DUT-68(Hf)	TDC	0.38	0.29	-	0.34	Survives HCl sol. (1 mol L^{-1}), 3 days	121
UiO-67(Zr)	BPDC	0.5	0.29	-	-	> 99% loss in S_{BET} after 1 cycle	147
ISE-1(Ni)	BTC/btre	-	0.28	-	0.51	No loss in Δq over 10 ads. cycles	289
UiO-66(Zr)-CF$_3$	BDC-CF$_3$	0.32	0.28	-	0.36	-	271
UiO-66(Zr)-(CH$_3$)$_2$	BDC-(CH$_3$)$_2$	0.38	0.28	-	0.35	after a long term storage (>2 years) under ambient air	271
UiO-66D(Zr)-(CF$_3$)$_2$	ABDC-(CF$_3$)$_2$	0.87	0.28	-	0.88	Structure collapses after water adsorption	271
FeFFIVE-1-Ni	Pyrazine	0.02	0.27 (308K)	64.7	0.13	Crystallinity was retained at 95% RH	204
MOF-801(Zr) (Scaled-up)	FA	0.09	0.27	-	0.21	With hysteresis	74
UiO-66(Zr)-(COOH)$_2$	(COOH)$_2$-BDC	0.15	0.27 (303K)	-	0.21	No loss in q_{max} after 2 ads. cycles	290
UiO-66(Zr)-NH$_2$	BDC-NH$_2$	0.24	0.27	-	-	-	212
DMOF(Zn)-A	ADC/DABCO	0.30	0.27	-	0.33	4% loss in S_{BET} after 90% RH	291

https://dx.doi.org/10.1021/acs.chemrev.9b00746
Chem. Rev. XXXX, XXX, XXX−XXX

Table 2. continued

Material	Linker	α [-][b]	q_{max} [g g^{-1}][c]	$-\Delta_{ads}H$ [kJ mol^{-1}][d]	V_p [cm^3 g^{-1}][e]	Stability	REF
DMOF-TM1(Zn)	TMBDC/BDC/ DABCO	0.44	0.27	-	0.53	30% loss in S_{BET} after 90% RH	291
Cd(BTTB)	BTTB	0.50	0.27	-	0.19	100% loss in S_{BET} after 90% RH	292
Zn(BTTB)(BPY)	BTTB/BPY	0.70	0.27	-	0.38	no loss in S_{BET} after 90% RH	292
UiO-66(Zr)-1,4-Napthyl	1,4-NDC	0.25	0.26	-	0.40	No loss in crystallinity after ads.	259
DUT-69(Zr)	TDC	0.30	0.26	-	0.31	Survives HCl sol. (1 mol L^{-1}), 1 day	121
SIFSIX-2-Cu-i	BPA	0.51	0.26	-	-	Crystallinity and porosity were retained after 14 days exposure to 75% RH	293
Lc^3-Zr_6^8-bcu	Lc^3	0.55	0.26	-	0.54	9% loss in q_{max} after 4 ads. cycles	234
UiO-66(Zr)-CH_3	BDC-CH3	0.22	0.25	-	0.32	after a long term storage (>2 years) under ambient air	271
CAU-1(Al)-$NHCOCH_3$	$NHCOCH_3$-BDC	0.26	0.25	-	0.30	-	249
Zn(NDI-SO_2Et)	NDI-SO_2Et	0.35	0.25 (293K)	-	0.31	-	261
Zn(NDI-SEt)	NDI-SEt	0.41	0.25 (293K)	-	0.39	-	261
Co(BTTB)(AZPY)	BTTB/AZPY	0.55	0.25	-	0.39	56% loss in S_{BET} after 90% RH	292
[Dy(ox)(Bpybc)(H_2O)]	Ox/ Bpybc	0.60	0.25	-	-	-	294
UiO-66(Zr)-C_2F_5	BDC-C_2F_5	0.61	0.25	-	0.26	after a long term storage (>2 years) under ambient air	271
ValZnOAc	Val	0.78	0.25	-	-	-	295
MUF-77(Zn)-ethyl	HETT, BPDC, BDC	0.81	0.25	-	1.55	Structure was retained after 20 ads. cycles between 10% and 70% RH / with significant hysteresis	296
AlaZnOAc	Ala	0.88	0.25	-	-	-	295
AlFFIVE-1-Ni	Pyrazine	0.02	0.24 (308K)	63	0.1	No loss in Δq over 14 ads. cycles	204
DUT-52(Zr)	2,6-NDC	0.35	0.24	-	0.54	-	297
[PbL_2]·2DMF·6H_2O	L	0.8	0.24	-	-	-	298
(H_2dab)[$Zn_2(ox)_3$]	ox/dab	0.70	0.23	-	-	-	299
MIL-91(Ti)	PMPA	0.01	0.23	-	0.16	No loss in q_{max} over 3 ads. cycles	300

https://dx.doi.org/10.1021/acs.chemrev.9b00746
Chem. Rev. XXXX, XXX, XXX−XXX

Table 2. continued

Material	Linker	α [-][b]	q_{max} [g g^{-1}][c]	$-\Delta_{ads}H$ [kJ mol^{-1}][d]	V_p [cm^3 g^{-1}][e]	Stability	REF
CAU-10(Al)-OH	1,3-BDC-OH	0.15	0.23	-	-	-	278
CAU-10(Al)-NH_2	1,3-BDC-NH_2	0.16	0.23	-	-	Survives liq. water (18 hr.)	68
UiO-67(Zr)-BIPY	BIPY	0.2	0.23	-	-	> 99% loss in S_{BET} after 1 cycle	147
MOF-804(Zr)	$(OH)_2$-BDC	0.4	0.23	-	0.46	Unstable/strong H_2O ads.	75
UiO-66(Zr)-$(CH_3)_2$	$(CH_3)_2$-BDC	0.43	0.23	-	0.40	Stable after 1 ads. cycle	301
MIL-53(Al)-F_2	F_2-BDC	0.70	0.23	-	0.16	-	302
MUF-77(Zn)-butyl	HBTT, BPDC, BDC	0.83	0.23	-	1.21	With significant hysteresis	296
MIL-53(Al)-$(OH)_{0.53}(NH_2)_{.47}$	NH_2-/OH-BDC	0.88	0.23	-	-	-	283
$[Co_4L_3(\mu 3\text{-}OH)(H_2O)_3](SO_4)_{0.5}$	TAPP	0.09	0.22	-	-	9% loss in q_{max} over 1-2 ads. cycles, no loss in q_{max} over 2-3 ads. cycles	287
Cu_2(dmcapz)$_2$	dmcapz	0.33	0.22	-	0.23	Reversible structural change upon ads.	303
DUT-53(Hf)	2,6-NDC	0.38	0.22	-	0.31	-	297
Zn(BTTB)	BTTB	0.70	0.22	-	0.25	100% loss in S_{BET} after 90% RH	292
Zn(BTTB)(DMBPY)	BTTB/DMBPY	0.85	0.22	-	0.27	1.2% loss in S_{BET} after 90% RH	272
Zn_3L_2	TCBPTA	0.48	0.21	-	-	With hysteresis	304
Zn-Trimesate	BTC	0.10	0.2	-	-	20% loss of q_{max} over 1-20 ads. cycles, and no loss of q_{max} over 20-40 ads. cycles	305
Cu_2(pmpmd)$_2$(CH_3OH)$_4$(opd)$_2$	pmpmd/opd	0.15	0.20	-	-	-	306
DUT-69(Hf)	TDC	0.28	0.20	-	0.22	-	121
IPM-MOF-201(Ni)	IPA	0.44	0.2	-	-	The uptake of methyl orange from aqueous solution was retained over 3 ads. cycles / with hysteresis	60
[Co(DPE)]·0.5DPE	DPE	0.45	0.20	-	0.14	-	307
Basolite™ A100 (MIL-53)(Al)	BDC	0.48	0.2	52.1	-	-	235
Zn(BTTB)(AZPY)	BTTB/AZPY	0.55	0.20	-	0.36	43% loss in S_{BET} after 90% RH	292
MUF-77(Zn)-methyl	HMTT, BPDC, BDC	0.72	0.2	-	1.85	With significant hysteresis	296

https://dx.doi.org/10.1021/acs.chemrev.9b00746
Chem. Rev. XXXX, XXX, XXX−XXX

Table 2. continued

Material	Linker	α [-][b]	q_{max} [g g^{-1}][c]	$-\Delta_{ads}H$ [kJ mol^{-1}][d]	V_p [cm^3 g^{-1}][e]	Stability	REF
Co(BTTB)(DMBPY)	BTTB/DMBPY	0.85	0.20	-	0.29	0.2% loss in S_{BET} after 90% RH	272
Cd_2(sdb)$_2$(pcih)$_2$	SDB, PCIH	0.22	0.19	48.9	0.22	No loss in q_{max} over 35 ads. cycles	175
UiO-66(Zr)-$(CF_3)_2$	BDC-$(CF_3)_2$	0.35	0.19	-	0.30	-	271
MIL-53(Ga)-NH_2	NH_2-BDC	0.02	0.18	-	-	-	202
CuEBTC	C_2H_5-BTC	0.15	0.18 (293K)	-	0.65	Loss of crystallinity after 90% RH	255
CAU-10(Al)-NH_2	1,3-BDC-NH_2	0.16	0.18	-	0.13	-	278
CuMBTC	CH_3-BTC	0.30	0.18 (293K)	-	0.79	Loss of crystallinity after 90% RH	255
CAU-8(Al)	BPDC	0.4	0.18	-	0.25	-	278
CAU-10(Al)-CH_3	1,3-BDC-CH_3	0.45	0.18	-	-	Survives liq. water (18 hr.)	68
UiO-67(Zr)	BPDC	0.6	0.18	75-50	0.97	-	227
MIL-47(V)-F	F-BDC	0.60	0.18	-	0.36	50% loss in hexane capacity after 1 ads. cycle	308
L_A^1-Zr_6^8-flu	L_A^1	0.70	0.18	-	1.31	80% loss in q_{max} over 2 ads. cycles	234
MIL-47(V)-F_2	F_2-BDC	0.70	0.18	-	0.34	-	302
Cu_2(pzdc)$_2$bpy	Pzdc/bpy	0.09	0.17 (303K)	-	-	-	288
UiO-66(Zr)-$(OH)_2$	BDC-$(OH)_2$	0.17	0.17	-	-	-	212
CAU-10(Al)-NO_2	1,3-BDC-NO_2	0.32	0.17	-	0.21	Survives liq. water (18 h)	68
L_B^1-Zr_6^8-flu	L_B^1	0.59	0.17	-	0.94	83% loss in q_{max} over 2 ads. cycles	234
STAM-17(Cu)-OEt	MPA	0.04	0.16	-	-	No loss in Δq over 8 ads. cycles	309
MIL-53(Fe)-$(COOH)_2$	$(COOH)_2$-BDC	0.05	0.16	-	-	-	198
UiO-66(Zr)-OH	BDC-OH	0.16	0.16	-	-	-	212
Zn_2(bptc)	Bptc	0.18	0.16	-	-	-	310
CAU-13(Al)	CDC	0.22	0.16	-	0.15	-	311
Al(OH)-(1,4-NDC)	1,4-NDC	0.45	0.16	-	0.22	-	312

https://dx.doi.org/10.1021/acs.chemrev.9b00746
Chem. Rev. XXXX, XXX, XXX−XXX

Table 2. continued

Material	Linker	α [-][b]	q_{max} [g g^{-1}][c]	$-\Delta_{ads}H$ [kJ mol^{-1}][d]	V_p [cm^3 g^{-1}][e]	Stability	REF
AlaZnCl	ALa	0.45	0.16	-	-	Stable for 6 months in H_2O	313
MUF-7a(Zn)	BTB, BPDC, BDC	0.5	0.16	-	2.16	With significant hysteresis	296
CoNIm	NIm	0.55	0.16	-	-	-	314
SIFSIX-3-Ni	Pyrazine	-	0.15	-	-	Crystallinity was retained at 75% RH	293
SIFSIX-14-Cu-i	BPDA	-	0.15	-	-	Porosity was completely lost after exposure to 75% RH	293
[Cd(L7)(DMF)]	L7	0.1	0.15	-	-	Stable in boiling water, 1 day	315
MOS-2(Co)	IDC, PHEN	0.15	0.15	-	-	-	173
ThrZnOAc	Thr	0.25	0.15	-	-	-	295
Zn(NO_2-BDC)(dmbpy)$_{0.5}$	BDC-NO_2, DMBPY	0.47	0.15	-	-	No loss in q_{max} over 3 ads. cycles / With slight hysteresis	183
SIFSIX-1-Cu	BPD	-	0.14	-	-	Porosity was completely lost after exposure to 75% RH	293
MIL-53(Al)-Cl	Cl-BDC	0.18	0.14	-	0.32	-	273
SIM-1(Zn)	mImca	0.27	0.14	-	0.30	-	202
DMOF(Zn)-NO_2	NO_2-BDC/DABCO	0.40	0.14	-	0.53	97% loss in S_{BET} after 90% RH	291
ValZnCl	Val	0.8	0.14	-	-	Stable for 6 months in H_2O	313
MUF-77(Zn)-hexyl	HHTT, BPDC, BDC	0.9	0.14	-	1.0	With significant hysteresis	296
MOS-3(Co)	IDC, BPY	0.15	0.13	-	-	-	173
Cd_3L_2	TCBPTA	0.29	0.13	-	-	With hysteresis	304
kag-MOF-1(Zn)	HCN_4	0.07	0.12	60	0.12	Survive in boiling water for 24 h	168
MIL-53(Al)-NO_2	NO_2-BDC	0.10	0.12	-	0.34	-	273
Cu_2(pzdc)$_2$pyz	Pzdc/pyz	0.10	0.12 (303K)	-	-	-	288
([Ni(L6)$_2$]·4H_2O)$_n$	L6	0.11	0.12	-	-	Stable after 1 ads. cycle	316
MIL-125(Ti)-NHCyp	BDC-NHCyp	0.33	0.12 (308K)	-	-	1% loss in BET after 5 ads. cycles	161
1DUT-84(Zr)	2,6-NDC	0.38	0.12	-	0.27	-	297

https://dx.doi.org/10.1021/acs.chemrev.9b00746
Chem. Rev. XXXX, XXX, XXX−XXX

Table 2. continued

Material	Linker	α [-][b]	q_{max} [g g^{-1}][c]	$-\Delta_{ads}H$ [kJ mol^{-1}][d]	V_p [cm^3 g^{-1}][e]	Stability	REF
UiO-66(Zr)-(C_2H_5)$_2$	BDC-(C2H5)2	0.48	0.12	-	0.16	after a long term storage (>2 years) under ambient air	271
MIL-53(Al)-(OH)$_{0.34}$(NH_2)$_{0.66}$	NH_2-/OH-BDC	0.02	0.11	-	-	-	283
[Cd(L'3)(Cl)](H_2O)$_2$	L'3	0.15	0.11	-	-	-	279
JUC-110(Cd)	THIPC	0.2	0.11	-	-	Survives boiling water (10 days)	317
MIL-53(Al)-CH_3	CH_3-BDC	0.25	0.11	-	0.32	-	273
DMOF(Zn)-OH	OH-BDC/DABCO	0.30	0.11	-	0.54	100% loss in S_{BET} after 90% RH	291
MIL-53(Al)-Br	Br-BDC	0.50	0.11	-	0.14	-	273
PCP-1(La)	BTN	0.59	0.11	-	0.12	CO_2 uptake was maintained after treated with water	142
MUF-77(Zn)-octyl	HOTT, BPDC, BDC	0.85	0.11	-	0.65	With significant hysteresis	296
MUF-77(Zn)-decyl	HDTT, BPDC, BDC	0.88	0.11	-	0.48	With significant hysteresis	296
MIL-53(Cr)	BDC	0.15	0.1	60-40	-	-	318
HV-MOF-1(Er)	DCBP	0.40	0.10	-	-	3% loss in q_{max} after 9 ads. cycles	319
MIL-53(Al)-NH_2	NH_2-BDC	0.02	0.09	-	-	-	198
[Cd(L'2)(Cl)](H_2O)	L'2	0.1	0.09	-	-	-	279
MIL-53(Al)	BDC	0.14	0.09	-	0.51	-	202
MIL-53(Al)	BDC	0.30	0.09	-	-	-	198
DMOF(Zn)	BDC/DABCO	0.30	0.09	-	0.75	100% loss in S_{BET} after 90% RH	244
MOF-802(Zr)	PZDC	0.4	0.09	-	<0.01	Stable over 5 ads. cycles	75
Zn(BTTB)(BDC)	BTTB/BDC	0.50	0.09	-	0.21	50% loss in S_{BET} after 90% RH	292
CALF-25(Ba)	PytPh	0.60	0.09	45	-	Stable over 4 ads. cycles	95
MIL-53(Al)-NH_2	NH_2-BDC	0.04	0.08	-	0.37	-	202
Zn(PM)$_{0.5}$(AT)	PM, AT	0.07	0.08	-	-	-	320
MIL-53(Al)$_{ionothermal}$	BDC	0.15	0.08	-	0.36	-	321

https://dx.doi.org/10.1021/acs.chemrev.9b00746
Chem. Rev. XXXX, XXX, XXX−XXX

Table 2. continued

Material	Linker	α [-][b]	q_{max} [g g^{-1}][c]	$-\Delta_{ads}H$ [kJ mol^{-1}][d]	V_p [cm^3 g^{-1}][e]	Stability	REF
CAU-10(Al)-OCH$_3$	1,3-BDC-OCH$_3$	0.25	0.08	-	-	Survives liq. water (18 hr.)	68
DMOF(Zn)-NH$_2$	NH$_2$-BDC/DABCO	0.30	0.08	-	0.58	100% loss in S_{BET} after 90% RH	244
Ga-MIL-53	BDC	0.03	0.07	71-32	-	-	322
DMOF(Zn)-Cl$_2$	Cl$_2$-BDC/DABCO	0.35	0.07	-	0.45	100% loss in S_{BET} after 90% RH	291
AlaZnBr	Ala	0.60	0.07	-	-	Stable for 6 months in H$_2$O	313
ZIF-412(Zn)	BIM, NIM, IM	0.78	0.07	-	-	No loss in q_{max} over 4 ads. cycles	97
MIL-53(Al)-F	F-BDC	0.80	0.07	-	0.48	No reduction in hexane capacity after 1 ads. cycle	308
MOF-1 (Ce, Eu)	OAA	0.44	0.06	-	-	Crystallinity was retained after being soaked in water for 15d	323
MIL-53(Ga)	BDC	0.02	0.05	-	0.47	-	202
DMOF(Zn)-Br	Br-BDC/DABCO	0.45	0.05	-	0.53	100% loss in S_{BET} after 90% RH	291
23R (Co)	(R)-3-Cl-man	0.81	0.05	-	-	Structure was maintained after ads.	324
[Cd$_2$(L'2)$_2$(Br)$_2$](H$_2$O)$_3$	L'2	0.5	0.04	-	-	-	279
33R (Co)	(R)-4-Cl-man	0.55	0.04	-	-	Structure was maintained after ads.	324
Cu(mtpm)Cl$_2$	MTPM	0.16	0.03	-	-	-	325
3S (Co)	(S)-man	0.66	0.03	-	-	Structure was maintained after ads. / Significant hysteresis	324
La(pyzdc)$_{1.5}$	PYZDC	0.37	0.02	-	-	Structure was retained after 59 days air exposure	326
13R (Co)	(R)-2-Cl-man	0.6	0.02	-	-	Structure was maintained after ads.	324
43R (Co)	(R)-4-Me-man	0.67	0.02	-	-	Structure was maintained after ads.	324
Ni(BTTB)	BTTB	0.80	0.02	-	0.20	No loss in S_{BET} after 90% RH	292
Co(BTTB)(BPY)	BTTB/BPY	0.30	0.01	-	0.40	No loss in S_{BET} after 90% RH	292
ZIF-8(Zn)	mIm	-	-	-	0.49	-	267
MAF-4(ZIF-8)	mIm	-	-	-	0.65	-	267
DMOF(Zn)-N	NDC/DABCO	-	-	-	0.57	26% loss in S_{BET} after 90% RH	291

https://dx.doi.org/10.1021/acs.chemrev.9b00746
Chem. Rev. XXXX, XXX, XXX−XXX

Table 2. continued

Material	Linker	α [-][b]	q_{max} [g g^{-1}][c]	$-\Delta_{ads}H$ [kJ mol^{-1}][d]	V_p [cm^3 g^{-1}][e]	Stability	REF
ZIF-71(Zn)	dcIm	-	-	-	0.39	-	286

[a]The rows are arranged in order of decreasing mass specific values of q_{max} (from highest to lowest). The rows of the selected MOFs are colored with pink background. [b]Inflection point of water uptake step, the relative pressure for which capacity is 50% of q_{max}. [c]Maximum capacity, measured at 298 K unless otherwise stated. [d]Heat of adsorption (isosteric or average of isosteric heat). Note that values below the water heat of condensation (~40.7 kJ/mol) seem physically unrealistic. [e]Pore volume, from N_2 adsorption at 77 K.

Mg^{2+}, and Al^{3+}).[110] The same reasoning can be used to interpret the integrity of MIL-121(Al) in NaCl solution. PCN-602(Ni) demonstrated excellent stability in aqueous solutions of 1 M KF, K_3PO_4, and Na_2CO_3 as corroborated by N_2 sorption isotherms and PXRD patterns. This is indeed because the soft metal ion Ni has a stronger interaction with soft azolate linkers than with hard linkers (F^-, PO_4^{3-}, and CO_3^{2-}), although the inertness of Ni^{2+}[111] and the high framework connectivity[109] are other factors to strengthen its structure.

3.1.4. In Acidic Water. After a thorough survey (Table 1), we conclude that MOFs constructed from high-valent metal ions and carboxylate-based linkers exhibit excellent robustness in acids but with moderate resistance in alkaline media. In principle, the degradation in acid of MOFs that are stable in neutral water can be rationalized by the competition between proton and metal ion for the coordinating linkers. Not surprisingly, the low pK_a values of carboxylic acids endow these MOFs with excellent stability in acids. However, owing to the high affinity between high-valency metal ions and OH^-, this type of MOFs will easily decompose in a basic solution.[112]

Trivalent Cr, Al, and Fe-carboxylate MOFs could stand normal acid solutions. For instance, the crystallinity of MIL-53(Cr, Al) was well-retained in HCl solutions (pH ~ 2).[88,113] MIL-101(Cr) was unaltered in a more acid solution with pH ~ 1.[114] After 1 day treatment in 10 M H_2SO_4 or concentrated HCl, the structure of BUT-8A(Cr) was still intact.[115] Furthermore, the stability of trivalent In-,[116−118] and Sm-carboxylate MOFs[119] was described in acid solutions and the framework hydrophobicity may be a possible reason for the latter case.

Apart from the aforementioned trivalent metal−carboxylate MOFs, tetravalent Zr, Ti, and Hf-carboxylate frameworks with a much greater number and variety of stable MOFs have become accessible. UiO-66(Zr) together with its broad range of analogues has extensively been studied. Concentrated HCl, pH = 12 alkaline, and 5% H_2O_2 are conditions that UiO-66(Zr) can stand.[113,114] Missing linkers and clusters defects are always found in zirconium MOFs, such as UiO-66, when modulated synthesis is adopted.[120] Strikingly, the chemical stability of UiO-66 is not compromised by these defects.[113] PCN-222(Fe)(Zr,Fe),[70] MOF-808(Zr),[113] DUT-67(Zr),[121] DUT-68(Zr),[121] BUT-12(Zr),[122] BUT-13(Zr),[122] MIP-200-(Zr),[123] spiro-1(Zr),[124] and MIL-177-LT(Ti)[125] are compelling examples that could maintain their framework integrity in concentrated HCl or H_2SO_4 or H_3NO_3 or aqua regia or H_3PO_4. More strikingly, the porosity of PCN-222(Fe)-(Zr,Fe),[70] MOF-808(Zr),[126] MIP-200(Zr),[123] spiro-1(Zr),[124] and MIL-177-LT(Ti)[125] was well-retained after acid treatment.

Moreover, some acid-tolerant bivalent Zn[101,127] and Cu[56]-carboxylate MOFs were documented by virtue of the hydrophobicity,[127] interpenetration,[101] and buffer environment[56] of frameworks. Besides carboxylate-linkers, MOFs constructed by other linkers are rarely known on standing strong acid. BUT-83(Co)[128] and SZ-3(Zr)[129] linked by azolate and phosphonate linkers, respectively, are among the few examples benefiting from their compact structure[128] and strong coordinative bond.[129]

3.1.5. In Alkaline Water. As indicated in Table 1, MOFs composed of low-valency metal ions and azolate-based linkers display great stability in alkaline solutions but moderate tolerance in acids. The high stability in alkaline solutions can be attributed to the strong bonds between the low-valency metals and azolate linkers and the weak interaction of the low-valency metals with hydroxyls, even if the framework hydrophobicity sometimes is probably another reason. The relatively high pK_a values of azoles denote a strong affinity between azolate linkers and protons and consequently the related MOFs are labile in acidic solutions.[112]

Bivalent Zn, Co, and Ni-azolate MOFs are representative samples that are robust under very basic conditions. ZIF-8(Zn) is the pioneering base-resistant MOF studied in 8 M NaOH at 373 K.[41] Besides, MAF-X27-Cl(Co) could well maintain its crystalline structure after treating with 1.0 M KOH for 7 days.[86] Furthermore, both the structure and porosity of $Ni_3(BTP)_2(Ni)$[85] and PCN-601(Ni)[59] were not affected after immersing in pH ~ 14 and saturated NaOH solutions, respectively. Strong base-resistant MOFs are hardly found beyond this family. On account of the hydrophobicity, trivalent La-carboxylate MOF La(BTB)[130] is an exception, which could stand pH ~ 14 NaOH solution at 373 K for 3 days.

In general, given by the continuous efforts of the scientific community, dozens of MOFs are available that survive in water under harsh conditions. This mitigates the concerns of MOF applications in water systems. However, the MOF durability in the devices for the specific applications discussed below is only reported or addressed for a few samples. The corrosion issue among MOFs, substrates (for example, aluminum fins),[24] binders (for example, polysiloxane),[24] and additives (for example, graphite)[74] is one of the future directions to implement. For example, the color of MOF coatings changed from white to brown after a few days cooling test runs, caused by the diffusion of iron oxide from the steel substrate.[24]

3.2. Adsorption Mechanisms

The water adsorption properties in MOFs have been extensively studied since Chang's pioneering work in 2006.[190−193] Three categories of mechanisms were distinguished for water adsorption in MOFs:[10] (a) chemisorption on open metal sites, (b) capillary condensation (physisorption), and (c) layer/cluster adsorption (physisorption). Water cluster adsorption is prevalent over layer formation because most of the studied MOFs are comprised of hydrophobic aromatic linkers. Water clusters can be formed following the water nucleation on hydrophilic sites in MOFs, including open metal

https://dx.doi.org/10.1021/acs.chemrev.9b00746
Chem. Rev. XXXX, XXX, XXX−XXX

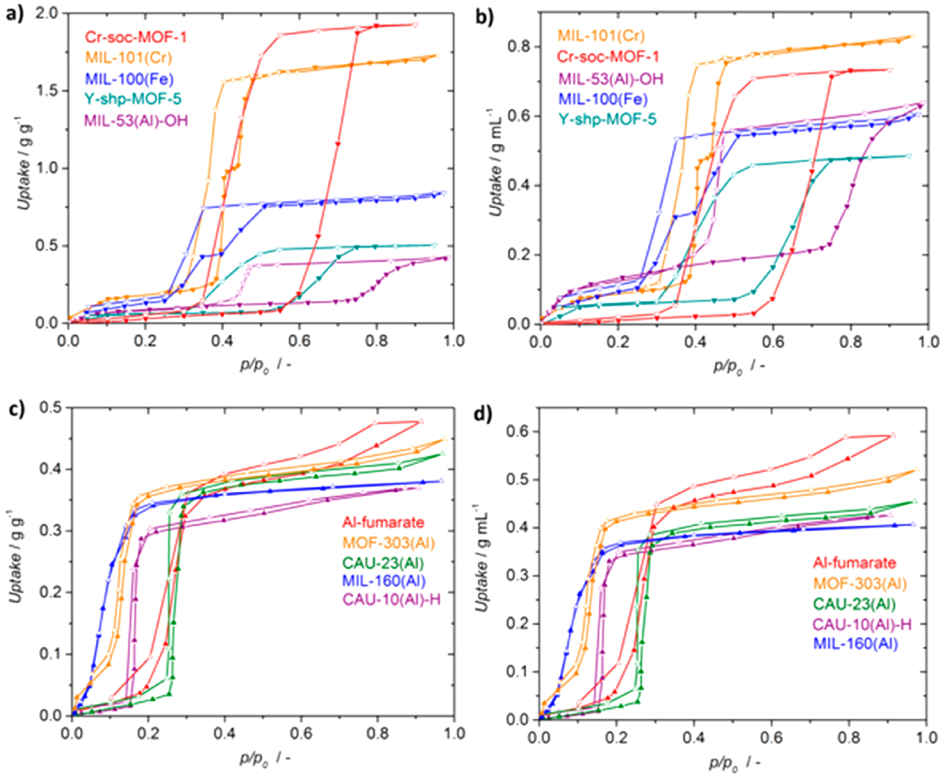

Figure 7. Water adsorption (filled symbols) and desorption (empty symbols) isotherms of M(III)-carboxylate MOFs mostly discussed in this work, presented in gravimetric (a,c) and volumetric (b,d) uptake at 298 K. Samples and data used for MIL-101(Cr),[7,196] MIL-100(Fe),[197] MIL-53(Al)-OH,[198] Y-shp-MOF-5,[195] Cr-soc-MOF-1,[194] Al-fumarate,[199] CAU-10(Al)-H,[200] CAU-23(Al),[99] MIL-160(Al)(@303K),[100] and MOF-303(Al).[74] The crystal density of MOFs is taken from Table 3. Lines are shown to guide the eye.

sites and μ-OH groups on SBUs, defects, and hydrophilic functional groups on linkers.

Six criteria have been outlined to determine suitable MOFs for water adsorption-related applications:[7,75,194]

1. hydrothermal stability
2. a steep uptake isotherm at a specific relative pressure for pore filling or condensation
3. a large water working capacity for the requisite maximum delivery of water or energy effect
4. minimal or no hysteresis in desorption (indoor humidity control is an exception)[195]
5. high cycling durability
6. facile adsorption−desorption, fast mass and heat kinetics for the desired energy efficiency

The water adsorption properties of 383 MOF samples (Table 2) have been systemically evaluated in this section according to these criteria, resulting in 18 types of MOFs that stand out complying with the above criteria. The rows of the selected MOFs are colored with pink background in Table 2, and their water adsorption/desorption isotherms are replotted in Figure 7 and Figure 8 based on their literature data. Both mass specific (g/g_{MOF}) and volume specific (g/cm^3_{MOF}) isotherms are presented. The former are mostly presented in literature, while the latter, corrected for crystal density, are more relevant for application by specifying the occupied sample volume for a certain water capacity. High mass specific capacities are not synonymous with a preferred material, and relative differences between MOFs change considerably by this transformation.[7]

The structure and water adsorption properties of these 18 selected MOFs are discussed below according to the type of adsorption mechanism and the types of linkers and metal valencies. The categories of some adsorption isotherms are designated referring to the IUPAC definition.[206]

3.2.1. Chemisorption on Open Metal Sites. The UiO-66(Zr)[43,107] framework consists of $Zr_6O_4(OH)_4$ cores bridged by BDC linkers forming a face-centered cubic lattice (*fcu* topology). The diameters of the tetrahedral and octahedral cavities are ∼0.9 and ∼1.1 nm, respectively, connected by triangular apertures (diameter ∼ 0.6 nm). The zirconium is initially eight-coordinated and turned into seven-coordinated after dehydration (523−573 K). The structural transformation was evidenced by PXRD, EXAFS,[43,207] pair distribution function (PDF),[208] and neutron powder diffraction[209] analyses together with DFT computation. Strikingly, the chemisorption of water in the SBU is fully reversible.

3.2.2. Capillary Condensation. For pores with diameters larger than a critical value D_c, water is adsorbed because of capillary condensation and preceded by cluster adsorption. A hysteresis loop is always found between adsorption and desorption branches because the adsorption branch does not reach thermodynamic equilibrium.[206] The equation to calculate the D_c is expressed as follows:

$$D_c = \frac{4\sigma T_c}{T_c - T} \quad (2)$$

Here, σ represents the Van der Waals diameter of water (0.28 nm), T_c is the critical temperature (647 K) for water, and T is the actual temperature. So, at room temperature, the value of D_c is determined to be around 2.0 nm. Pores larger than 2.0

https://dx.doi.org/10.1021/acs.chemrev.9b00746
Chem. Rev. XXXX, XXX, XXX−XXX

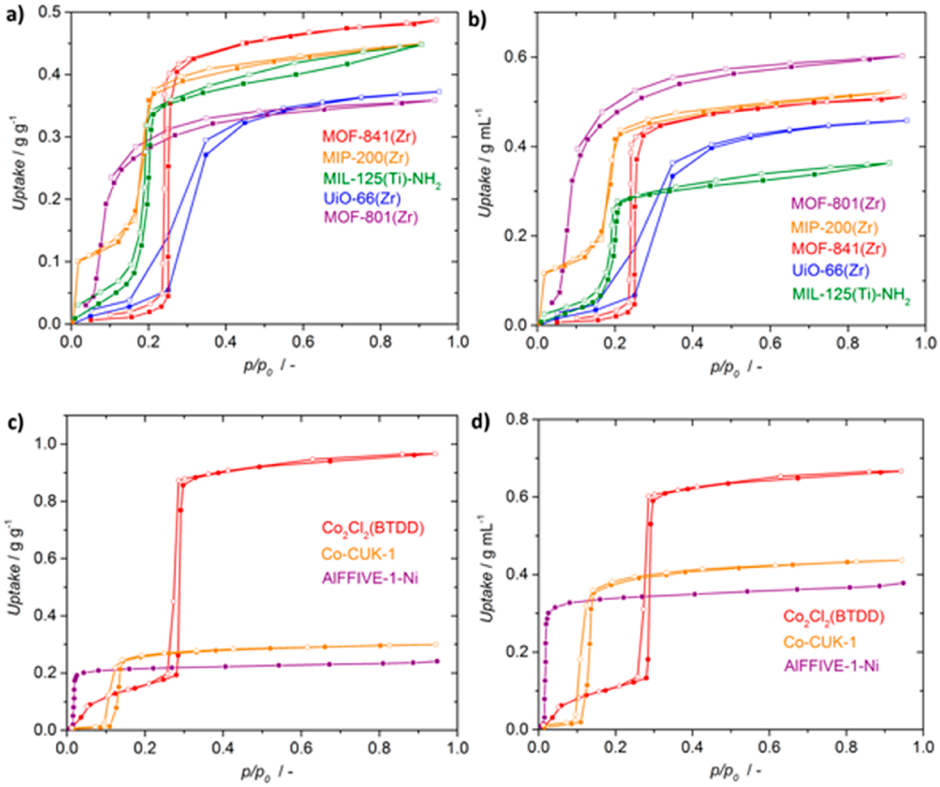

Figure 8. Water adsorption (filled symbols) and desorption (empty symbols) isotherms of M(IV)-carboxylate (a,b) and M(II)-azolate (c,d) MOFs mostly discussed in this work, presented in gravimetric (a,c) and volumetric (b,d) uptake at 298 K. Samples and data used for UiO-66(Zr),[201] MOF-801(Zr),[75] MOF-841(Zr),[75] MIP-200(Zr)(@303 K),[123] MIL-125(Ti)-NH_2,[202] Co_2Cl_2(BTDD),[203] AlFFIVE-1-Ni (@308 K),[204] and Co-CUK-1 (@303 K).[205] The crystal density of MOFs is taken from Table 3. Lines are shown to guide the eye.

nm are predicted to exhibit capillary condensation behavior and adsorption−desorption hysteresis.

MIL-101(Cr)[42] has two types of mesoporous cages present in a ratio of 2:1 with internal free diameters of 2.9 and 3.4 nm, respectively. The smaller cages possess pentagonal aperture with a diameter of 1.2 nm, while the larger cages have both pentagonal and hexagonal (1.47 nm and 1.6 nm) apertures. The high framework porosity endows MIL-101(Cr) with a large water capacity (up to 1.73 g/g).[7,196] Moreover, a good cycling durability[210−212] is guaranteed by its high hydrothermal stability. So, MIL-101(Cr) has received significant attention for applications in water adsorption.[197] Its adsorption isotherm displays two distinct steps (Figure 7[7,196]). An initial low uptake is recorded at relative pressures below p/p_0 = 0.39, assigned to water nucleation and cluster growth. The high heat of adsorption (~80 kJ mol^{-1}) in this stage reflects the possible chemisorption on coordinated unsaturated metal sites.[210] The first steep step at around p/p_0 = 0.39 and the second at around p/p_0 = 0.44 correspond to the pore filling of the smaller and larger cages, respectively.[210,213] The heat of adsorption (44.5 kJ/mol) in these two steps is close to the evaporation enthalpy of water (40.7 kJ/mol), supporting that most of these water molecules are physisorbed.[210] As capillary condensation happens in the mesoporous cages, the strong hysteresis loop can be well explained.

MIL-100 (Cr)[66] has the same MTN zeotype architecture as MIL-101(Cr), but with a different linker (BTC and BDC for MIL-100(Cr) and MIL-101(Cr), respectively), smaller mesoporous cages (diameters of 2.5 and 2.9 nm), and apertures (0.48 nm × 0.58 nm and 0.86 nm × 0.86 nm for pentagonal and hexagonal windows, respectively). The water adsorption behavior is marginally influenced when chromium was replaced with iron.[197,214−216] The latter is not harmful to the human body.[212] So, MIL-100(Fe) features basically isotherms of similar shape as MIL-101(Cr), a lower capacity (up to 0.87 g/g)[210] and a lower inflection point (α = ~0.35, where α = ~0.4 for MIL-101(Cr)) (Figure 7).[197] 2000 adsorption cycles were conducted without capacity loss, which highlights its brilliant durability.[214]

Mesopores (~3.0 nm) are also found in NU-1000(Zr).[71] However, the MOF framework undergoes pore collapse during water desorption because of capillary forces.[217] Metal node functionalization is utilized to afford a recyclable modified NU-1000(Zr) (SALI-5(Zr) and SALI-9(Zr)).[217]

3.2.3. Cluster Adsorption. MIL-53 (M = Cr, Fe, Al, Ga)[65] is constructed by infinite rod-like SBUs linked by BDC linkers to build 1D channels. It shows a pronounced breathing effect triggered by water molecules, as exemplified by functionalized MIL-53(Al)-OH.[198] At saturated vapor pressure, only one water molecule is adsorbed on each metal unit in initial MIL-53(Al), which is in its narrow pore configuration.[198] The introduction of OH groups on the BDC linkers makes the breathing possible at a relative pressure around p/p_0 = 0.75.[198] Pore filling happens, and finally five water molecules are adsorbed per metal unit in the large pore phase (free dimensions of 1.7 nm × 1.2 nm) MIL-53(Al)-OH. The structure returns to the narrow pore phase (free dimensions of 1.9 nm × 0.8 nm) at a relative pressure around p/p_0 = 0.47 in the desorption branch, leaving a large hysteresis loop attributed to the breathing behavior (Figure 7).

Al-fumarate,[98,218] also named as MIL-53(Al)-FA and the commercial Basolite A-520, is built up from rod-like SBUs

https://dx.doi.org/10.1021/acs.chemrev.9b00746
Chem. Rev. XXXX, XXX, XXX−XXX

linked together by FA linkers to form lozenge-shaped 1D channels with free dimensions of 0.57 nm × 0.60 nm. It is an analogue of the MIL-53(Al) but with a more rigid framework. The water adsorption shows a type V isotherm with a favorable S-shape (Figure 7).[199] The linker hydrophobicity is reflected by an initial low uptake. Steep uptake happens in a narrow relative pressure range (p/p_0 = 0.2−0.3), and further loading follows in a gentle slope above p/p_0 = 0.3. The hysteresis is fairly narrow, designated to the reversible and continuous pore filling. A qualified hydrothermal stability is corroborated by 4500 adsorption cycles.[199]

CAU-10(Al)-H[68] has *cis*-connected corner-sharing rod-like SBUs in its structure linked by 1,3-BDC linkers to form square shaped, sinusoidal channels with a diameter around 0.7 nm. The material shows a beneficial S-shaped adsorption isotherm (Figure 7), with the main loading lift at p/p_0 = 0.16 and no hysteresis.[200] The capacity is around 0.37 g/g, with an average isosteric heat about 54 kJ/mol pointing at a moderate guest−host interaction. The CAU-10(Al)-H exhibits fantastic recyclability over 10000 water adsorption cycles.[219]

CAU-23(Al)[99] has rod-like SBUs in its chiral structure which is coordinated by hydrophilic TDC linkers (150° opening angle) to form 1D square channels (side length of 0.76 nm) along the *b*-axis. The SBUs are built from alternating units of four consecutive *trans* (as observed in MIL-53 series) and *cis* corner-sharing AlO_6 polyhedra, as observed in CAU-10(Al)-H. The measurements indicate an S-shaped isotherm with a steep uptake at p/p_0 = 0.27 (Figure 7). The adsorption mechanism is simulated by GCMC simulations.[99] The formation of hydrogen bonding between the adsorbed water and the μ-OH groups on the SBUs provides a driving force and initiates the adsorption process. Subsequently, pore filling happens and leads to a sudden increase in water content. To this end, for a single adsorbed water molecule, the average number of hydrogen bond connections is ∼3.65, which is very close to that of bulk water, interpreting the moderate adsorption heat (48 kJ/mol) and easy achievement of desorption. Long-term stability is confirmed by 5000 consistent adsorption cycles.

MIL-160(Al)[100] is isostructural to CAU-10, which is built from *cis* corner-sharing rod-like SBUs linked by FDC linkers, leading to a 3D framework delimiting square-shaped sinusoidal 1D channels with a diameter around 0.5 nm. It adsorbs water at a low inflection point (α = 0.09) and without any hysteresis (Figure 7). The inflection point α is the relative pressure at 50% of q_{max}. The adsorption mechanism is intensively studied by GCMC simulation, adsorption enthalpy calculation coupled with solid-state ^{1}H MAS NMR measurements. The adsorbed water molecules preferentially interact with the OH groups from the SBUs and then the pore wall, probably the O atoms from the FDC linkers and the water molecules already present in the pore. Because of the hydrophilic nature of FDC linkers, the inflection point of water adsorption on MIL-160(Al) (α = 0.09) is lower than on CAU-10(Al)-H (p/p_0 = 0.16).[200] The MIL-160(Al) is recyclable as evidenced by 10 water adsorption cycles and stable in boiling water for three days.

MOF-303(Al)[74] is built up from infinite rod-like aluminum SBUs coordinated with PDC linkers to form 1D hydrophilic channels with a diameter around 0.6 nm. The water adsorption displays a type IV isotherm with a low inflection point at α = 0.13 and a plateau commencing at p/p_0 = 0.3 (Figure 7),[17,74] and features minimal hysteresis, moderate constant isosteric heat of adsorption (∼52 kJ/mol), and excellent durability, demonstrated by 150 repeatable adsorption cycles.[74]

Y-shp-MOF-5[195] structure is composed of 12-coordinated nonanuclear SBUs coordinated with 12 BTEB linkers to give triangular 1D channels with an opening of 1.2 nm. The type-IV-like, S-shaped adsorption and desorption isotherms display inflection points at p/p_0 = ∼0.63 and p/p_0 = ∼0.45, respectively (Figure 7). On the basis of SCXRD measurements and Dubinin−Serpinsky theory,[220] the characteristic adsorption behavior is interpreted as follows. The initial low uptake below 10% RH is due to the water affinity on the open metal sites and hydroxyl groups from SBUs. At 50% RH, a steep uptake is manifested because the dispersive energy of clusters of at least five water molecules[220] is enough to be sustained inside the pores. The wide hysteresis loop is explained by the appearance of water superclusters, and a driving force is required to break the superclusters into smaller ones before escaping from the pore. The Y-shp-MOF-5 maintains its uptake over more than 1000 adsorption cycles between 25% and 85% RH at room temperature.[195]

Cr-soc-MOF-1[194] features well-defined 1D infinite channels with an estimated diameter of 1.7 nm (just below the D_c of water) and cubic-shaped cages with six HTPC linkers on the faces and 8 SBUs on the vertices. As depicted in Figure 7, the isotherms have an S-shape with significant hysteresis between the adsorption−desorption branches. On the basis of the crystal structure analysis of hydrated Cr-soc-MOF-1, the initial adsorption is promoted by the water nucleation located at the vertices of the cubic cages, which corroborates the stated energy barrier, followed by the formation of water clusters, i.e., the steep uptake of water between 60% and 75% RH. The hysteresis is understandable because the energy barrier for dissociating the hosted water hydrogen-bonded network must be surmounted.[194] The high porosity (2.1 cm^3/g) affords Cr-soc-MOF-1 with a water capacity of 1.95 g/g, surpassing carbons, inorganic materials, and all other MOFs. Accounting for the nearly three times lower density (Table 3), however, arranges it among other MOFs on the basis of volume specific capacity, although still high (Figure 7). The water uptake remained unaltered over 100 adsorption cycles between 25% and 85% RH at 298 K.

The structure information of UiO-66 is reviewed in sections 3.1.2 and 3.2.1. UiO-66 exhibits an initial low water uptake till around 25% RH, corresponding to the hydrophobicity of the phenol rings from the BDC linkers (Figure 8). Pore filling takes place between 30% and 50% RH and the uptake levels off around 0.37 g g^{-1}.[201] A hysteresis loop is observed, which could possibly arise from the water−linker interaction and the different pore sizes and the presence of defects in the UiO-66 structure.[202] Given by the outstanding structural stability, the water capacity was well-retained in repeated cycling.[75,201,211,221,222]

MOF-801(Zr),[75] also named as Zr-fumarate,[223] is isostructural with UiO-66 with the shorter FA as linker. So, smaller apertures (0.33−0.46 nm)[224] and tetrahedral (0.56 and 0.48 nm) and octahedral (0.74 nm) cavities are formed in its structure. The adsorbed amount of water smoothly increases with pressure up to p/p_0 = 0.05, followed by a steep uptake in the relative pressure range from p/p_0 = 0.05 to 0.1, and a final capacity of 0.36 g/g is reached at p/p_0 = 0.9 (Figure 8). The relative pressure of the step is much lower than that of UiO-66, highlighting a higher hydrophilicity for this material.

https://dx.doi.org/10.1021/acs.chemrev.9b00746
Chem. Rev. XXXX, XXX, XXX−XXX

Table 3. Selected MOFs and Benchmark Materials for Heat Pump Performance Assessment[a]

material	pore structure	d_{window} (Å)[b]	d_{pore} (Å)[b]	ρ_c (g mL^{-1})[c]	$\langle -\Delta_{ads}H \rangle$ (kJ mol^{-1})	W_{sat} (mL mL^{-1})[h]	α	ref
MOFs-H_2O								
Al-fumarate	1-D	5.7 × 6.0	5.7 × 6.0	1.24	42.8[d,i]	0.59	0.27	98,199
CAU-10(Al)-H	1-D	5.6	7	1.15, 1.60	53.5[d]	0.38	0.16	75,100,360
CAU-23 (Al)	1-D			1.07	48.2	0.43	0.27	99
Co-CUK-1	1-D	13.4 × 13.0	13.4 × 13.0	1.46	46.9 (0.22 g g^{-1})	0.41	0.12	205
Co_2Cl_2(BTDD)	1-D	22	22	0.69	45.8	0.67	0.29	203,264
Cr-soc-MOF-1	1D	17	17	0.381	NA	0.74	0.41, 0.69 (hysteresis)	194
MIP-200	1-D	13, 6.8	13, 6.8	1.16	55	0.55	0.18	123
Ni_2Cl_2(BBTA)	1-D	13	13	1.1	55 (zero loading)	0.46	0.03	264
Ni-MOF-74	1-D	11	11	1.19	62.6 (zero loading)	0.55	0.05	75,242
Ni-MOF-74-BPP	1-D	17	17	NA	62.1 (zero loading)	0.81 g/g	0.23	242
Ni-MOF-74-TPP	1-D	23	23	NA	60.0 (zero loading)	0.90 g/g	0.5	242
MIL-53(Al)-TDC	1-D	8 × 8.2	8 × 8.2	NA	46.8	0.434 g/g	0.37	263,361
MIL-53 (Cr)	1-D, flexible	7−13		1.50$^{(np),m}$−1.14 $^{(lp),n}$	57.0[g]	0.56$^{(lp),n}$	0.15	202,318
MIL-100 (Fe)	3-D	5.5, 8.6	25, 29	0.72	50.6[d]	0.56	0.3, 0.35 (hysteresis)	66,215,362
MIL-101 (Cr)	3-D	12, 15	29, 34	0.48	45.5[d]	0.62−0.82	0.34, 0.4 (hysteresis)	42,196,202,236
MIL-125 (Ti)	3-D	5−7	6.13, 12.55	0.81		0.84	0.35	78,225
NH_2-MIL-125 (Ti)	3-D	3.4−4.2	6, 12.5	0.81	56.0[d]	0.46−0.84	0.2	225,227
MIL-160 (Al)	1-D, flexible	5.5	2.5	1.068		0.40	0.09	100,285,360,363
MOF-303 (Al)	1-D	6	6	1.159	40−50[e]	0.56	0.13	74
MOF-801 (Zr)	3-D	4.8, 5.6, 7.4	8	1.68	58.4[d]	0.76	0.09	75
MOF-841 (Zr)	3-D	9.2	13.3	1.05	50.4[d]	0.55	0.22	75
DUT-67 (Zr)	3-D		16.6, 8.8	1.04	47−58[e]	0.65	0.35	75,364
Y-shp-MOF-5	1-D	12	12	0.963	NA	0.48	0.45, 0.63 (hysteresis)	195
Zn(BDC)$(DABCO)_{0.5}$	3-D, flexible	3.2, 4.8, 7.5$^{(lp),n}$	3.2, 4.8, 7.5$^{(lp),n}$	1.42$^{(np),m}$−1.35 $^{(lp),n}$	42.8$^{(MeOH),d}$	0.89$^{(lp),n}$		365,366
COF								
COF-432	1-D		7.5	0.875	48[d]	0.20	0.33	44
Zeolite-H_2O								
$AlPO_4$-LTA	3-D	flexible	flexible	1.412		0.59	0.15	338
MOFs-Hydrofluorocarbons (e.g., R-134a)								
MCF-61	1-D	20 × 21	20 × 21	0.564	∼30	1.10 (R-134a)		346
MCF-62	1-D	30 × 34	30 × 34	0.375	24−29	1.73 (R-134a)		346
MCF-63	1-D	35 × 40	35 × 40	0.318	23−29	2.07 (R-134a)		346
Ni-MOF-74	1-D	11	11	NA	50.6 (zero loading)	0.58 (R-134a)		242
Ni-MOF-74-BPP	1-D	17	17	NA	44.2 (zero loading)	0.75 (R-134a)		242
Ni-MOF-74-TPP	1-D	23	23	NA	40.6 (zero loading)	0.77 (R-134a)		242
Benchmarks								
AQSOA-Z01	1-D	7.4	8.3	1.75[j]	56.1[d]	0.42		20,367,368
AQSOA-Z02	3-D	3.7	7.4	1.43	57.0[d]	0.45		20,367,369
AQSOA-Z05	1-D	7.4	8.3	1.75	52.6[d]	0.39		20,367,368
silica gel	3-D, irregular			0.72$^{(bd),k}$	55.7[d]	0.22$^{(bd),k}$		370
activated carbon	3-D, irregular	<6, 8, 12 $^{(N2),o}$		2.17$^{(rd),l}$	43.0$^{(MeOH),d}$	1.05$^{(rd),l}$		339,371

https://dx.doi.org/10.1021/acs.chemrev.9b00746
Chem. Rev. XXXX, XXX, XXX−XXX

Table 3. continued

[a]Pore structure, window and pore size, crystal density, loading averaged enthalpy of adsorption, and saturation volume adsorbed per volume of adsorbent, are indicated where meaningful. [b]As reported, unless noted otherwise. [c]Crystal density, determined from crystallographic structure, unless noted otherwise. [d]Average enthalpy of adsorption, as calculated according to ref 7 over the loading range for which the enthalpy (or else isosteric heat) of adsorption is determined. Value is for water as adsorptive, unless noted otherwise. [e]Isosteric adsorption heat. [f]Calculated from DTG curve. [g]Microcalorimetry. [h]Saturation capacity (in g g^{-1}) is converted using the crystal density of the material, where possible, and liquid density of the working fluid. [i]The reported isosteric heat of adsorption at higher loadings[199] becomes lower than the evaporation enthalpy of water, yielding this physically unrealistic low average. [j]AQSOA-Z01 is a partially Fe-exchanged $AlPO_4$-5 material. The fraction of iron is not accurately reported and neglected in the density calculations. [k]bd refers to the bulk density of the packed bed. [l]rd refers to the real density of the solid. [m]np is the narrow pore configuration. [n]lp is the large pore configuration. [o]N_2 was derived from pore-size distribution of N_2 physisorption isotherm (at 77 K).

MIP-200(Zr)[123] has typical eight-coordinated SBUs linked with eight carboxylate groups from two MDIP linkers and four formate groups, which constitute a 3D Kagome-type framework with 1D triangular (0.68 nm) and hexagonal channels (1.3 nm) along the *c*-axis. The water adsorption isotherm has two regions with almost no hysteresis on the desorption branch above p/p_0 = 0.05 (Figure 8). As supported by the ^{1}H MAS NMR spectra and GCMC simulations,[123] the initial steep uptake is driven by the strong affinity between the water molecules and the hydroxyl groups and the water molecules originally coordinated to the SBUs. A heat of adsorption up to 70 kJ/mol is reached in the first stage, followed by relative low values (55−45 kJ/mol) in the pore filling process above p/p_0 = 0.1. The cyclability of MIP-200(Zr) is deduced from repeated 40 adsorption cycles between 70% RH at 303 K and 9.5% RH at 343 K.

The combination of eight-coordinated zirconium SBUs with tetrahedral MTB linkers constitutes the 3D MOF-841(Zr)[75] framework with *flu* topology. This structure has only one cage type, with an internal diameter of around 1.2 nm. The isotherm of MOF-841 can be categorized as type V. The adsorption steeply increases at p/p_0 = 0.2 and begins to level off at p/p_0 = 0.3 with a final capacity of around 0.5 g/g (Figure 8). Hardly any desorption hysteresis is identified. The adsorption durability was examined by five repeated cycles, after which a slight capacity loss (∼7%) is observed.

MIL-125(Ti)[78] has a 3D interconnected porosity built with octahedral (diameter ∼ 1.3 nm) and tetrahedral (diameter ∼ 0.6 nm) cages connected by triangular apertures (diameter in the range 0.5−0.7 nm). To afford a more hydrophilic and robuster[222,225−227] framework, the isostructural MIL-125(Ti)-NH_2[228] with narrower apertures (diameter in the range 0.34−0.42 nm) was deliberately prepared by decorating NH_2 groups on the BDC linkers. The MIL-125(Ti)-NH_2 exhibits a type V isotherm with a characteristic S-shape (Figure 8),[202] which can be explained by the hierarchical pore structure where narrow necks acting as pore gates for large internal voids.[161,225] A steep loading occurs at a low relative pressure p/p_0 = 0.2, benefiting from the framework hydrophilicity, and desorption hysteresis is absent.

Co_2Cl_2(BTDD)[87] features 1D mesoporous channels with a diameter of 2.2 nm. After the initial adsorption on the open metal sites, the pore diameter is reduced to slightly below the D_c of water (∼2.0 nm at room temperature), allowing water uptake and release without hysteresis due to capillary condensation.[203] The MOF displays a large and steep uptake step at p/p_0 = 0.29 and a capacity of 0.97 g/g is reached at 298 K (Figure 8). The initial capacity is well maintained when the MOF is cycled at a constant water vapor pressure of 1.7 kPa (p_0 = 3.2 kPa at 298 K) between 298 and 393 K, with a decline of 6.3 wt.% after 30 cycles.[203]

AlFFIVE-1-Ni (KAUST-8)[204] structure results from pillaring of layers of Ni(II)-pyrazine 2-periodic square-grids with $[AlF_5(H_2O)]^{2-}$ pillars, which adopts tetragonal space groups with primitive cubic topology and 1D channel. The water adsorption has a type I isotherm, and a saturated uptake of 0.22 g/g is reached at a very low relative pressure (p/p_0 = 0.05) (Figure 8). The water adsorption heat is correspondingly higher, 63 kJ/mol as quantified by TG-DSC. A good recyclability is realized between 298 and 378 K.

M-CUK-1 (M = Co, Mg, Ni)[205,229,230] has an infinite 1D square grid channel system (wall-to-wall distance around 1.1 nm) supported by highly connected PDC linkers that are

https://dx.doi.org/10.1021/acs.chemrev.9b00746
Chem. Rev. XXXX, XXX, XXX−XXX

arranged in orthogonal fashion around rod-like, edge- and vertex-sharing SBUs. The water sorption isotherms of Co-CUK-1 feature an S-shape with a very steep uptake at p/p_0 = ~0.12 for Ni and Co and at p/p_0 = ~0.25 for Mg, indicative of the presence of a uniform micropore (Figure 8).[205] The isosteric heat of adsorption is moderate (~47 kJ/mol) below the water uptake of 0.22 g/g at 303 K. The water capacity is around 0.3 g/g with good cycling stability, and the adsorption is fully reversible with almost no hysteresis. The initial low uptake is assigned to the framework hydrophobicity as simulated by GCMC. At low coverage, the water molecules tend to preferentially adsorb on the hydrophilic sites, i.e., μ-OH groups from the SBUs, followed by water cluster formation (4−7 molecules) filling the pore.

On the basis of the above literature overview, differences in the adsorption isotherms shapes, the step location, steepness, leading adsorption, and hysteresis originate from the MOF structure and hydrophilicity or hydrophobicity of the building blocks. It is striking that 12 of these 18 selected MOFs present a 1D pore system, and with pore sizes close to ~0.7 nm, very steep uptakes are observed, and also for the MOFs with a 3D pore structure. Apparently, the size of the pores or cavities and interaction with water molecules create a favorable situation for the formation of well-defined water cluster structures at low relative pressures. The observed uptake step and absence of hysteresis could even be considered as a phase change. For CAU-10-H, this ordering appears as new reflections in the XRD pattern, suggesting a very regular and immobile fashion.[200] Indeed, entropic analysis of the adsorbed phase show a much lower mobility than in liquid water (~58 vs 70 J mol^{-1} K^{-1}), although still somewhat higher than in ice (45 J mol^{-1} K^{-1}). XRD refinement suggests that water molecules are preferentially located close to the oxygens of the aluminum hydroxide chains of the framework, serving as the primary interaction sites for the polar water, followed by a regular cluster formation. Similar regular cluster formation has been revealed by SCXRD for MOF-801.[231] Molecular modeling of the adsorption in Al-fumarate (0.6 nm pore) also suggests a regular ordening of water molecules.[232] Considering the structural similarity of the other 1D porous MOFs this picture applies to most of these. The location of the step for isostructural MOFs is strongly related to the polarity of the linker and the interaction with water, e.g., compare CAU-10-H, CAU-23, and MIL-160 (Table 2). Also modifying the MOF by functionalization of the linker with hydrophilic groups moves the step to lower relative pressures, while with hydrophobic groups it moves upward.[231] Even changing the metal in CUK-1 from Ni or Co to Mg increases hydrophobicity, attributed to a different effect on the local electron density distribution, moving the step from p/p_0 = 0.12 to 0.25. The leading uptake at low relative pressures is generally ascribed to the nucleation of water at hydrophilic locations, but also defects can play a role and can explain uptake differences in this region for the same MOF. A reduced pore size due to this (strong) adsorption may explain the absence of hysteresis for MOFs with larger pore sizes (MIL-125(Ti)-NH_2, MOF-841(Zr), Co-CUK-1, MIP-200(Zr)). The highly hydrophobic COF-432 (1D, pore size 0.75 nm, water uptake step at p/p_0 = ~0.33, no hysteresis (Table 3)[44]) shows virtually no leading uptake, confirming the role of polarity. MIL-101 and MIL-100 exhibit two distinct steps, clearly related to the presence of two different sized cavities. The steepness of the step decreases with increasing distribution of pore dimensions (pore, cage, windows, defects), where the clustering of water molecules becomes less defined. The origins of hysteresis are (i) capillary condensation in pores above the critical size (~2 nm), (ii) the formation in smaller pores of superclusters that require more energy to be broken down, and (iii) flexible frameworks. These insights in the parameters that affect the adsorption mechanism and how they modify the adsorption, serve the development of new or fine-tuning existing MOFs.

4. APPLICATIONS AND PERFORMANCE ASSESSMENT

The aforementioned adsorption properties and isotherms endow MOFs with various applications. Five important types are studied in this work which are classified on the inflection points in the isotherm steps (Figure 9). Very low inflection

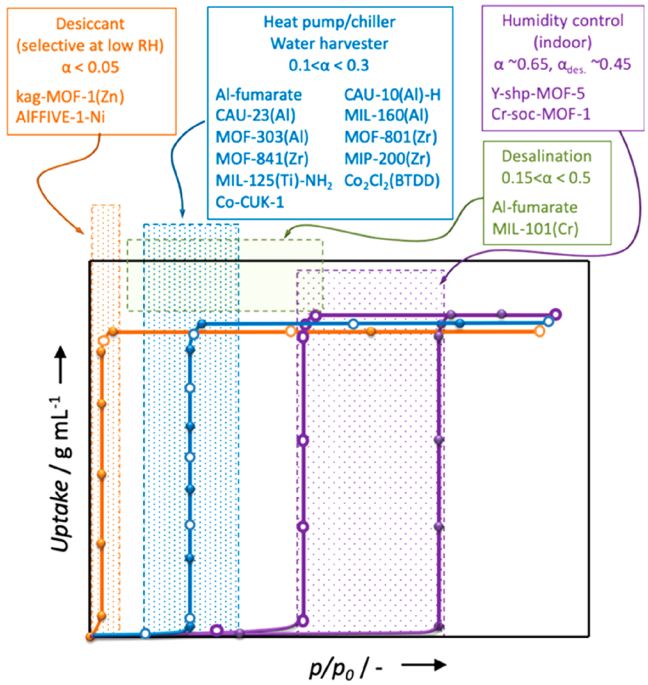

Figure 9. Relative pressure ranges of water adsorption (filled symbols) and desorption (open symbols) isotherms (assuming room temperature) and corresponding selected MOFs compatible with the various applications reviewed in this work.

points (α < 0.05) indicate a strong interaction between water and the MOF framework, which can provide the capability for selective removal of water molecules from other species (e.g., CO_2 and CH_4 for natural gas dehydration). Inflection points located in the α-range between 0.1 and 0.3 represent a facile desorption and a proper relative pressure range for being used as heat pumps/chillers and water harvesters. Inflection points around α = 0.65 for adsorption branches (and around 0.45 for desorption branches) could perfectly match with the humidity range of healthy indoor environments. The associated heat effects can be utilized simultaneously in air conditioning. Desalination covers a broader range and is connected to the operation conditions, also here cooling can be cogenerated. The MOFs evaluated for these specific applications are discussed in this section.

4.1. Desiccation

Desiccation is meant here for deep water removal, although this term is also used in air conditioning in combination with cooling (vide infra).[25,38] The MOFs with appreciable water

https://dx.doi.org/10.1021/acs.chemrev.9b00746
Chem. Rev. XXXX, XXX, XXX−XXX

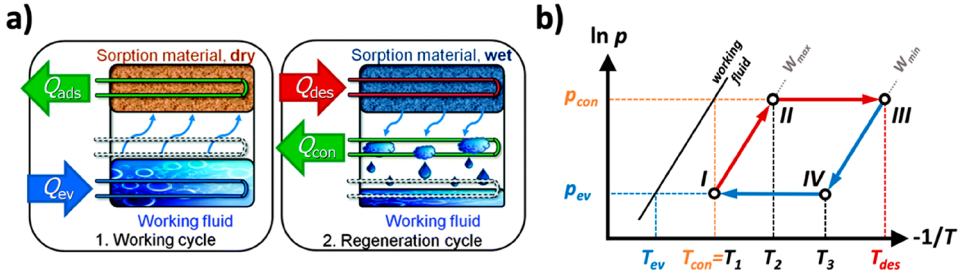

Figure 10. (a) Principle of operation of an adsorption-driven heat cycle with the adsorption stage and the desorption stage.[227] (b) Isosteric cycle diagram of an adsorption heat pump cycle, including the vapor pressure of water, minimum and maximum isosteres, lines of equal loading, W_{min} and W_{max}, temperature and pressure of the evaporator and condenser, desorption temperature, and intermediate cycle temperatures. (a) Reprinted with permission from ref 227. Copyright 2013 Royal Chemical Society.

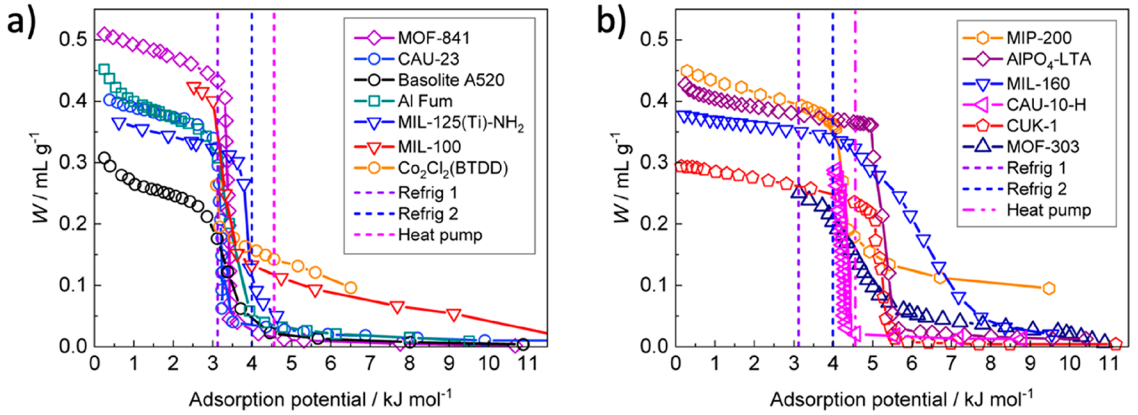

Figure 11. Characteristic curves determined using eq 1, using adsorption isotherms from various literature sources. The optimal adsorption potential for refrig-1 cooling (purple), refrig-2 cooling (blue), and heat pump heating (pink) is indicated by the dashed lines. (a) MOFs suited only for refrig-1 cooling: MOF-841,[75] CAU-23,[99] Basolite A520,[337] Alfum,[337] MIL-125-NH_2 (Ti),[161] MIL-100 (Fe),[215] and Co_2Cl_2(BTDD).[203] (b) MOFs that can be used for both cooling and heating: AlPO-LTA,[338] MIP-200,[123] CUK-1,[205] CAU-10,[280] MIL-160,[100] MOF-303.[74]

uptake capacity at low H_2O partial pressures would be an attractive alternative to solid desiccants (Figure 9). Besides the cycling capacity, the remaining challenge is the cost of MOFs sorbents.[327] Cadiau et al.[204] reported hydrolytically stable fluorinated metal−organic frameworks, AlFFIVE-1-Ni (KAUST-8) and FeFFIVE-1-Ni (KAUST-9), selectively removed trace water vapor from natural gas (e.g., p/p_0 = 0.05). The complete desorption of the adsorbed water molecules requires a relatively moderate temperature (~105 °C) and about half the energy input for commonly used desiccants such as zeolites 4A (heating to ~250 °C).[12,328] Silica gel desiccants can be recycled at moderate temperature but have only a nominal water adsorption uptake at relatively low water vapor partial pressures. The *fcu*-MOFs based on rare-earth metals (e.g., Tb and Y) and heterofunctional linkers feature high localized charge density and contracted one-dimensional channels, thus give enhanced sorption energetics.[329] To reduce the cost, the cheaper combination of tetrazolate linkers and zinc cations was demonstrated to yield *fcu*-MOFs, kag-MOF-1, which shows steep water vapor adsorption isotherm and could be used for the dehydration of gas streams.[168] Interestingly, the performance of CO_2 adsorption is not affected by the presence of water vapor because of the different adsorption sites for H_2O and CO_2,[330] demonstrating kag-MOF-1 can be used to adsorb water vapor and acid gas simultaneously.

It is speculated here that the limited effect of water vapor in gas adsorption processes may be related to the water adsorption step.[331] As long as the relative pressure is below the onset of the step, water will hardly tend to adsorb (unless secondary effects like interaction with adsorbed species occur),[332] keeping the capacity for the other components intact.

Another example where MOFs are used as selective adsorbents is the organic solvent dehydration.[326] The water uptake of MIL-101(Cr) was 7−8.5 times higher than those commercial 3A and 4A zeolite for 2-dimethyl amino ethyl azide dehydration.[233] Together with the hydrothermal stability, MIL-101 was easily regenerated at 343 K in contrast to the zeolite regenerated at 573 K.[233]

4.2. Heat Pump/Chiller

Reallocation of heat and cold through ad- and desorption is conveniently realized in heat pumps.[7,235,289] The heat pump cycle is briefly described in the Clausius−Clapeyron diagram, wherein the *x*-axis and *y*-axis are typically shown as $(-1/T)$ and $(\ln p)$ (Figure 10). In this case, the isosteric lines are straight and the lowest transport temperature is at the left of the figure. For a given working pair (i.e., water and specified MOFs in this review), the operational conditions are fully fixed when evaporator (T_{ev}), adsorption ($T_1 = T_{con}$), and desorption (T_{des}) temperature are chosen. Generally, this cycle can be used for heating or cooling, wherein the process is evaluated by the coefficient of performance (COP) for heating (the ratio of energy output and energy input, <2.0) or cooling (the ratio of cooling energy extracted and energy input, <1.0), the specific energy capacity and power. More details on the thermodynamic model and thermodynamic properties were described in

https://dx.doi.org/10.1021/acs.chemrev.9b00746
Chem. Rev. XXXX, XXX, XXX−XXX

our previous review paper,[7] where four cases were distinguished to compare various MOFs (Table 5). Here only a status update is given.

A promising adsorbent material should exhibit a large working capacity (ΔW) between the isosteric heating (I–II) and isosteric cooling (III–IV), as $\Delta W = W_{max} - W_{min}$ (Figure 10). The COP approaches its maximum value already at $\Delta W >$ (0.1–0.15) mL/$g_{sorbent}$ for water adsorption and is no longer dependent on ΔW for larger values.[333] To increase the energy capacity, especially for heat storage,[333] the working capacity ΔW must be maximized. The characteristic curve (eq 1 and Figure 11), obtained after transformation of the relative pressure and temperature dependency of the adsorption data to the adsorption potential A, is conveniently used for modeling of cycle performance,[7,334,335] although also other relations for the uptake can be applied.[7,336]

Adsorptive heating is considered as a single case, while cooling is subdivided into three different applications depending on the desired temperature.[7] The optimal adsorbents should have a maximum water uptake (W_{max}) at A = 3.12 kJ mol^{-1} for cooling in refrig-1 region (cooling to 283 K), at A = 3.99 kJ mol^{-1} for cooling in refrig-2 region (cooling to 278 K), and at A = 4.56 kJ mol^{-1} for heating region (318 K) (Figure 11). Thus, the adsorbent optimal for cooling should have higher affinity toward water than that for heating. In the case of ice making (refrig-3), alternatives for water, such as methanol,[339–342] ethanol,[340] ammonia,[343,344] saline water,[345] or fluorocarbon,[242,346] are needed, this is outside the scope of this review.[347]

In choosing a sorbent, a balance must be found between a high affinity for water vapor and the energy required for desorption. A material that binds water more strongly will function at lower RH, but more energy will be required to release and then collect the water. If the evaporation temperature and adsorption temperature are fixed for the heating and cooling (e.g. T_{ev} = 283 K and $T_1 = T_{con}$ = 303 K for refrig-1 cooling[7]), the minimal desorption temperature ($T_{des,min}$) can be estimated by equating the adsorption potential for the isosteric heating and isosteric cooling. This value is equal to that calculated by simple Trouton's rule within an accuracy of ±1 K.[333] Evidently, if the available temperature of desorption T_{des} is lower than $T_{des,min}$, the cycle cannot be realized at all. The temperature lift during the adsorption half-cycle can be defined as the difference between T_{con} and T_{ev}.[7] During desorption, this is the difference between T_{des} and T_{con}.[7] A large temperature lift can be obtained only if the adsorbent has a high regeneration temperature T_{des} and a strong affinity to the adsorptive. However, an increase in COP is often observed at lower T_{des} (Figure 12).

For the realization of an efficient adsorption heat pump or chiller, the MOF has to meet more requirements than a high working capacity and a high COP. Most importantly, the MOF must be thermally coupled to the water sorption circuit as efficiently as possible, as the adsorption kinetics, the specific power and power density directly depend on the mass transport of sorbate to/from and heat transfer of adsorption/desorption energy away/toward the adsorption site.[24] This can be realized by using packed beds with heat exchange plates in between or using packed metal foams, or coating MOFs directly on heat exchange surfaces. A comparison of such a packed bed performance of MIL-101(Cr) and NH_2-MIL-53(Al) shows that mass and heat transport are slow in these systems, resulting in lower efficiency and power density than a

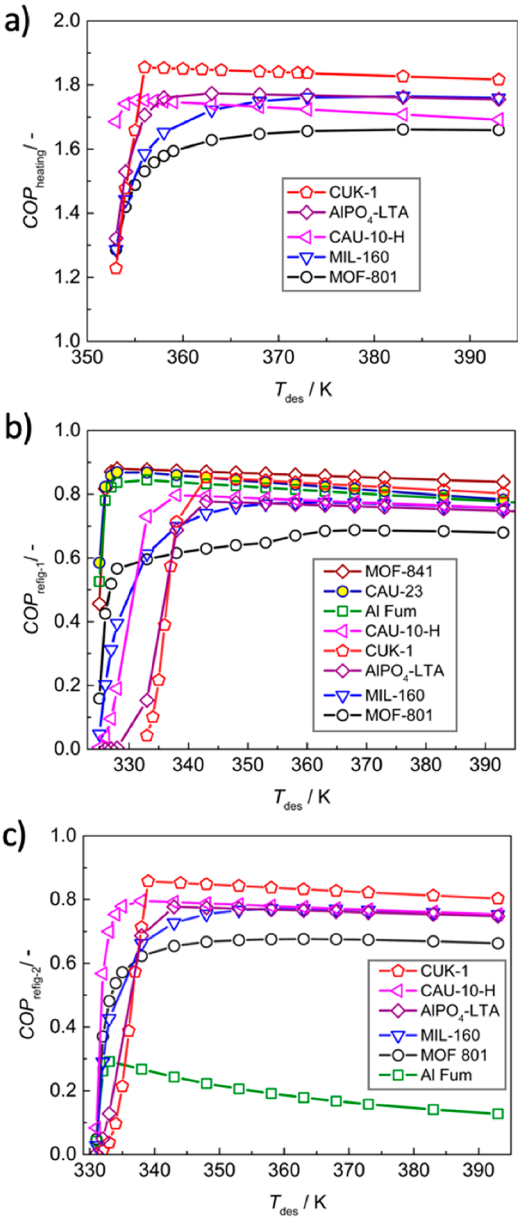

Figure 12. COP as a function of desorption temperature (a) for heat pump heating, (b) for cooling in refrig-1 region, and (c) for cooling in refrig-2 region. The water isotherms used for COP calculation is from various literature sources: CAU-10-H,[200] CAU-23,[99] MIL-160,[100] MOF-841,[75] CUK-1,[205] MOF-801,[334] AlPO-LTA,[338] and Al-Fum.[265,348]

silica gel.[336] Betke et al. improved the heat transportation of CAU-10 (0.08 W m^{-1} K^{-1} for compacted pellet) by intergrowth with reticulated open-cellular alumina foams (0.9–1.78 W m^{-1} K^{-1}).[349] Heat exchangers coated with the adsorbent are by far superior to packed beds, similar as for catalytic reactors,[28] in terms of power delivered per mass of adsorbent.[200,278,280] The optimum coating thickness represented the cases where, as the coating thickness increased, the opposite effects of the increase in adsorbent mass (capacity) and slower transport phenomena (so increasing cycle duration) were most favorable and led to the maximization of power.[23,350] The optimum thickness for triazolyl phoshponate MOF was established as 150 μm.[350] Furthermore, such coating has to be mechanically and chemically stable toward

https://dx.doi.org/10.1021/acs.chemrev.9b00746
Chem. Rev. XXXX, XXX, XXX–XXX

thermal stress during cyclic operation, mechanical shocks, and vibration, for example, due to transportation. These issues are addressed in the literature by the development and evaluation of several routes to obtain thick and sturdy binder-based or binder-free coatings of CAU-10-H,[200,278,280] HKUST-1,[351,352] MIL-125-NH_2,[353] Basolite A520,[24] MOF-801,[334] and MIL-101(Cr).[352] Kummer et al.[24] fabricated a functional full-scale heat exchanger coated with commercial aluminum fumarate (Basolite A520) for adsorption heat transformation (Figure 13). The heat exchanger was evaluated resulting in a gross

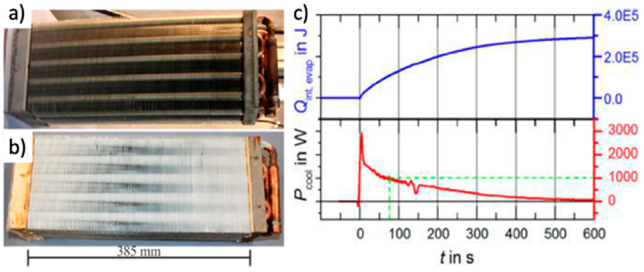

Figure 13. A state-of-the-art water/air finned heat exchanger with aluminum fins pressed onto copper tubes before (a) and after (b) coating with Basolite A520. (c) Gross cooling power P_{cool} and heat of evaporation $Q_{int,evap}$. The green line indicates P_{cool} = 1000 W for a half cycle time of t = 74 s. Reproduced with permission from ref 24. Copyright 2017 American Chemical Society.

cooling power of 2900 W (at the beginning of the adsorption cycle) or, respectively, an average cooling power of 690 W (up to a limit of 90% equilibrium loading in 7 min) under the working conditions of a realistic adsorption chiller of 90 °C/30 °C/18 °C (temperature level of heat source, heat rejection/condenser, and evaporator) (Figure 13). The capacity of the coating remained at 95% after 360 cycles.[24] Another application of adsorptive cooling concerns the production of cooling water for heat removal in a data center.[354] It shows how IT waste heat can be used effectively to cool the storage racks of a large high-performance computing system. The adsorption chiller setup is more than three times as efficient at generating cold than the mechanical chiller supported cold water infrastructure.

An overview of literature learns that several MOF materials have been identified for the reallocation of heat but predominantly on the basis on high working capacity and maximum COP. For real applications, the mass and heat transport properties are essential. The highly porous MOFs are in themselves poor heat conducting materials, while mass transport is comparable with that encountered in adsorption/separation and catalytic processes. Thermal and mass diffusivities in MOFs are to be determined to provide a basis for better comparative modeling and smart ways to improve transport phenomena are to be designed.[21,336,355] In view of the intimate contact between MOF and heat exchange surface coatings seem preferred for higher power delivery (rapid cycling), but system capacities are lower due to the lower sorbent to metal mass ratio.[23] If speed or cycle times are less important (e.g., in seasonal heat storage), then packed beds can be an option.

Considering seasonal storage for, e.g., providing domestical heating, it must be realized that for a family house, ~8 GJ (~2225 kWh) is needed in wintertime (The Netherlands). This corresponds to a required MOF volume of 8−10 m^3, excluding the equipment and water supply. The geographic location, period, and housing size strongly affect this quantity.[356] Clearly, MOF availability and cost are impeding such an application at present.

This paragraph only considered single stage heating devices, but low temperature−high temperature (LT-HT) cascaded systems are also considered for MOFs.[264] However, for the HT stage, much higher regeneration temperatures are required than available from waste heat, and the advantage of low temperature regeneration is lost and classical materials could be used as well. High-throughput computational screening suggest the use of wide pore COFs (1−2 nm) for the LT stage, and more narrow pore MOFs (0.5−1 nm) for the HT stage.[357]

Next to the extensive library of MOFs the first studies with COFs for water adsorption are reported.[44,358,359] They exhibit similar isotherm characteristics as MOFs and may become alternatives without metals.

4.3. Water Harvesting

Water scarcity is a critical challenge in desert and arid regions, which are landlocked and have limited infrastructure. Mature

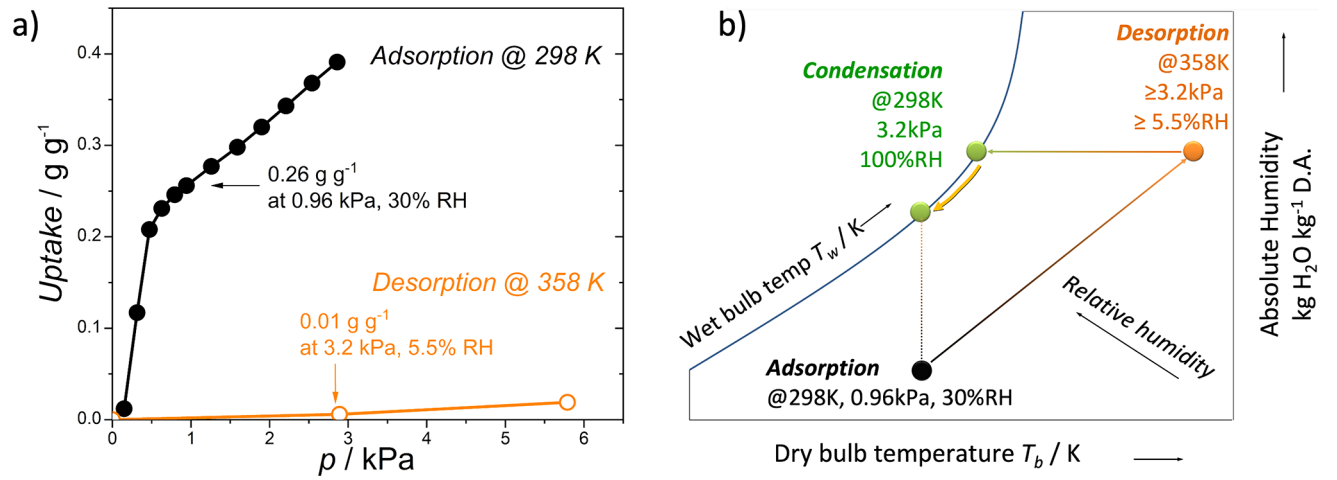

Figure 14. (a) Water adsorption (298 K) and desorption (358 K) isotherms of MOF-801(Zr). The data points are taken from literature,[376] and the desorption branch is built from its adsorption branch at 358 K.[376] (b) Adsorption-based atmospheric water harvesting (AAWH) cycle illustrated with psychrometric chart (atmospheric pressure) using MOF-801(Zr) as an example. Lines are shown to guide the eye.

https://dx.doi.org/10.1021/acs.chemrev.9b00746
Chem. Rev. XXXX, XXX, XXX−XXX

Table 4. MOFs for Water-Adsorption-Driven Chillers (ADCs)

material	T_{evp}	T_{ads}	T_{des}	SCP[c]	$C_{p,MOF}$[i]	COP_C	ΔW g g^{-1}[n]	$\langle -\Delta_{ads}H \rangle$ kJ mol^{-1}	ref
MOF Powder									
Al-fumarate	25	25	60	922	1.05−1.35		0.32	49.8	199,257,265
Al-fumarate (formic acid modulated)	25	25	60	1732			0.36	49.9	265
CAU-23 (Al)	10	30	60	858.9[d]	1.2	0.78	0.35	48.2	99
Co-CUK-1	5	30	70	624.96[d]	NA	0.83	0.24		205
MIP-200	5	30	63	423.72[d]	NA	0.78	0.35		123
Co_2Cl_2(BTDD)	10	30	55	1654[d]	1[k]	0.885	0.65	45.8	203
Ni_2Cl_2(BBTA)	5	30	127	820[d]	1[k]	0.70	0.36	55−50	264
MIL-160	5	30	80	780[d]	1[k]	0.74	0.26	54	100
MWCNT/MIL-100(Fe)	13.5	31.5	100	NA	455	1.25	0.65		372

material	d (thickness) μm	T_{evp}	T_{ads}	T_{des}	t_{ads} s	V_{HX}[a]/VSCP[b]	SCP[c]	$C_{p,MOF}$[i]	COP_C	ΔW g g^{-1}[n]	ref
MOF Coating											
CAU-10(Al)-H[m]	229				NA	NA	337[d,g]	NA	NA	0.14	349
NH_2-MIL-125[m]	400−500	10	30	70−90	200[f]	NA	3200	0.89−1.18	0.77−0.80	NA	226,353
MOF-801	400−500	5	30	85	100[f]	NA	2550	0.76	NA	0.21	73,334
triazolyl phosphonate MOF	150	2	20	110	NA	NA	66700	NA	NA	NA	350

material	d (μm)	T_{evp}	T_{ads}	T_{des}	t_{ads} (s)	V_{HX}[a]/VSCP[b]	SCP[c]	$C_{p,MOF}$[i]	COP_C	ref
MOF Coating on Full Heat Exchanger										
Al fumarate (Basolite A520)[l]	300−330	18	30	90	630[e]	0.68/101[e]	1394[e]	1.20	0.61	24
CAU-10(Al)-H[l]	550	10	30	70	483[e]	0.94/201[e]	1204[e]	1.20[j]	NA	280
CAU-10(Al)-H[l]	550	14	34	70	430[e]	0.94/229[e]	1369[e]	1.21[j]	NA	280
SAPO-34	100	15	25	90	300[h]	0.81/93[h]	675[h]	NA	0.24	373
TiAPSO SCT-323	212	10	35	90	288[e]	1.43/220[e]	2128[e]	NA		23
TiAPSO SCT-323	165	4	39	110	310[e]	1.43/66[e]	1854[e]	NA		23

[a]Volume of heat exchanger, L. [b]Volumetric specific cooling power, W·L^{-1}. [c]Mass specific cooling power, W·kg_{ads}^{-1}; only the mass of MOF was accounted for. [d]Energy capacity, kJ·kg_{ads}^{-1}. [e]Calculation based on the adsorption 0−90% RH. [f]Calculation based on the 0.8 uptake. [g]Calculation based on the adsorption 0−75% RH. [h]Calculation based on the adsorption time. [i]Specific heat capacity, J·K^{-1}·g^{-1}. [j]Temperature dependent by linear regression of 0.87 + 0.0011 × T [J·K^{-1}·g^{-1}]. [k]Assumption. [l]Coating with binder. [m]Pure MOF, without binder. [n]Delivery capacity in g g^{-1}.

water purification technologies including reverse osmosis and multistage flash are impractical to implement. Atmospheric water harvesting (AWH)[374,375] is a potential alternative which can utilize renewable or waste energy from ambient surroundings, for instance, solar and wind energy. State-of-the-art AWH technology captures water using direct cooling. However, a decreasing humidity causes a dramatic increase of energy penalty because larger quantity of air has to be cooled down and the dew point of water can be hardly reached above 273 K. One way to revitalize AWH technology is exploring adsorption-based atmospheric water harvesting (AAWH),[231,376] where water vapor from arid atmosphere is first enriched in an adsorbent, followed by desorption and condensation. Hygroscopic salts play an important role in such water sorption technology, but leakage of salt solution is an issue. Considering the adsorption−desorption characteristics of water on MOFs it was merely a matter of time before these were considered for this application. In 2012, the first public example of fresh water production is given in supplementary info using MIL-100(Fe),[210] and in 2014, Yaghi et al.[75] proposed MOFs as adequate adsorbents for AAWH in arid atmospheres. A few MOF samples, e.g., UiO-66(Zr),[377] MIL-53(Al),[377] Basolite F300 (Fe),[377] MOF-801(Zr),[73,74,76] MOF-303(Al),[74] and Al-fumarate[74] have been investigated. Here, we take MOF-801(Zr) as an example to illustrate the working principle of AAWH.

Figure 14 shows water adsorption and desorption isotherms at 298 and 358 K, respectively. First, 0.26 g water (per gram MOF-801(Zr)) is adsorbed at 298 K (@0.96 kPa and 30% RH, setting as the typical arid condition in this work), and then almost all water (0.25 g g^{-1}) is released at 358 K (3.2 kPa and 5.5% RH). A schematic psychrometric chart (Figure 14) illustrates the AAWH process. Adsorption of water vapor from the atmosphere is the first step (@30% RH, 0.96 kPa, 298 K), concentrating water in the adsorbent (exothermal process). Subsequently, water desorption (@358 K, 5.5% RH, 3.2 kPa) is induced by heating and the absolute humidity is increased (endothermal process). Finally, the dew point is reached by cooling, and condensation (@100% RH, 3.2 kPa, 298 K) takes place (exothermal process). Pressurization increases the water yield but at an additional energy penalty.

The minimum energy for evaporating water is 40.7 kJ/mol, but in practice more energy is needed as the ideal process design can be hardly realized. From an energy-saving point, the temperature for condensation is set identical to that of adsorption and the sensible heat removal for cooling can be supplied by the environment. The final water vapor pressure at the desorption stage is higher or equal to the saturated vapor pressure at the temperature of condensation. This desorption temperature should be as low as possible to minimize the sensible energy for heating the sample but must be high enough to stay below the steep step of the desorption branch (see Figure 3). The latter is identical to the adsorption uptake step if hysteresis is absent.

Several following parameters are defined to evaluate the performance of one capture cycle:

Gravimetric productivity per cycle (P_c^g)

$$P_c^g = \frac{m_{collected}}{m_{MOF} n_c} \quad (3)$$

https://dx.doi.org/10.1021/acs.chemrev.9b00746
Chem. Rev. XXXX, XXX, XXX−XXX

where $m_{collected}$, m_{MOF}, and n_c are the mass of water collected, mass of MOF adsorbents, and the number capture cycles. P_c^g is converted into volumetric productivity (P_c^v) using crystal density (ρ_c):

$$P_c^v = \rho_c P_c^g \tag{4}$$

Similarly, daily productivities can be defined using the number of cycles per day (24 h).

Energy taken up (minimum to be provided) per unit mass water released in desorption

$$Q_d = -\Delta_{ads}H + \frac{(m_{captured}c_{p,water} + m_{MOF}c_{p,MOF})(T_{des} - T_{ads})}{m_{released}} \tag{5}$$

and energy released (minimum to be removed) per unit mass water collected in condensation:

$$Q_c = \Delta_{vap}H + \frac{(m_{captured}c_{p,water} + m_{MOF}c_{p,MOF})(T_{des} - T_{con})}{m_{collected}} \tag{6}$$

where $\Delta_{vap}H$ is the enthalpy of water evaporation; $m_{captured}$ and $m_{released}$ are the mass of water captured in adsorption and released in desorption, respectively; $c_{p,water}$ and $c_{p,MOF}$ represent the heat capacity of water and MOFs, respectively. The values of $c_{p,MOF}$ are taken from Table 4 or assumed to 1 J/(g·K), if unavailable. T_{ads}, T_{des}, and T_{con} are the temperatures for adsorption, desorption, and condensation, respectively. Further, it is assumed that $m_{collected} = m_{released}$ and $T_{ads} = T_{con}$. The material properties for both reported and potential MOFs for AAWH are summarized in Table 6 together with the calculated parameters.

Table 5. Operational Temperatures of Heat Pump for Heating and Cooling

	heat pump	refrig-1	refrig-2	refrig-3[a]
T_{ev} (K)	288	283	278	268
T_{con} (K)[b]	318	303	303	298

[a]Water cannot be employed as working fluid. [b]$T_{ads} = T_{con}$.[7]

To quantify the minimum energy required for a water capture cycle, we assume the heat released in adsorption and condensation processes can be removed by the surrounding cool air at night, and Q_d is selected for comparison, although it can partially be supplied by the ambient hot air during daytime. Alternatively, application of electricity from PV panels can be considered. Ideal MOFs for AAWH should have a high P_c^v while keeping Q_d as low as possible (Figure 15). On the basis of the eqs 3−5, the following properties are the rational criteria for selecting MOFs: high volumetric working capacity, low adsorption heat (i.e., $-\Delta_{ads}H$), low heat capacity ($c_{p,MOF}$), and low desorption temperature (T_{des}). A low inflection point of the uptake step (for instance 0.09 for MOF-801(Zr)[75,376] and MIL-160(Al)[100]) is mandatory in the case of a very arid atmosphere (e.g., RH < 15%). As indicated in Figure 15, Co_2Cl_2(BTDD)[203] delivers the highest P_c^v (0.51 g mL^{-1} c^{-1}) and Co-CUK-1[205] requires the lowest Q_d (54.0 kJ mol^{-1}). It is noted that, for the aforementioned calculation, the crystal density is used instead of a particle or coating density and the energy for heating the construction[23] and air are not considered. Nevertheless, in a real case, the overall consumed energy (i.e., the operating cost) is always several times higher, as exemplified for the MOF-303(Zr) based water harvester calculated with the device power.[17] The thermal efficiency is around 14%,[76] so 6 times more energy must be provided.

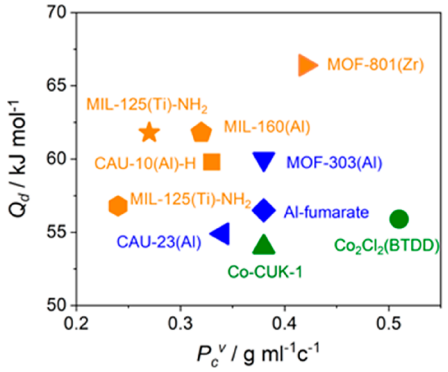

Figure 15. Volumetric productivity per cycle (P_c^v) versus energy taken up per mol water released in desorption (Q_d). The data points are taken from Table 6.

Table 6. MOF Properties for Adsorption-Based Atmospheric Water Harvesting

MOFs	α [−][a]	q_{water} [g g^{-1}][b]	T_{des} [K][c]	RH_{des} [−][d]	p_{des} [kPa][e]	P_c^g [g g^{-1}c^{-1}]	P_c^v [g mL^{-1}c^{-1}][f]	P_d^g [g g^{-1}d^{-1}]	P_d^v [g mL^{-1}d^{-1}][g]	$-\Delta_{ads}H$ [kJ mol^{-1}]	Q_d [kJ mol^{-1}]	Q_c [kJ mol^{-1}]
MOF-801(Zr)[75,376]	0.09	0.26	358	5.5%	3.2	0.25[h]	0.42	0.1[i]	0.168[i]	58.4[75]	66.4	52.1
MOF-303(Al)[74]	0.13	0.37	358	5.5%	3.2	0.33[h]	0.38	1.3[j], 0.7[k]	1.5[j], 0.8[k]	49	60.0	55.1
Al-fumarate[199]	0.27	0.33	333	16%	3.2	0.31	0.38	0.55[j]	0.68[j]	50	56.5	50.6
Co_2Cl_2(BTDD) [203]	0.29	0.87	328	20%	3.2	0.74	0.51			45.8	55.9	54.1
MIL-125(Ti)-NH_2[202]	0.2	0.36	333	16%	3.2	0.30[l]	0.24			50.5[226]	56.8	50.4
MIP-200(Zr) [123]	0.18	0.40[m]	333	16%	3.2	0.23	0.27			55	61.8	50.9
CAU-23(Al) [99]	0.27	0.35	333	16%	3.2	0.32	0.34			48.2	54.9	50.8
MIL-160(Al) [100]	0.09	0.35	353	6.8%	3.2	0.30[285]	0.32			52	61.8	53.9
CAU-10(Al)-H[200]	0.16	0.31	333	16%	3.2	0.29[284]	0.33			53.5	59.8	50.4
Co-CUK-1[205]	0.12	0.28[m]	343	10%	3.2	0.26[n]	0.38			46.9	54.0	51.2

[a]Inflection point, the relative pressure for which capacity is 50% of q_{max}. [b]Water uptake at 298 K, 30% RH (0.96 kPa). [c]Desorption temperature. [d]Desorption relative humidity (RH). [e]Desorption vapor pressure. [f]P_c^g is converted using crystal density from Table 3. [g]Productivity for 24 h. [h]Equilibrium uptake in desorption is taken from adsorption branch. [i]Desert of Arizona.[74] [j]Indoor environment.[17] [k]Mojave Desert.[17] [l]Equilibrium uptake in desorption taken from adsorption branch at 3.7 kPa.[226] [m]303 K. [n]Equilibrium uptake in desorption taken at 4.2 kPa.

https://dx.doi.org/10.1021/acs.chemrev.9b00746
Chem. Rev. XXXX, XXX, XXX−XXX

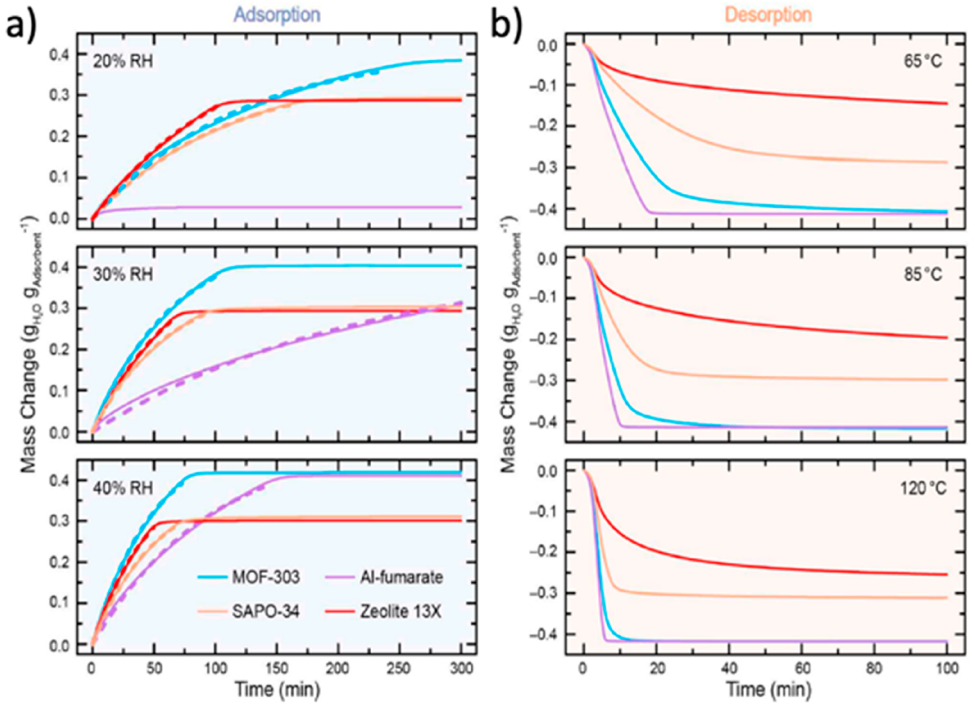

Figure 16. Water adsorption (a, 303 K) and desorption (b, 0% RH) profiles on MOFs (MOF-303(Al) and Al-fumarate) and zeolites (SAPO-34 and 13X). The dashed lines are the monoexponential curve fits. Prior to adsorption (desorption), the adsorbents were fully activated (saturated at 303 K under 40% RH). Reproduced with permission from ref 17. Copyright 2019 American Chemical Society.

In addition to the volumetric productivity per cycle (P_c^v) and energy required for desorption Q_d, the capture rate is another vital parameter for evaluating the performance of AAWH, which can be reflected by the volumetric productivity per day (P_d^v) converted from the mass productivity (P_d^g) with the crystal density (ρ_c):

$$P_d^g = \frac{m_{collected}}{m_{MOF} n_d} \tag{7}$$

$$P_d^v = \rho_c P_d^g \tag{8}$$

Also here the intra/intercrystalline mass and heat transport properties dictate the capture rate, which determines the footprint and the capital cost of AAWH systems. A framework for optimizing the AAWH systems on adsorption kinetics was recently discussed by Wang et al.,[376] which is not repeated here.

A systematic experimental study on the adsorption kinetics was conducted by Yaghi et al.[17] using MOF-303(Al), Al-fumarate, zeolite SAPO-34, and 13X as probe adsorbents. At 20% RH, the zeolite 13X is the fastest for adsorbing water while MOF-303(Al) has the most favorable kinetics at higher RH (Figure 16). In desorption, Al-fumarate responds faster than MOF-303(Al). Both zeolites exhibit relatively slow kinetics and the trapped water in zeolite 13X could not be desorbed within 10 h even at 393 K. These results recommend MOF-303(Al) and Al-fumarate as superior adsorbents over the zeolites. The P_d^v value of MOF-303(Al) (1.5 g $mL_{MOF}^{-1}d^{-1}$) is more than 2 times of Al-fumarate (0.68 g mL_{MOF}^{-1} d^{-1}) due to the different uptake kinetics and confirmed by the further indoor experiment (Table 6), highlighting the primary importance of adsorption kinetics. The feasibility of the MOF-303(Al) harvester in practice was examined in the extremely dry Mojave Desert (Figure 17),[17] employing a construction similar as the so-called "three-levels-of-porosity" (TLP) catalytic reactor.[30] The P_d^v value is 0.8 g mL^{-1} d^{-1} in a continuous 3 day run.

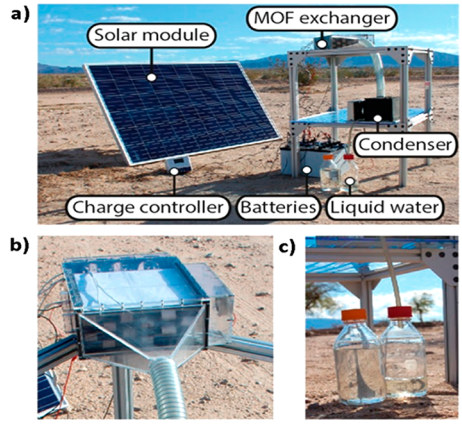

Figure 17. (a) MOF-303(Al) harvester unit in the Mojave Desert, (b) MOF adsorber, and (c) water container. Reproduced with permission from ref 17. Copyright 2019 American Chemical Society.

MOF AAWH is still in its infancy stage. Until now, only MOF-801(Zr) and MOF-303(Al) have been tested under practical conditions (Table 6). The following points require further attention: (1) More potential MOFs are to be tested under practical conditions, identifying their optimal applicability range of conditions. (2) The quality of the harvested water should be reported. Water produced by systems with MOFs based on certain transition metals may not stand the hygiene tests for human consumption.[378] (3) Combination and comparison with mature harvesting technology (e.g., direct cooling) should be evaluated to broaden the range of climates.

https://dx.doi.org/10.1021/acs.chemrev.9b00746
Chem. Rev. XXXX, XXX, XXX−XXX

Further optimization of the whole AAWH system seems realistic. (4) How to realize the large continuous supply of air in arid regions and the effect on the capital and operating expenses.

4.4. Humidity Control

As advised by the American Society of Heating, Refrigerating, and Air-Conditioning Engineers (ASHRAE), the proper indoor relative humidity (RH) for comfortable and healthy environment for human beings falls in the range from 45% to 65%.[195] MOF adsorbents could well regulate the humidity level[210] if these materials sharply adsorb water vapor when the RH is above 65% and swiftly release vapor as RH is below 45% (Figure 18). Such an adsorptive humidity control avoids the classical cooling−dew pointing−reheating cycle resulting in a better energy efficiency.

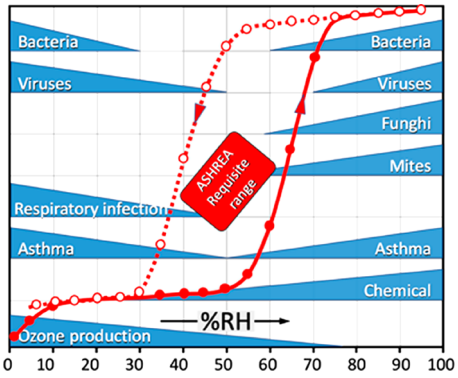

Figure 18. Recommended relative humidity window for a healthy indoor atmosphere and the achievable control window by using MOFs. Adapted with permission from ref 195. Copyright 2017 American Chemical Society.

As reported by Eddaoudi et al., Y-shp-MOF-5[195] shows type IV water adsorption/desorption isotherms with inflection points at 63% (adsorption) and 37% RH (desorption) (Figure 7), which perfectly matches the recommended working range (45−65%) for the indoor humidity level control. Not surprisingly, under the cycling conditions (45−65% RH), Y-shp-MOF-5 retains its performance with a working capacity of nearly 33 wt % and outperforms mesoporous MCM-41 by virtue of its good stability. Furthermore, another candidate, Cr-soc-MOF-1[194] developed by the same team, exhibits outstanding working capacity under various indoor humidity levels. It outperforms both Y-shp-MOF-5 and MCM-41 by its excellent capacity, even on a volume basis (Figure 7).

For air-conditioning and drying, other MOFs with lower inflection points (Figure 7, 8, and 9) can also be utilized for dehumidification together with process optimization,[12,210,327] which potentially consume less energy compared to the dew-pointing step. This is well summarized in previous reviews.[12,25]

In these open systems, coadsorption of volatile organic compounds (VOCs) and moisture can occur, beneficial to improving indoor air quality, but unwanted release of harmful VOCs is undesired. Controlled release and degradation of VOCs into nontoxic products[12,379,380] could possibly mitigate this issue, e.g., by incorporating a catalytic function on the MOF.[381,382]

More applications of humidity control are for industrial cooling and drying,[383] in combined cooling−heating and power cogeneration (CCHP), and in data centers.[354] Clearly other specific MOF characteristics may apply, not only regarding application but also on the geographical location.[354] A home appliance for dishwashing has been successfully commercialized with a zeolitic material.[384] An energy reduction of ∼1 kWh and an excellent drying performance is achieved.[385,386] The low regeneration temperature suggests MOFs as extremely interesting alternative sorbents.

4.5. Desalination

Various commercial desalination technologies exist to produce fresh water from brackish or seawater.[387,388] A relatively new, emerging technology is the adsorption desalination (AD).[389] It is based on a combination of adsorption−desorption cycles integrated with low-grade heat utilization, providing high quality water and cooling.

The adsorption desalination system basically consists of an evaporator, a packed bed adsorber, and a condenser operated at reduced pressure. In one half-cycle, evaporated water is adsorbed in a cold bed, and in the next half-cycle, the sorbent is regenerated with a low temperature heat source, typically 50−85 °C. Heat exchange is integrated in all units. Chilled water is produced in the evaporator and used to cool the condenser. The sorbent is often packed in a tube-fin heat exchanger. Cooling water is used to remove the adsorption heat during loading. After saturation, the adsorber is regenerated with low-grade heat and the desorbed water vapor is liquified and collected in the cold condenser.

The use of a pair of parallel beds allows a more continuous swing operation, one in adsorption and one in regeneration mode, and in various designs several bed pairs are used, thereby increasing the specific daily water production (SDWP) and changing cycle times.

The thermodynamic cycle is similar as for a heat pump (Figure 10),[390] but now as an open system with the focus on water production, although in cogeneration, cooling effects can also be achieved by a lower temperature in the evaporator relative to the adsorber and condenser. An equal or higher temperature restricts the operation to desalination only.

The development of the AD technology is demonstrated for traditional silica gel[391] and used in benchmarking other materials. Pilot plants (Figure 19) have been demonstrated at academia, the National University of Singapore and the King Abdullah University of Science and Technology.[392] Reported SDWP values range up to 10 $m^3/(tonne_{silica}$ day) for a two-bed system. The performance ratio (PR), the ratio between the energy used for evaporation of the produced water and the heat used for regeneration of the bed, increases with decreasing regeneration temperature (0.6−0.75). In cogeneration the specific cooling power (SCP), the amount of cooling per mass of sorbent is another assessment parameter.[393]

Here the use of MOFs become interesting for their peculiar adsorption and regeneration properties.

Using CPO-27(Ni), also reported as MOF-74(Ni), an SDWP of 22.8 $m^3/(tonne_{MOF}$ day) and an SCP of 750 W/kg_{MOF} could be realized in a one-bed system at evaporation−condenser−desorption temperatures of 40, 5, and 95 °C, respectively, highlighting the potential of MOFs in AD.[394] A comparative study with CPO-27(Ni), Al-fumarate, and MIL-101(Cr) demonstrated the use of MOFs in AD. At evaporation−adsorption−condenser temperatures of 20, 25, and 25 °C, SDWP values of 4.6, 6.3, and 11 $m^3/(tonne_{MOF}$ day) were reached, respectively, but at a high regeneration temperature of 150 °C. Although on a mass basis this was the

https://dx.doi.org/10.1021/acs.chemrev.9b00746
Chem. Rev. XXXX, XXX, XXX−XXX

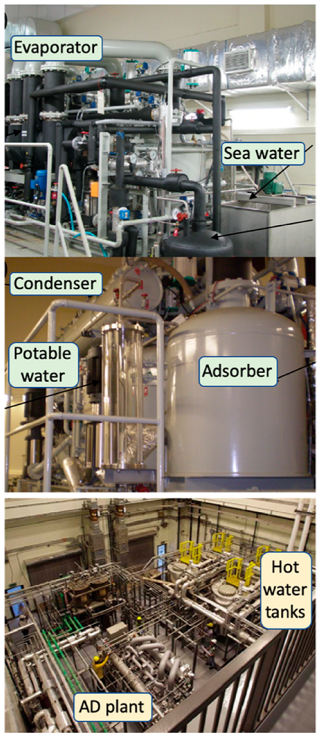

Figure 19. Pictures of adsorption desalination test facilities at NUS (top, middle) and KAUST (bottom). Reproduced with permission from ref 392. Copyright 2013 Elsevier.

highest for MIL-101,[232] correcting for the density (Table 3) shows that Al-fumarate stands out per unit volume sorbent by ~40%. Lower regeneration temperatures down to 70 °C did not affect its SDWP but strongly impacted the other MOFs' performances due to the desorption hysteresis of MIL-101 (Figure 7) or to the strong adsorption in CPO-27. Al-fumarate hardly exhibits hysteresis and can therefore be regenerated at lower temperatures (see Figures 3 and 7). A recent study of the same team with a two-bed system confirmed that Al-fumarate outperformed both silica and CPO-27(Ni) depending on the operation temperatures and the operation mode (pure desalination or cogeneration).[395] The water (SDWP up to 14 $m^3/(tonne_{MOF}$ day)) has a high distilled water quality, is produced at a low thermal and electricity consumption, and at the lowest cost (0.3 $/$m^3$) in comparison with other standard operations (reversed osmosis, multieffect distillation, and multistage flash).[395] The reported AD productivities are an order of magnitude large than in water harvesting. Apart from the technology development level, this is importantly due to the wider range of humidities in AD.

These data exemplify the potential of MOFs in AD. The step location in the MOF isotherm and absence of hysteresis determine the operation temperatures window in the system. Not many MOFs have been explored yet for this application, but the demonstrated low regeneration temperature for Al-fumarate is especially attractive for an energy efficient operation.

5. EVALUATION AND OUTLOOK

MOFs exhibit a characteristic uptake step of water, easy water release and high mass specific capacities, distinguishing them from most other porous sorbents, and making them attractive for various applications and processes where humidity control, water production, and evaporation and energy reallocation using water as benign component is the essential basis. In this review, specifically desiccation, heating/cooling, water harvesting, humidity control, and desalination, have been presented as those are the most advanced, although other applications, such as drying and storage, can be thought of.

The steep water adsorption/desorption step much below 100% RH allows energy efficient operation over a small temperature and relative humidity window, without formation or presence of liquid water, interesting in, e.g., food preservation. This eliminates growth of microorganisms and avoids water condensation−evaporation energy management in humidity control. The "ultralow" driving temperature range of ~55−85 °C for water desorption allows the use of low-grade waste heat or renewable energy from solar panel heating, increasing energy utilization from renewable sources, and decreasing the consumption of primary fossil sources, thereby reducing the impact on the environment.[7]

Apart from the essential hydrothermal stability of the MOFs under long-term cyclic operation, in most lab-scale studies predominantly only basic characterization parameters for a certain application are determined. These include the location (relative pressure) of the adsorption and desorption step, the working capacity, and COP's depending on the applied operating temperatures. Although most uptake capacities are given on a mass basis (g_{H2O}/g_{MOF}), reporting in volumetric units (g_{H2O}/mL_{MOF}) is essential for judging the system volume needed, moderating the high mass specific working capacities of low-density MOFs, and placing them in better perspective. From an extensive suite, 18 interesting MOFs have been identified for adsorptive heat reallocation, many possessing 1D channels. Several MOFs are also suited for water harvesting, air-conditioning, and desalination, although R&D with MOFs in these latter cases is still limited and more materials should be evaluated.

On the basis of the many MOFs that have been explored, the insight in the factors affecting the shape of the water isotherm, location, and steepness of the adsorption step and presence or absence of hysteresis (hydrophobicity/hydrophilicity, pore size, and pore structure) can be used for further development of dedicated MOFs. Even COFs appear at the horizon with similar characteristics as MOFs.

As stated in the introduction, for the application mass and heat transport kinetics are essential and appear to have an adverse effect on the expected performance based on the thermodynamically determined basic parameters. MOFs are highly porous and consequently are poor heat conductors, with similar low thermal conductivities ($\lambda \sim 0.2-1.2$ $W{\cdot}m^{-1}{\cdot}K^{-1}$) and heat capacities ($C_p = \sim 0.5-1$ $J{\cdot}g^{-1}{\cdot}K^{-1}$) as zeolites.[99,231] In packed beds, this transport mainly occurs through the porous particle contact points, lowering at least 1 order of magnitude the pristine (crystal) MOF values.[396,397] The use of binders and coatings is used to alleviate this drawback.[280,336] Because not only conduction plays a role but also the heat capacity of the materials, a better parameter to characterize the thermal transport is the thermal diffusivity $a = \lambda/(\rho{\cdot}c_p)$ [m^2 s^{-1}] that describes how fast temperature profiles move in the system (see Figure 2). The low heat capacity is positive in this sense, but particle and bed porosity and conductive support structures have an adverse effect.

Mass transport occurs by pore diffusion,[336] strongly coupled with adsorption and heat release, phenomena having a strong impact on the response time of the application.[17,75,280] As in

https://dx.doi.org/10.1021/acs.chemrev.9b00746
Chem. Rev. XXXX, XXX, XXX−XXX

heterogeneous catalytic processes, one has to combine intensive (scale independent) and extensive (scale dependent) variables. Structuring of the system on the micro-, meso-, and macro level can to a certain extent decouple these phenomena, leaving more degrees of design freedom.[398,399] Coatings versus packed beds have opposite effects regarding heat and mass transport, and optimization is required by smart engineering, where additive manufacturing opens new opportunities.[400] Determination of water diffusivity and heat conductivity of MOFs in the systems under study is still limited and requires more attention to evaluate if promising properties of a MOF can be successfully translated into an application.

Most applications are stationary systems in which the cyclic swing operation is engineered into semicontinuous or continuous mode by multibed or rotating wheel use, where cycle times of tens of minutes to hours are acceptable. Small-scale mobile applications, e.g., vehicle air conditioning or personal water harvesting in dry areas require continuous operation with shorter cycle times. In the absence of waste heat sources, an alternative such as electricity is obvious.

Regarding applications, more factors than performance play a role, like availability, economics, and acceptability. For test systems, more than lab-scale amounts of MOFs are needed, and their availability and cost evaluation should be considered.[280] Production scale-up developments will improve availability and may cut the lab-scale cost price (e.g., CAU-10-H ~ 60 €/kg)[280] to levels that the MOF-based application can compete with those using benchmark materials.[401] Conceptual process designs and sensitivity analyses are essential to provide the insight to what extent and at what price MOF-based systems outperform those based on classical sorbents, similarly as, e.g., done for CO_2 capture.[402]

Concerning acceptability, the type of MOF used will be subjected to scrutiny regarding toxicity of the used building blocks, linker, and metal, and regarding the application, being an open or closed system.[378,403] In water harvesting, no harmful species may end up in the produced drinking water and unsuspected MOF building blocks should be used, or even metal-free COF alternatives can be considered. On the other hand, in long-term cyclic operations around ambient conditions, microorganism growth should be avoided and some metal nodes (Ag^+, Cu^{2+}, and Ni^{2+}) can have an antibacterial function.[193] Addition of a catalytic function can be considered.

In all cases, applications should be compared against competing systems and their developments. Utilizing renewable energy to drive MOF applications also holds for these competitors. Renewable electricity may become increasingly available and cheaper, changing the operating cost picture in comparative analyses.

Considering all these elements needed to develop MOFs toward adsorption-based applications, a collaborative effort of chemists, materials scientists, and engineers is required.

6. CONCLUSIONS

Metal−organic frameworks have an exciting potential for application in water adsorption-based applications for humidity control and reallocation of heat, like heat pumps, energy storage, drying, air-conditioning, and emerging technologies of water harvesting and desalination. The characteristic uptake step at defined relative pressure allows energy efficient operation over a small temperature and relative humidity window with a large working capacity, unlike classical sorbents. Regeneration can be achieved at ultralow driving temperature levels of low-grade heat (~55−85 °C), allowing the use of the abundantly available industrial waste heat and renewable energy from solar panel heating. The insight in the factors that determine the shape of the isotherm, the location of the step, and the presence of a hysteresis allows the further development or fine-tuning of MOFs for a specific application.

For heat reallocation, 18 MOFs have been identified from an extensive suite that combine an excellent hydrothermal stability under humid conditions with good working capacity at optimal relative humidities. Several MOFs have been operated for thousands of adsorption−regeneration cycles without deterioration. Some of these MOFs are also suited for water harvesting and air-conditioning, although R&D in the latter cases is still limited and more materials should be evaluated.

Apart from the intrinsic adsorption and stability qualities, scale-dependent heat and mass transport in MOFs and packings are often rate controlling in the application. This topic needs more R&D. Structuring the MOFs on different levels can improve a lot, e.g., by coatings and additive manufacturing.

It is recommended further that the working capacity of MOFs is given and compared on a volume basis to account for the large differences in density, after all in practice volume counts. For heat transport, the thermal diffusivity should be used, as it accounts for both the thermal conductivity and the heat capacity of the MOF system under study.

Next to performance, availability, economics, and acceptability of MOFs for the specific applications have to be considered. Sufficient amounts are required and at acceptable cost, while conceptual process designs (CPD) and life cycle analyses (LCA) can guide essential further R&D directions. This requires a concerted effort bridging chemistry, materials science, and engineering.

AUTHOR INFORMATION

Corresponding Author

Freek Kapteijn − *Catalysis Engineering, Chemical Engineering Department, Delft University of Technology, 2629 HZ Delft, The Netherlands;* orcid.org/0000-0003-0575-7953; Phone: +31 15 278 3516; Email: f.kapteijn@tudelft.nl

Authors

Xinlei Liu − *Catalysis Engineering, Chemical Engineering Department, Delft University of Technology, 2629 HZ Delft, The Netherlands; Chemical Engineering Research Center, School of Chemical Engineering and Technology and Tianjin Key Laboratory of Membrane Science and Desalination Technology, State Key Laboratory of Chemical Engineering, Tianjin University, 300072 Tianjin, China;* orcid.org/0000-0001-7552-1597

Xuerui Wang − *Catalysis Engineering, Chemical Engineering Department, Delft University of Technology, 2629 HZ Delft, The Netherlands; State Key Laboratory of Materials-Oriented Chemical Engineering, Jiangsu National Synergetic Innovation Center for Advanced Materials, College of Chemical Engineering, Nanjing Tech University, 210009 Nanjing, China;* orcid.org/0000-0003-2220-7531

Complete contact information is available at: https://pubs.acs.org/10.1021/acs.chemrev.9b00746

https://dx.doi.org/10.1021/acs.chemrev.9b00746
Chem. Rev. XXXX, XXX, XXX−XXX

Author Contributions

X. L. and X. W. contributed equally.

Notes

The authors declare no competing financial interest.

Biographies

Xinlei Liu (1985) received his Ph.D. in 2013 at Dalian Institute of Chemical Physics. After postdoc positions at Imperial College London (2013−2016) and Delft University of Technology (2016−2019), he became a professor at Tianjin University in 2019. He is interested in membranes and porous framework chemistry for energy and environmental science.

Xuerui Wang (1987) received his Ph.D. in 2014 at Nanjing Tech University. After postdoc positions at National University of Singapore (2015−2017) and Delft University of Technology (2017−2019), he became a professor at Nanjing Tech University in 2019. He is interested in microporous membranes and (noble) gas separation in energy- and environment-related fields.

Freek Kapteijn (1952), M.Sc. in Chemistry and Mathematics, received his Ph.D. in 1980 at the University of Amsterdam. After postdoc positions (Coal Science) in Amsterdam and Nancy (ENSIC), he became Associate Professor in Amsterdam. He moved to Delft University of Technology in 1992 and was appointed "Anthonie van Leeuwenhoek professor" in 1999 and chaired the Catalysis Engineering team from 2008 till 2019. He holds the prestigious Golden Hoogewerff award and is among the highly cited "Cross-Field" scientists 2018 and 2019. His research interest focuses on the interplay of catalysis and engineering, comprising structured and multifunctional catalysts, adsorption, separation, and (catalytic) membranes. He co-authored over 650 publications in peer-reviewed journals and as book chapters.

ACKNOWLEDGMENTS

We acknowledge valuable input and discussions with Prof. J.-S. Chang (KRICT), Dr. S. Marx (BASF), Dr. S.J. Ernst (ISE Fraunhofer), Prof. S. Wang (USTC), and Prof. M. Eddaoudi (KAUST). X.L. is grateful to the Peiyang Scholars Program (Tianjin University) for the New Professors Starting Grant. X.W. acknowledges the financial supports from the National Natural Science Foundation of China (21908097) and the Jiangsu Specially-Appointed Professors Program.

ABBREVIATIONS

Symbols

A = adsorption potential, kJ·mol^{-1}
α = relative pressure at inflection point adsorption step
$C_{p,water}$ = specific heat capacity of water, J· K^{-1}·g^{-1}
$C_{p,MOF}$ = specific heat capacity of MOF, J· K^{-1}·g^{-1}
COP = coefficient of performance
d = coating thickness, μm
d_{pore} = size of MOF cage or cage, Å
d_{window} = size of MOF aperture or cage window, Å
D_c = critical diameter for capillary condensation, nm
E = characteristic adsorption energy, kJ·mol^{-1}
E_a = activation energy, kJ·mol^{-1}
ΔG = free Gibbs energy change, kJ·mol^{-1}
$(-\Delta_{ads}H)$ = heat of adsorption, kJ·mol^{-1}
$\Delta_{vap}H$ = enthalpy of evaporation, kJ·mol^{-1}
λ = thermal conductivity, W·m^{-1}·K^{-1}
$m_{captured}$ = mass of water captured, g
$m_{collected}$ = mass of water collected, g
m_{MOF} = mass of MOF adsorbents, g
$m_{released}$ = mass of water released, g
n = fit parameter in DA equation
n_c = number of capture cycles
p = partial pressure of water vapor, kPa
p_0 = saturated pressure of water vapor, kPa
(p/p_0) = relative vapor pressure
P_c^g = gravimetric water productivity per cycle, g g_{MOF}^{-1} c^{-1}
P_c^v = volumetric water productivity per cycle, g mL_{MOF}^{-1} c^{-1}
P_d^g = gravimetric water productivity per day, g g_{MOF}^{-1} d^{-1}
P_d^v = volumetric water productivity per day, g mL_{MOF}^{-1} d^{-1}
PR = performance ratio, energy water evaporation/bed regeneration
q_{max} = maximum water uptake capacity, g·g_{MOF}^{-1}
q_{water} = water uptake at specific conditions, g·g_{MOF}^{-1}
Δq = working capacity, g·g_{MOF}^{-1}
Q_c = energy released per unit mass water collected in condensation, kJ·mol^{-1}
Q_d = energy taken up per unit mass water released in desorption, kJ·mol^{-1}
R = universal gas constant, J·mol^{-1}·K^{-1}
RH = relative humidity, %
S_{BET} = BET area, m^2·g^{-1}
SCP = mass specific cooling power, W·kg_{ads}^{-1}
SDWP = specific daily water production, often given in (m^3/(tonne$_{MOF}$ day)), L kg^{-1} d^{-1}
t_{ads} = adsorption time, s
T_{ads} = adsorption temperature K, °C
T_b = dry bulb temperature K, °C
T_c = critical temperature K
T_{con} = condensation temperature K, °C
T_{des} = desorption temperature K, °C
T_{ev} = evaporator temperature K, °C
T_w = wet bulb temperature K, °C
V_{HX} = volume of heat exchanger, L
VSCP = volumetric specific cooling power, W·L^{-1}
V_p = pore volume, cm^3·g^{-1}
σ = Van der Waals diameter, nm
ρ_c = crystal density, g·mL^{-1}
W_{sat} = saturation water uptake, g·mL_{MOF}^{-1}
W_{max} = maximum water uptake, g·mL_{MOF}^{-1}
W_{min} = minimum water uptake, g·mL_{MOF}^{-1}
ΔW = working capacity, g·mL_{MOF}^{-1}

MOF Acronyms

BUT = Beijing University of Technology
CALF = Calgary Framework
CAU = Christian Albrechts University
COF = covalent organic framework
CUK = Cambridge-University-KRICT
DUT = Dresden University of Technology
HKUST = Hong-Kong University of Science and Technology
IISERP = Indian Institute of Science Education and Research, Pune
JUC = Jilin University, Changchun
KAUST = King Abdullah University of Science and Technology
MAF = metal azolate framework
MIL = Matériel Institut Lavoisier
MIP = Materials of the Institute of Porous Materials from Paris

https://dx.doi.org/10.1021/acs.chemrev.9b00746
Chem. Rev. XXXX, XXX, XXX−XXX

MOF = metal−organic framework
NENU = Northeast Normal University
NU = Northwestern University
PCN = Porous Coordination Network
UiO = University of Oslo
ZIF = zeolitic imidazolate framework
ZJNU = Zhejiang Normal University

Other

AAWH = adsorption-based atmospheric water harvesting
ADC = adsorption-driven chiller
AD = adsorptive desalination
ASHRAE = American Society of Heating, Refrigerating, and Air-Conditioning Engineers
AWH = atmospheric water harvesting
CCHP = combined cooling-heat and power
CPD = conceptual process design
DA = Dubinin−Astakhov
EHS = environment, health, and safety
FTIR = Fourier-transform infrared
HSAB = hard/soft acid/base principle
ICP-OES = inductively coupled plasma optical emission spectrometry
LCA = life cycle analysis
NMR = nuclear magnetic resonance
PALS = positronium annihilation lifetime spectroscopy
PDF = pair distribution function
PXRD = powder X-ray diffraction
SBU = secondary building unit
SCXRD = single crystal X-ray diffraction
SEM = scanning electron microscopy
TLP = three levels of porosity
UV−vis = ultraviolet−visible
VOC = volatile organic compound

Linkers

ABDC = 4,4′-azobenzenedicarboxylate
ABTA = 1-(4-aminobenzyl)-1,2,4-triazolate
ADC = 9,10-anthracenedicarboxylate
ALA = alanine
AT = aldrithiol
AZPY = azopyridine
BA = benzoate
BBTA = 1*H*,5*H*-benzo(1,2-*d*:4,5-*d*′)bistriazolate
BDA = 2,2′-biphenyl dicarboxylate
BDB = 4,4′-(benzene-1,3-diyl)dibenzoate
BDC = 1,4-benzene dicarboxylate (TPA)
BDP = 1,4-benzenedi(4-pyrazolyl)
BDPO = 2,4-bis(3,5-dicarboxyphenylamino)-6-oltriazine
BDTT = bis(1,2,3-triazolo[4,5-*b*],[40,50-*i*])dibenzo[1,4]-dioxin)
BFBPDC = 2,2′-bistrifluoromethyl-biphenyl-4,4′-dicarboxylate
BIM = benzimidazolate
BIPY = 2,2′-bipyridine-5,5′-dicarboxylate
BNDCA = 1,1′-binaphthyl-4,4′-dicarboxylate
BPA = 1,2-bis-(4-pyridyl)acetylene)$_2$
BPANCH = 9,10-bis(4-pyridyl)anthracene
BPDC = 4,4′-biphenyldicarboxylate
BPE = *trans*-1,2-bis(4-pyridyl)ethylene
BPT = [1,1′-biphenyl]-3,4′,5-tricarboxylate
BPTC = 4,4′-bipyridine-2,6,2′,6′-tetracarboxylate
BPY = 2,2′-dipyridyl
BPYBC = 1,1′-bis(4-carboxybenzyl)-4,4′-bipyridine
BTBbenzene = benzenetribenzoate
BTBA = 4,4′,4″-(1*H*-benzo[*d*]imidazole-2,4,7-triyl)-tribenzoate
BTC = 1,3,5-benzene tricarboxylate
BTDD = bis(1*H*-1,2,3-triazolo[4,5-*b*],[4′,5′-*i*])dibenzo-[1,4]dioxin
BTEB = 1,2,4,5-tetrakis(4-carboxyphenyl)benzene
BTEC = pyromellitate
BTP = 1,3,5-tris(1*H*-pyrazol-4-yl)benzene
BTRE = 1,2-bis(1,2,4-triazol-4-yl)ethane
BTN = 1,3,5-tri(6-hydroxycarbonylnaphthalen-2-yl)benzene
BTTA = 1*H*,5*H*-benzo-(1,2-d:4,5-d′)bistriazolate
BTTB = 4,4′,4″,4″-benzene-1,2,4,5-tetrayltetrabenzoate
CDC = *trans*-1,4-cyclohexane dicarboxylate
(*R*)-2-Cl-man = (*R*)-2-chloromandelate
(*R*)-3-Cl-man = (*R*)-3-chloromandelate
(*R*)-4-Cl-man = (*R*)-4-chloromandelate
CPP = (*S* or *R*)-3,3′-di-*tert*-butyl-5,5′-dicarboxyphenyl-6,6′-dimethylbiphenyl-2,2′-diyl hydrogen phosphate
CTTA = 5′-(4-carboxyphenyl)-2′,4′,6′-trimethyl-[1,1′:3′,1″-terphenyl]-4,4″-dicarboxylate
DAB = 1,4-diamino-butane
DABCO = 1,4-diazabicyclo[2.2.2]octane (TED)
DCBP = 4,4′-dicarboxy-2,2′-bipyridine
DCDPP = 5,15-di(4-carboxylphenyl)-10,20-di(4-pyridyl)-porphyrin
DCDPS = 4,4′-dicarboxydiphenyl sulfone
DCI = 4,5-dicyanoimidazolate
DCIM = dichloroimidazolate
DCPBA = 3,5-di(4′-carboxylphenyl) benzoate
DOBDC = 2,5-dihydroxyterephthalate
DMBPY = 2,2′-dimethyl 4,4′-bipyridine
DMCAPZ = 3,5-dimethyl-4-carboxypyrazolate
DPE = 1,2-di(4-pyridyl)ethylene
DTTDC = dithieno[3,2-*b*;20,30-*d*]-thiophene-2,6-dicarboxylate
EDDA = 5,5′-(ethane-1,2-diylbis(oxy))diisophthalate
FA = fumarate
FCP1 = (*R*)-6,6′-dimethyl-3,3′-di(3,5-bis(trifluoromethyl))-phenyl-5,5′-di(3,5-bis(methoxycarb -onyl))phenyl-1,1′-biphenyl-2,2′-hydrogen phosphate
FCP3 = (*R*)-6,6′-dimethyl-3,3′-di(3,5-difluoro)phenyl-5,5′-di(3,5-bis(methoxycarbonyl))pheny -l-1,1′-biphenyl-2,2′-hydrogen phosphate
FDA = 1,3,6,8-tetrakis(*p*-benzoate)pyrene
FDC = 2,5-furandicarboxylate
Gd-H-DOTA-4AmP = Gd(III)-1,4,7,10-tetraazacyclododecane-1,4,7,10-tetraacetamidomethylene phosphonate
HBTT = 5,5′,10,10′,15,15′-hexabutyltruxene-2,7,12-tricarboxylate
HDTT = 5,5′,10,10′,15,15′-hexadecyltruxene-2,7,12-tricarboxylate
HETT = 5,5′,10,10′,15,15′-hexaethyltruxene-2,7,12-tricarboxylate
HHTT = 5,5′,10,10′,15,15′-hexahexyltruxene-2,7,12-tricarboxylate
HMTT = 5,5′,10,10′,15,15′-hexamethyltruxene-2,7,12-tricarboxylate
HOTT = 5,5′,10,10′,15,15′-hexaoctyltruxene-2,7,12-tricarboxylate
ICA = imidazole-2-carboxaldehyde
IDC = 4,5-imidazoledicarboxylate
IM = imidzolate

https://dx.doi.org/10.1021/acs.chemrev.9b00746
Chem. Rev. XXXX, XXX, XXX−XXX

IPA = isopthalate
L = *N*-(4-carboxyphenyl)isonicotinamide 1-oxide for $[PbL_2]\cdot 2DMF\cdot 6H_2O$
L1 = structural formula, see ref 124 for spiro-1
L1 = 1*H*-pyrazole-4-carboxylate for $Ni_8(L1)_6$
L2 = structural formula, see ref 124 for spiro-2
L2 = 4-(1*H*-pyrazole-4-yl)benzoic acid for $Ni_8(L2)_6$
L3 = 4,4′-benzene-1,4-diylbis(1*H*-pyrazole)
L4 = 4,4′-buta-1,3-diyne-1,4-diylbis(1*H*-pyrazole)
L5 = 4,4′-(benzene-1,4-diyldiethyne-2,1-diyl)bis(1*H*-pyrazole)
L6 = 3,5-di(pyridine-4-yl)benzoate
L7 = 5-(4-pyridyl)-isophthalate
L22 = structural formula, see ref 137
L′1 = 2-((pyridin-4-yl)methylamino)-4-methylpentanoate
L′2 = 2-(pyridin-4-yl)methylamino)-3-hydroxypropanoate
L′3 = 2-((pyridin-4-yl)methylamino)-3-hydroxybutanoate
L_A^1 = structural formula, see ref 234
L_A^2 = structural formula, see ref 234
L_A^3 = structural formula, see ref 234
L_B^1 = structural formula, see ref 234
L_B^2 = structural formula, see ref 234
L_B^3 = structural formula, see ref 234
L_C^1 = structural formula, see ref 234
L_C^2 = structural formula, see ref 234
L_C^3 = structural formula, see ref 234
(*S*)-man = (*S*)-mandelate
MCP = (*R*)-6,6′-dimethyl-3,3′-di(3,5-dimethyl)phenyl-5,5′-di(3,5-bis(methoxycarbonyl))phenyl-1,1′-biphenyl-2,2′-hydrogen phosphate
MDIP = 3,3′,5,5′-tetracarboxydiphenylmethane
(*R*)-4-Me-man = (*R*)-4-methylmandelate
MIM = 2-methylimidazolate
MIMCA = 4-methylimidazolate-5-carbaldehyde
MPA = dimethyl 5-ethoxy isophthalate
MTB = 4,4′,4″,4‴-methanetetrayltetrabenzoate
MTPM = tetrakis(*m*-pyridyloxymethylene)methane
MTZ = 3-methyl-1,2,4-triazolate
NDB = 4,4′-(naphthalene-2,7-diyl)dibenzoate
NDC = naphthalene-2,6-dicarboxylate
NDI-H = structural formula, see ref 261
NDI-SEt = structural formula, see ref 261
NDI-SOEt = structural formula, see ref 261
NDI-SO_2Et = structural formula, see ref 261
NIM = nitroimidazolate
OAA = oxalate (OX)
OBA = 4,4′-oxybis(benzoate)
OPD = *o*-phthalate
PA = phytate
PAIP = 5-(1*H*-pyrazol-4-yl)-isophthalate
PCIH = 4-pyridinecarboxaldehyde hydrazine
PDA = 1,2-diaminopropane
PDAD = 5,5′-(pyridine-3,5-dicarbonyl)bis(azanediyl)-diisophthalate
PDC = pyridine-2,4-dicarboxylate for Co-CUK-1
PDC = 3,5-pyrazoledicarboxylate for MOF-303(Al)
PEDB-$(OMe)_2$ = 4,4′-[(2,5-dimethoxy-1,4-phenylene)bis-(ethyne-2,1-diyl)]dibenzoate
PHEN = 1,10-phenanthroline
PM = pyromellitate
PMPA = *N*,*N*′-piperazinebis(methylenephosphonate)
PMPMD = *N*,*N*′-bis(4-pyridylmethyl)phenyldiimide
PYC = 4-pyridine carboxylate
PYTPH = tetraethyl-1,3,6,8-pyrenetetraphosphonate
PYZ = pyrazine
PYZDC = pyrazine-2,5-dicarboxylate
PZDC = 2,3-pyrazinedicarboxylate for $Cu_2(pzdc)_2bpy$
PZDC = 1*H*-pyrazole-3,5-dicarboxylate for MOF-802(Zr)
Q = hydroquinone
RABL = resorcin[4]arene-based linker
SDB = 4,4′-sulfonyldibenzoic carboxylate
TAIP = 5-(1*H*-1,2,3-triazol-4-yl)isophthalate
TAPP = 4-(4*H*-1,2,4-triazol-4-yl)-phenyl phosphonate
TATB = 4,4′,4″-*s*-triazine-2,4,6-triyl-tribenzoate
TBAPY = 4,4′,4″,4‴-(pyrene-1,3,6,8-tetrayl)tetrabenzoate
TBPP = 4′,4‴,4⁗,4′′′′′-(porphyrin-5,10,15,20-tetrayl)-tetrakis([1,10-biphenyl]-4-carboxylate)
TCBPTA = 2,4,6-tris-(4-carboxyphenoxy)-1,3,5-triazine
TCS = tetrakis(4-oxycarbonylphenyl)silane)
TCP-2 = structural formula, see ref 156
TCP-3 = structural formula, see ref 156
TCPP = tetrakis(4-carboxyphenyl)porphyrin
TCPT = 3,3″,5,5′′-tetrakis(4-carboxyphenyl)-*p*-terphenyl
TCTPA = 4,4′,4′′-tricarboxyltriphenylamine
TCYM = 2,4,6-tris[1-(3-carboxylphenoxy)ylmethyl]-mesitylene
TDC = 2,5-thiophenedicarboxylate
TDHB = 3,3′,5,5′-tetrakis(3,5-dicarboxyphenyl)-2,2′,4,4′,6,6′-hexamethylbiphenyl)
THIPC = (*S*)-4,5,6,7-tetrahydro-1*H*-imidazo[4,5-*c*]-pyridine-6-carboxylate
THR = 2-(pyridin-4-yl)methylamino-3-hydroxybutanoate
TIB = 1,3,5-tris(1-imidazolyl)benzene
TMBDC = 2,3,5,6-tetramethyl-1,4-benzenedicarboxylate
TPADPA = 5,5′-(triphenylamine-4,4′-diyl)diisophthalate
TPDC-o-$2CF_3$ = 3,3″-bis(trifluoromethyl)-[1,1′:4′,1′′-terphenyl]-4,4′′-dicarboxylate
TPHB = 4,4′,4″,4‴,4⁗,4′′′′-(triphenylene-2,3,6,7,10,11-hexayl)hexabenzoate
TPO = tris(paracarboxylphenyl) phosphine oxide
TPP = 5,10,15,20-tetra(1*H*-pyrazol-4-yl)-porphyrin
TPPA = 1,3,5,7-tetrakis(4-phosphonophenyl)adamantine
TPPM = tetrakis[4-(dihyroxyphosphoryl)phenyl]methane
TPPP = 5,10,15,20-tetrakis(4-(1*H*-pyrazol-4-yl)-phenyl)-porphyrin
TPT = 2,4,6-tris(4-pyridyl)-1,3,5-triazine
TRZ = 1,2,4-triazolate
TTFTB = tetrathiafulvalene tetrabenzoate
TTNA = 6,6′,6″-(2,4,6-trimethylbenzene-1,3,5-triyl)tris(2-naphthoate)
TTTA = (2*E*,2′*E*,2″*E*)-3,3′,3″-(2,4,6-trimethylbenzene-1,3,5-triyl)-triacrylate
TZBPDC = 4′-(1*H*-tetrazol-5-yl)-[1,1′-biphenyl]-3,5-dicarboxylate
TZE = tetrazole-5-ethylester
TZG = 5,5′-(1,2,4,5-tetrazine-3,6-diyl)bis(benzene-1,2,3-triol)
VAL = 3-methyl-2-(pyridine-4-ylmethylamino) butanoate

REFERENCES

(1) Forman, C.; Muritala, I. K.; Pardemann, R.; Meyer, B. Estimating the global waste heat potential. *Renewable Sustainable Energy Rev.* **2016**, *57*, 1568−1579.
(2) Rattner, A. S.; Garimella, S. Energy harvesting, reuse and upgrade to reduce primary energy usage in the USA. *Energy* **2011**, *36*, 6172−6183.

https://dx.doi.org/10.1021/acs.chemrev.9b00746
Chem. Rev. XXXX, XXX, XXX−XXX

(3) Ikink, H., Warmte-integratie: Van technologie naar implementatie. *NPT Procestechnologie*, March, 2020, pp 20−21.
(4) Polanyi, M. Section III.—Theories of the adsorption of gases. A general survey and some additional remarks. Introductory paper to section III. *Trans. Faraday Soc.* **1932**, *28*, 316−332.
(5) Dubinin, M. M. The potential theory of adsorption of gases and vapors for adsorbents with energetically nonuniform surfaces. *Chem. Rev.* **1960**, *60*, 235−241.
(6) Dubinin, M. M.; Astakhov, V. A. Development of the concepts of volume filling of micropores in the adsorption of gases and vapors by microporous adsorbents. *Bull. Acad. Sci. USSR, Div. Chem. Sci.* **1971**, *20*, 3−7.
(7) de Lange, M. F.; Verouden, K. J. F. M.; Vlugt, T. J. H.; Gascon, J.; Kapteijn, F. Adsorption-driven heat pumps: The potential of metal−organic frameworks. *Chem. Rev.* **2015**, *115*, 12205−12250.
(8) Burtch, N. C.; Jasuja, H.; Walton, K. S. Water stability and adsorption in metal-organic frameworks. *Chem. Rev.* **2014**, *114*, 10575−612.
(9) Bai, Y.; Dou, Y.; Xie, L.-H.; Rutledge, W.; Li, J.-R.; Zhou, H.-C. Zr-based metal-organic frameworks: Design, synthesis, structure, and applications. *Chem. Soc. Rev.* **2016**, *45*, 2327−67.
(10) Canivet, J.; Fateeva, A.; Guo, Y.; Coasne, B.; Farrusseng, D. Water adsorption in MOFs: Fundamentals and applications. *Chem. Soc. Rev.* **2014**, *43*, 5594−617.
(11) Aristov, Y. I. Challenging offers of material science for adsorption heat transformation: A review. *Appl. Therm. Eng.* **2013**, *50*, 1610−1618.
(12) Wang, W.; Wu, L.; Li, Z.; Fang, Y.; Ding, J.; Xiao, J. An overview of adsorbents in the rotary desiccant dehumidifier for air dehumidification. *Drying Technol.* **2013**, *31*, 1334−1345.
(13) Meunier, F. Adsorption heat powered heat pumps. *Appl. Therm. Eng.* **2013**, *61*, 830−836.
(14) Vasta, S.; Brancato, V.; La Rosa, D.; Palomba, V.; Restuccia, G.; Sapienza, A.; Frazzica, A. Adsorption heat storage: State-of-the-art and future perspectives. *Nanomaterials* **2018**, *8*, 522.
(15) Zhang, L. Z.; Niu, J. L. Performance comparisons of desiccant wheels for air dehumidification and enthalpy recovery. *Appl. Therm. Eng.* **2002**, *22*, 1347−1367.
(16) Kodama, A.; Hirayama, T.; Goto, M.; Hirose, T.; Critoph, R. E. The use of psychrometric charts for the optimization of a thermal swing desiccant wheel. *Appl. Therm. Eng.* **2001**, *21*, 1657−1674.
(17) Hanikel, N.; Prévot, M. S.; Fathieh, F.; Kapustin, E. A.; Lyu, H.; Wang, H.; Diercks, N. J.; Glover, T. G.; Yaghi, O. M. Rapid cycling and exceptional yield in a metal-organic framework water harvester. *ACS Cent. Sci.* **2019**, *5*, 1699−1706.
(18) Felder, R. M.; Rousseau, R. W., *Elementary Principles of Chemical Processes*, 3rd ed.; Wiley: New York, 2005.
(19) *Zeolitic Water Vapor Adsorbent: Aqsoa (product leaflet)*; Mitsubishi Plastics, 2010; http://www.aaasaveenergy.com/products/001/pdf/AQSOA_1210E (accessed 2020-03-07).
(20) Thu, K.; Kim, Y. D.; Xi, B. J.; Ismail, A.; Ng, K. C., Thermophysical properties of novel zeolite materials for sorption cycles. In *Advances in Thermofluids*; Wahid, M. A., Alhamid, I., Pamitran, A.; Sheriff, J. M., Eds.; Trans Tech Publishing, 2013; Vol. *388*, pp 116−122.
(21) Velte, A.; Füldner, G.; Laurenz, E.; Schnabel, L. Advanced measurement and simulation procedure for the identification of heat and mass transfer parameters in dynamic adsorption experiments. *Energies* **2017**, *10*, 1130.
(22) Schnitzlein, K. Modelling radial dispersion in terms of the local structure of packed beds. *Chem. Eng. Sci.* **2001**, *56*, 579−585.
(23) Bendix, P.; Füldner, G.; Möllers, M.; Kummer, H.; Schnabel, L.; Henninger, S.; Henning, H.-M. Optimization of power density and metal-to-adsorbent weight ratio in coated adsorbers for adsorptive heat transformation applications. *Appl. Therm. Eng.* **2017**, *124*, 83−90.
(24) Kummer, H.; Jeremias, F.; Warlo, A.; Füldner, G.; Fröhlich, D.; Janiak, C.; Gläser, R.; Henninger, S. K. A functional full-scale heat exchanger coated with aluminum fumarate metal−organic framework for adsorption heat transformation. *Ind. Eng. Chem. Res.* **2017**, *56*, 8393−8398.
(25) Vivekh, P.; Kumja, M.; Bui, D. T.; Chua, K. J. Recent developments in solid desiccant coated heat exchangers - A review. *Appl. Energy* **2018**, *229*, 778−803.
(26) Grabowska, K.; Krzywanski, J.; Nowak, W.; Wesolowska, M. Construction of an innovative adsorbent bed configuration in the adsorption chiller - Selection criteria for effective sorbent-glue pair. *Energy* **2018**, *151*, 317−323.
(27) Freni, A.; Dawoud, B.; Bonaccorsi, L.; Chmielewski, S.; Frazzica, A.; Calabrese, L.; Restuccia, G., *Characterization of Zeolite-Based Coatings for Adsorption Heat Pumps*. 1st ed.; Springer International Publishing: Heidelberg, 2015.
(28) Kolios, G.; Frauhammer, J.; Eigenberger, G. Efficient reactor concepts for coupling of endothermic and exothermic reactions. *Chem. Eng. Sci.* **2002**, *57*, 1505−1510.
(29) O'Connor, D.; Calautit, J. K.; Hughes, B. R. A novel design of a desiccant rotary wheel for passive ventilation applications. *Appl. Energy* **2016**, *179*, 99−109.
(30) van Hasselt, B. W.; Calis, H. P. A.; Sie, S. T.; van den Bleek, C. M. Pressure drop characteristics of the three-levels-of-porosity reactor. *Chem. Eng. Sci.* **1999**, *54*, 3701−3708.
(31) Lebens, P. J. M.; Kapteijn, F.; Sie, S. T.; Moulijn, J. A. Potentials of internally finned monoliths as a packing for multifunctional reactors. *Chem. Eng. Sci.* **1999**, *54*, 1359−1365.
(32) Bakker, W. J. W.; Vriesendorp, M.; Kapteijn, F.; Moulijn, J. A. Sorbent development for continuous regenerative H_2S removal in a rotating monolith reactor. *Can. J. Chem. Eng.* **1996**, *74*, 713−718.
(33) Babich, I. V.; van Langeveld, A. D.; Zhu, W. D.; Bakker, W. J. W.; Moulijn, J. A. A rotating adsorber for multistage cyclic processes: Principle and experimental demonstration in the separation of paraffins. *Ind. Eng. Chem. Res.* **2001**, *40*, 357−363.
(34) Ghodsipour, N.; Sadrameli, M. Experimental and sensitivity analysis of a rotary air preheater for the flue gas heat recovery. *Appl. Therm. Eng.* **2003**, *23*, 571−580.
(35) Nobrega, C. E. L.; Brum, N. C. L. Modeling and simulation of heat and enthalpy recovery wheels. *Energy* **2009**, *34*, 2063−2068.
(36) Harrison, D. P. Sorption-enhanced hydrogen production: A review. *Ind. Eng. Chem. Res.* **2008**, *47*, 6486−6501.
(37) Wu, Y.-J.; Li, P.; Yu, J.-G.; Cunha, A. F.; Rodrigues, A. E. Progress on sorption-enhanced reaction process for hydrogen production. *Rev. Chem. Eng.* **2016**, *32*, 271−303.
(38) Jani, D. B.; Mishra, M.; Sahoo, P. K. Solid desiccant air conditioning - A state of the art review. *Renewable Sustainable Energy Rev.* **2016**, *60*, 1451−1469.
(39) Li, H.; Eddaoudi, M.; O'Keeffe, M.; Yaghi, O. M. Design and synthesis of an exceptionally stable and highly porous metal-organic framework. *Nature* **1999**, *402*, 276−279.
(40) Chui, S. S.-Y.; Lo, S. M.-F.; Charmant, J. P. H.; Orpen, A. G.; Williams, I. D. A chemically functionalizable nanoporous material $[Cu_3(TMA)_2(H_2O)_3]_n$. *Science* **1999**, *283*, 1148−1150.
(41) Park, K. S.; Ni, Z.; Côté, A. P.; Choi, J. Y.; Huang, R.; Uribe-Romo, F. J.; Chae, H. K.; O'Keeffe, M.; Yaghi, O. M. Exceptional chemical and thermal stability of zeolitic imidazolate frameworks. *Proc. Natl. Acad. Sci. U. S. A.* **2006**, *103*, 10186−10191.
(42) Férey, G.; Mellot-Draznieks, C.; Serre, C.; Millange, F.; Dutour, J.; Surblé, S.; Margiolaki, I. A chromium terephthalate-based solid with unusually large pore volumes and surface area. *Science* **2005**, *309*, 2040−2042.
(43) Cavka, J. H.; Jakobsen, S.; Olsbye, U.; Guillou, N.; Lamberti, C.; Bordiga, S.; Lillerud, K. P. A new zirconium inorganic building brick forming metal organic frameworks with exceptional stability. *J. Am. Chem. Soc.* **2008**, *130*, 13850−13851.
(44) Nguyen, H. L.; Hanikel, N.; Lyle, S. J.; Zhu, C.; Proserpio, D. M.; Yaghi, O. M. A porous covalent organic framework with voided square grid topology for atmospheric water harvesting. *J. Am. Chem. Soc.* **2020**, *142*, 2218−2221.

https://dx.doi.org/10.1021/acs.chemrev.9b00746
Chem. Rev. XXXX, XXX, XXX−XXX

(45) Rieth, A. J.; Wright, A. M.; Dincă, M. Kinetic stability of metal−organic frameworks for corrosive and coordinating gas capture. *Nat. Rev. Mater.* **2019**, *4*, 708−725.
(46) Hughes, J. T.; Bennett, T. D.; Cheetham, A. K.; Navrotsky, A. Thermochemistry of zeolitic imidazolate frameworks of varying porosity. *J. Am. Chem. Soc.* **2013**, *135*, 598−601.
(47) Low, J. J.; Benin, A. I.; Jakubczak, P.; Abrahamian, J. F.; Faheem, S. A.; Willis, R. R. Virtual high throughput screening confirmed experimentally: Porous coordination polymer hydration. *J. Am. Chem. Soc.* **2009**, *131*, 15834−15842.
(48) Mondloch, J. E.; Katz, M. J.; Planas, N.; Semrouni, D.; Gagliardi, L.; Hupp, J. T.; Farha, O. K. Are Zr_6-based MOFs water stable? Linker hydrolysis vs. capillary-force-driven channel collapse. *Chem. Commun.* **2014**, *50*, 8944−8946.
(49) DeCoste, J. B.; Peterson, G. W.; Schindler, B. J.; Killops, K. L.; Browe, M. A.; Mahle, J. J. The effect of water adsorption on the structure of the carboxylate containing metal−organic frameworks Cu-BTC, Mg-MOF-74, and UiO-66. *J. Mater. Chem. A* **2013**, *1*, 11922−11932.
(50) Liu, X.; Li, Y.; Ban, Y.; Peng, Y.; Jin, H.; Bux, H.; Xu, L.; Caro, J.; Yang, W. Improvement of hydrothermal stability of zeolitic imidazolate frameworks. *Chem. Commun.* **2013**, *49*, 9140−9142.
(51) Tan, K.; Zuluaga, S.; Gong, Q.; Canepa, P.; Wang, H.; Li, J.; Chabal, Y. J.; Thonhauser, T. Water reaction mechanism in metal organic frameworks with coordinatively unsaturated metal ions: MOF-74. *Chem. Mater.* **2014**, *26*, 6886−6895.
(52) Singh, M. P.; Dhumal, N. R.; Kim, H. J.; Kiefer, J.; Anderson, J. A. Influence of water on the chemistry and structure of the metal−organic framework $Cu_3(BTC)_2$. *J. Phys. Chem. C* **2016**, *120*, 17323−17333.
(53) Guo, P.; Dutta, D.; Wong-Foy, A. G.; Gidley, D. W.; Matzger, A. J. Water sensitivity in Zn_4O-based MOFs is structure and history dependent. *J. Am. Chem. Soc.* **2015**, *137*, 2651−2657.
(54) Flaig, R. W.; Osborn Popp, T. M.; Fracaroli, A. M.; Kapustin, E. A.; Kalmutzki, M. J.; Altamimi, R. M.; Fathieh, F.; Reimer, J. A.; Yaghi, O. M. The chemistry of CO_2 capture in an amine-functionalized metal−organic framework under dry and humid conditions. *J. Am. Chem. Soc.* **2017**, *139*, 12125−12128.
(55) Gul-E-Noor, F.; Jee, B.; Pöppl, A.; Hartmann, M.; Himsl, D.; Bertmer, M. Effects of varying water adsorption on a $Cu_3(BTC)_2$ metal−organic framework (MOF) as studied by ^1H and ^{13}C solid-state NMR spectroscopy. *Phys. Chem. Chem. Phys.* **2011**, *13*, 7783−7788.
(56) He, H.; Sun, Q.; Gao, W.; Perman, J. A.; Sun, F.; Zhu, G.; Aguila, B.; Forrest, K.; Space, B.; Ma, S. A stable metal−organic framework featuring a local buffer environment for carbon dioxide fixation. *Angew. Chem., Int. Ed.* **2018**, *57*, 4657−4662.
(57) Chen, Y.; Wang, B.; Wang, X.; Xie, L.-H.; Li, J.; Xie, Y.; Li, J.-R. A copper(II)-paddlewheel metal−organic framework with exceptional hydrolytic stability and selective adsorption and detection ability of aniline in water. *ACS Appl. Mater. Interfaces* **2017**, *9*, 27027−27035.
(58) Zhang, Y.-Z.; He, T.; Kong, X.-J.; Lv, X.-L.; Wu, X.-Q.; Li, J.-R. Tuning water sorption in highly stable Zr(IV)-metal−organic frameworks through local functionalization of metal clusters. *ACS Appl. Mater. Interfaces* **2018**, *10*, 27868−27874.
(59) Wang, K.; Lv, X.-L.; Feng, D.; Li, J.; Chen, S.; Sun, J.; Song, L.; Xie, Y.; Li, J.-R.; Zhou, H.-C. Pyrazolate-based porphyrinic metal−organic framework with extraordinary base-resistance. *J. Am. Chem. Soc.* **2016**, *138*, 914−919.
(60) Desai, A. V.; Roy, A.; Samanta, P.; Manna, B.; Ghosh, S. K. Base-resistant ionic metal-organic framework as a porous ion-exchange sorbent. *iScience* **2018**, *3*, 21−30.
(61) Pearson, R. G. Hard and soft acids and bases. *J. Am. Chem. Soc.* **1963**, *85*, 3533−3539.
(62) Férey, G.; Serre, C. Large breathing effects in three-dimensional porous hybrid matter: Facts, analyses, rules and consequences. *Chem. Soc. Rev.* **2009**, *38*, 1380−1399.
(63) Devic, T.; Serre, C. High valence 3p and transition metal based MOFs. *Chem. Soc. Rev.* **2014**, *43*, 6097−6115.
(64) Férey, G. Hybrid porous solids: Past, present, future. *Chem. Soc. Rev.* **2008**, *37*, 191−214.
(65) Serre, C.; Millange, F.; Thouvenot, C.; Noguès, M.; Marsolier, G.; Louër, D.; Férey, G. Very large breathing effect in the first nanoporous chromium(III)-based solids: MIL-53 or $Cr^{III}(OH)\cdot\{O_2C-C_6H_4-CO_2\}\cdot\{HO_2C-C_6H_4-CO_2H\}_x\cdot H_2O_y$. *J. Am. Chem. Soc.* **2002**, *124*, 13519−13526.
(66) Férey, G.; Serre, C.; Mellot-Draznieks, C.; Millange, F.; Surblé, S.; Dutour, J.; Margiolaki, I. A hybrid solid with giant pores prepared by a combination of targeted chemistry, simulation, and powder diffraction. *Angew. Chem., Int. Ed.* **2004**, *43*, 6296−6301.
(67) Ahnfeldt, T.; Guillou, N.; Gunzelmann, D.; Margiolaki, I.; Loiseau, T.; Férey, G.; Senker, J.; Stock, N. $[Al_4(OH)_2(OCH_3)_4(H_2N\text{-}bdc)_3]\cdot x\,H_2O$: A 12-connected porous metal−organic framework with an unprecedented aluminum-containing brick. *Angew. Chem., Int. Ed.* **2009**, *48*, 5163−5166.
(68) Reinsch, H.; van der Veen, M. A.; Gil, B.; Marszalek, B.; Verbiest, T.; de Vos, D.; Stock, N. Structures, sorption characteristics, and nonlinear optical properties of a new series of highly stable aluminum MOFs. *Chem. Mater.* **2013**, *25*, 17−26.
(69) Yuan, S.; Qin, J.-S.; Lollar, C. T.; Zhou, H.-C. Stable metal−organic frameworks with group 4 metals: Current status and trends. *ACS Cent. Sci.* **2018**, *4*, 440−450.
(70) Feng, D.; Gu, Z.-Y.; Li, J.-R.; Jiang, H.-L.; Wei, Z.; Zhou, H.-C. Zirconium-metalloporphyrin PCN-222: Mesoporous metal−organic frameworks with ultrahigh stability as biomimetic catalysts. *Angew. Chem., Int. Ed.* **2012**, *51*, 10307−10310.
(71) Mondloch, J. E.; Bury, W.; Fairen-Jimenez, D.; Kwon, S.; DeMarco, E. J.; Weston, M. H.; Sarjeant, A. A.; Nguyen, S. T.; Stair, P. C.; Snurr, R. Q.; Farha, O. K.; Hupp, J. T. Vapor-phase metalation by atomic layer deposition in a metal−organic framework. *J. Am. Chem. Soc.* **2013**, *135*, 10294−10297.
(72) Guillerm, V.; Ragon, F.; Dan-Hardi, M.; Devic, T.; Vishnuvarthan, M.; Campo, B.; Vimont, A.; Clet, G.; Yang, Q.; Maurin, G.; Férey, G.; Vittadini, A.; Gross, S.; Serre, C. A series of isoreticular, highly stable, porous zirconium oxide based metal−organic frameworks. *Angew. Chem., Int. Ed.* **2012**, *51*, 9267−9271.
(73) Kim, H.; Yang, S.; Rao, S. R.; Narayanan, S.; Kapustin, E. A.; Furukawa, H.; Umans, A. S.; Yaghi, O. M.; Wang, E. N. Water harvesting from air with metal-organic frameworks powered by natural sunlight. *Science* **2017**, *356*, 430−434.
(74) Fathieh, F.; Kalmutzki, M. J.; Kapustin, E. A.; Waller, P. J.; Yang, J.; Yaghi, O. M. Practical water production from desert air. *Sci. Adv.* **2018**, *4*, eaat3198.
(75) Furukawa, H.; Gándara, F.; Zhang, Y.-B.; Jiang, J.; Queen, W. L.; Hudson, M. R.; Yaghi, O. M. Water adsorption in porous metal-organic frameworks and related materials. *J. Am. Chem. Soc.* **2014**, *136*, 4369−4381.
(76) Kim, H.; Rao, S. R.; Kapustin, E. A.; Zhao, L.; Yang, S.; Yaghi, O. M.; Wang, E. N. Adsorption-based atmospheric water harvesting device for arid climates. *Nat. Commun.* **2018**, *9*, 1191.
(77) Baek, J.; Rungtaweevoranit, B.; Pei, X.; Park, M.; Fakra, S. C.; Liu, Y.-S.; Matheu, R.; Alshmimri, S. A.; Alshehri, S.; Trickett, C. A.; Somorjai, G. A.; Yaghi, O. M. Bioinspired metal−organic framework catalysts for selective methane oxidation to methanol. *J. Am. Chem. Soc.* **2018**, *140*, 18208−18216.
(78) Dan-Hardi, M.; Serre, C.; Frot, T.; Rozes, L.; Maurin, G.; Sanchez, C.; Férey, G. A new photoactive crystalline highly porous titanium(IV) dicarboxylate. *J. Am. Chem. Soc.* **2009**, *131*, 10857−10859.
(79) Serre, C.; Groves, J. A.; Lightfoot, P.; Slawin, A. M. Z.; Wright, P. A.; Stock, N.; Bein, T.; Haouas, M.; Taulelle, F.; Férey, G. Synthesis, structure and properties of related microporous N,N′-piperazinebismethylenephosphonates of aluminum and titanium. *Chem. Mater.* **2006**, *18*, 1451−1457.
(80) Assi, H.; Mouchaham, G.; Steunou, N.; Devic, T.; Serre, C. Titanium coordination compounds: From discrete metal complexes to metal-organic frameworks. *Chem. Soc. Rev.* **2017**, *46*, 3431−3452.

https://dx.doi.org/10.1021/acs.chemrev.9b00746
Chem. Rev. XXXX, XXX, XXX−XXX

(81) Li, P.; Vermeulen, N. A.; Gong, X.; Malliakas, C. D.; Stoddart, J. F.; Hupp, J. T.; Farha, O. K. Design and synthesis of a water-stable anionic uranium-based metal-organic framework (MOF) with ultra large pores. *Angew. Chem., Int. Ed.* **2016**, *55*, 10358−10362.
(82) Wang, Y.; Liu, Z.; Li, Y.; Bai, Z.; Liu, W.; Wang, Y.; Xu, X.; Xiao, C.; Sheng, D.; Diwu, J.; Su, J.; Chai, Z.; Albrecht-Schmitt, T. E.; Wang, S. Umbellate distortions of the uranyl coordination environment result in a stable and porous polycatenated framework that can effectively remove cesium from aqueous solutions. *J. Am. Chem. Soc.* **2015**, *137*, 6144−6147.
(83) Xie, J.; Wang, Y.; Liu, W.; Yin, X.; Chen, L.; Zou, Y.; Diwu, J.; Chai, Z.; Albrecht-Schmitt, T. E.; Liu, G.; Wang, S. Highly sensitive detection of ionizing radiations by a photoluminescent uranyl organic framework. *Angew. Chem., Int. Ed.* **2017**, *56*, 7500−7504.
(84) Demessence, A.; D'Alessandro, D. M.; Foo, M. L.; Long, J. R. Strong CO_2 binding in a water-stable, triazolate-bridged metal−organic framework functionalized with ethylenediamine. *J. Am. Chem. Soc.* **2009**, *131*, 8784−8786.
(85) Colombo, V.; Galli, S.; Choi, H. J.; Han, G. D.; Maspero, A.; Palmisano, G.; Masciocchi, N.; Long, J. R. High thermal and chemical stability in pyrazolate-bridged metal−organic frameworks with exposed metal sites. *Chem. Sci.* **2011**, *2*, 1311−1319.
(86) Lu, X.-F.; Liao, P.-Q.; Wang, J.-W.; Wu, J.-X.; Chen, X.-W.; He, C.-T.; Zhang, J.-P.; Li, G.-R.; Chen, X.-M. An alkaline-stable, metal hydroxide mimicking metal−organic framework for efficient electrocatalytic oxygen evolution. *J. Am. Chem. Soc.* **2016**, *138*, 8336−8339.
(87) Rieth, A. J.; Tulchinsky, Y.; Dincă, M. High and reversible ammonia uptake in mesoporous azolate metal−organic frameworks with open Mn, Co, and Ni sites. *J. Am. Chem. Soc.* **2016**, *138*, 9401−9404.
(88) Kang, I. J.; Khan, N. A.; Haque, E.; Jhung, S. H. Chemical and thermal stability of isotypic metal−organic frameworks: Effect of metal ions. *Chem. - Eur. J.* **2011**, *17*, 6437−6442.
(89) Liu, J.; Fan, Y.-Z.; Li, X.; Wei, Z.; Xu, Y.-W.; Zhang, L.; Su, C.-Y. A porous rhodium(III)-porphyrin metal-organic framework as an efficient and selective photocatalyst for CO_2 reduction. *Appl. Catal., B* **2018**, *231*, 173−181.
(90) Wang, K.; Huang, H.; Zhou, X.; Wang, Q.; Li, G.; Shen, H.; She, Y.; Zhong, C. Highly chemically stable MOFs with trifluoromethyl groups: Effect of position of trifluoromethyl groups on chemical stability. *Inorg. Chem.* **2019**, *58*, 5725−5732.
(91) Chen, X.; Jiang, H.; Hou, B.; Gong, W.; Liu, Y.; Cui, Y. Boosting chemical stability, catalytic activity, and enantioselectivity of metal−organic frameworks for batch and flow reactions. *J. Am. Chem. Soc.* **2017**, *139*, 13476−13482.
(92) Nguyen, N. T. T.; Furukawa, H.; Gándara, F.; Nguyen, H. T.; Cordova, K. E.; Yaghi, O. M. Selective capture of carbon dioxide under humid conditions by hydrophobic chabazite-type zeolitic imidazolate frameworks. *Angew. Chem., Int. Ed.* **2014**, *53*, 10645−10648.
(93) Xu, Y.-T.; Ye, Z.-M.; Ye, J.-W.; Cao, L.-M.; Huang, R.-K.; Wu, J.-X.; Zhou, D.-D.; Zhang, X.-F.; He, C.-T.; Zhang, J.-P.; Chen, X.-M. Non-3d metal modulation of a cobalt imidazolate framework for excellent electrocatalytic oxygen evolution in neutral media. *Angew. Chem., Int. Ed.* **2019**, *58*, 139−143.
(94) He, C.-T.; Jiang, L.; Ye, Z.-M.; Krishna, R.; Zhong, Z.-S.; Liao, P.-Q.; Xu, J.; Ouyang, G.; Zhang, J.-P.; Chen, X.-M. Exceptional hydrophobicity of a large-pore metal−organic zeolite. *J. Am. Chem. Soc.* **2015**, *137*, 7217−7223.
(95) Taylor, J. M.; Vaidhyanathan, R.; Iremonger, S. S.; Shimizu, G. K. H. Enhancing water stability of metal-organic frameworks via phosphonate monoester linkers. *J. Am. Chem. Soc.* **2012**, *134*, 14338−14340.
(96) Liu, X.-L.; Li, Y.-S.; Zhu, G.-Q.; Ban, Y.-J.; Xu, L.-Y.; Yang, W.-S. An organophilic pervaporation membrane derived from metal−organic framework nanoparticles for efficient recovery of bio-alcohols. *Angew. Chem., Int. Ed.* **2011**, *50*, 10636−10639.
(97) Yang, J.; Zhang, Y.-B.; Liu, Q.; Trickett, C. A.; Gutiérrez-Puebla, E.; Monge, M. Á.; Cong, H.; Aldossary, A.; Deng, H.; Yaghi, O. M. Principles of designing extra-large pore openings and cages in zeolitic imidazolate frameworks. *J. Am. Chem. Soc.* **2017**, *139*, 6448−6455.
(98) Alvarez, E.; Guillou, N.; Martineau, C.; Bueken, B.; Van de Voorde, B.; Le Guillouzer, C.; Fabry, P.; Nouar, F.; Taulelle, F.; de Vos, D.; Chang, J.-S.; Cho, K. H.; Ramsahye, N.; Devic, T.; Daturi, M.; Maurin, G.; Serre, C. The structure of the aluminum fumarate metal−organic framework A520. *Angew. Chem., Int. Ed.* **2015**, *54*, 3664−3668.
(99) Lenzen, D.; Zhao, J.; Ernst, S.-J.; Wahiduzzaman, M.; Ken Inge, A.; Fröhlich, D.; Xu, H.; Bart, H.-J.; Janiak, C.; Henninger, S.; Maurin, G.; Zou, X.; Stock, N. A metal−organic framework for efficient water-based ultra-low-temperature-driven cooling. *Nat. Commun.* **2019**, *10*, 3025.
(100) Cadiau, A.; Lee, J. S.; Damasceno Borges, D.; Fabry, P.; Devic, T.; Wharmby, M. T.; Martineau, C.; Foucher, D.; Taulelle, F.; Jun, C.-H.; Hwang, Y. K.; Stock, N.; De Lange, M. F.; Kapteijn, F.; Gascon, J.; Maurin, G.; Chang, J.-S.; Serre, C. Design of hydrophilic metal organic framework water adsorbents for heat reallocation. *Adv. Mater.* **2015**, *27*, 4775−4780.
(101) Qin, J.-S.; Du, D.-Y.; Guan, W.; Bo, X.-J.; Li, Y.-F.; Guo, L.-P.; Su, Z.-M.; Wang, Y.-Y.; Lan, Y.-Q.; Zhou, H.-C. Ultrastable polymolybdate-based metal−organic frameworks as highly active electrocatalysts for hydrogen generation from water. *J. Am. Chem. Soc.* **2015**, *137*, 7169−7177.
(102) Nugent, P.; Belmabkhout, Y.; Burd, S. D.; Cairns, A. J.; Luebke, R.; Forrest, K.; Pham, T.; Ma, S.; Space, B.; Wojtas, L.; Eddaoudi, M.; Zaworotko, M. J. Porous materials with optimal adsorption thermodynamics and kinetics for CO_2 separation. *Nature* **2013**, *495*, 80−84.
(103) Nandi, S.; Collins, S.; Chakraborty, D.; Banerjee, D.; Thallapally, P. K.; Woo, T. K.; Vaidhyanathan, R. Ultralow parasitic energy for postcombustion CO_2 capture realized in a nickel isonicotinate metal−organic framework with excellent moisture stability. *J. Am. Chem. Soc.* **2017**, *139*, 1734−1737.
(104) Xie, L.-H.; Liu, X.-M.; He, T.; Li, J.-R. Metal-organic frameworks for the capture of trace aromatic volatile organic compounds. *Chem* **2018**, *4*, 1911−1927.
(105) Choi, H. J.; Dincă, M.; Dailly, A.; Long, J. R. Hydrogen storage in water-stable metal−organic frameworks incorporating 1,3- and 1,4-benzenedipyrazolate. *Energy Environ. Sci.* **2010**, *3*, 117−123.
(106) Kim, M.; Cahill, J. F.; Fei, H.; Prather, K. A.; Cohen, S. M. Postsynthetic ligand and cation exchange in robust metal−organic frameworks. *J. Am. Chem. Soc.* **2012**, *134*, 18082−18088.
(107) Liu, X.; Demir, N. K.; Wu, Z.; Li, K. Highly water-stable zirconium metal-organic framework UiO-66 membranes supported on alumina hollow fibers for desalination. *J. Am. Chem. Soc.* **2015**, *137*, 6999−7002.
(108) Ou, R.; Zhang, H.; Wei, J.; Kim, S.; Wan, L.; Nguyen, N. S.; Hu, Y.; Zhang, X.; Simon, G. P.; Wang, H. Thermoresponsive amphoteric metal−organic frameworks for efficient and reversible adsorption of multiple salts from water. *Adv. Mater.* **2018**, *30*, 1802767.
(109) Lv, X.-L.; Wang, K.; Wang, B.; Su, J.; Zou, X.; Xie, Y.; Li, J.-R.; Zhou, H.-C. A base-resistant metalloporphyrin metal−organic framework for C−H bond halogenation. *J. Am. Chem. Soc.* **2017**, *139*, 211−217.
(110) Liu, X. Metal organic framework UiO-66 membranes. *Front. Chem. Sci. Eng.* **2020**, *14*, 216−232.
(111) Rieth, A. J.; Wright, A. M.; Skorupskii, G.; Mancuso, J. L.; Hendon, C. H.; Dincă, M. Record-setting sorbents for reversible water uptake by systematic anion exchanges in metal−organic frameworks. *J. Am. Chem. Soc.* **2019**, *141*, 13858−13866.
(112) Yuan, S.; Feng, L.; Wang, K.; Pang, J.; Bosch, M.; Lollar, C.; Sun, Y.; Qin, J.; Yang, X.; Zhang, P.; Wang, Q.; Zou, L.; Zhang, Y.; Zhang, L.; Fang, Y.; Li, J.; Zhou, H.-C. Stable metal−organic frameworks: Design, synthesis, and applications. *Adv. Mater.* **2018**, *30*, 1704303.

https://dx.doi.org/10.1021/acs.chemrev.9b00746
Chem. Rev. XXXX, XXX, XXX−XXX

(113) Cai, G.; Jiang, H.-L. A modulator-induced defect-formation strategy to hierarchically porous metal−organic frameworks with high stability. *Angew. Chem., Int. Ed.* **2017**, *56*, 563−567.
(114) Leus, K.; Bogaerts, T.; De Decker, J.; Depauw, H.; Hendrickx, K.; Vrielinck, H.; Van Speybroeck, V.; Van Der Voort, P. Systematic study of the chemical and hydrothermal stability of selected "stable" metal organic frameworks. *Microporous Mesoporous Mater.* **2016**, *226*, 110−116.
(115) Yang, F.; Xu, G.; Dou, Y.; Wang, B.; Zhang, H.; Wu, H.; Zhou, W.; Li, J.-R.; Chen, B. A flexible metal−organic framework with a high density of sulfonic acid sites for proton conduction. *Nat. Energy* **2017**, *2*, 877−883.
(116) Atallah, H.; Elcheikh Mahmoud, M.; Jelle, A.; Lough, A.; Hmadeh, M. A highly stable indium based metal organic framework for efficient arsenic removal from water. *Dalton Trans* **2018**, *47*, 799−806.
(117) Guo, Z.-J.; Yu, J.; Zhang, Y.-Z.; Zhang, J.; Chen, Y.; Wu, Y.; Xie, L.-H.; Li, J.-R. Water-stable In(III)-based metal−organic frameworks with rod-shaped secondary building units: Single-crystal to single-crystal transformation and selective sorption of C_2H_2 over CO_2 and CH_4. *Inorg. Chem.* **2017**, *56*, 2188−2197.
(118) Yang, C.; Cheng, J.; Chen, Y.; Hu, Y. Experimental investigation on the water stability of amino-modified indium metal−organic frameworks. *RSC Adv.* **2016**, *6*, 61703−61706.
(119) Ugale, B.; Dhankhar, S. S.; Nagaraja, C. M. Exceptionally stable and 20-connected lanthanide metal−organic frameworks for selective CO_2 capture and conversion at atmospheric pressure. *Cryst. Growth Des.* **2018**, *18*, 2432−2440.
(120) Wang, X.; Zhai, L.; Wang, Y.; Li, R.; Gu, X.; Yuan, Y. D.; Qian, Y.; Hu, Z.; Zhao, D. Improving water-treatment performance of zirconium metal-organic framework membranes by postsynthetic defect healing. *ACS Appl. Mater. Interfaces* **2017**, *9*, 37848−37855.
(121) Bon, V.; Senkovska, I.; Baburin, I. A.; Kaskel, S. Zr- and Hf-based metal−organic frameworks: Tracking down the polymorphism. *Cryst. Growth Des.* **2013**, *13*, 1231−1237.
(122) Wang, B.; Lv, X.-L.; Feng, D.; Xie, L.-H.; Zhang, J.; Li, M.; Xie, Y.; Li, J.-R.; Zhou, H.-C. Highly stable Zr(IV)-based metal-organic frameworks for the detection and removal of antibiotics and organic explosives in water. *J. Am. Chem. Soc.* **2016**, *138*, 6204−16.
(123) Wang, S.; Lee, J. S.; Wahiduzzaman, M.; Park, J.; Muschi, M.; Martineau-Corcos, C.; Tissot, A.; Cho, K. H.; Marrot, J.; Shepard, W.; Maurin, G.; Chang, J.-S.; Serre, C. A robust large-pore zirconium carboxylate metal−organic framework for energy-efficient water-sorption-driven refrigeration. *Nat. Energy* **2018**, *3*, 985−993.
(124) Gong, W.; Chen, X.; Jiang, H.; Chu, D.; Cui, Y.; Liu, Y. Highly stable Zr(IV)-based metal−organic frameworks with chiral phosphoric acids for catalytic asymmetric tandem reactions. *J. Am. Chem. Soc.* **2019**, *141*, 7498−7508.
(125) Wang, S.; Kitao, T.; Guillou, N.; Wahiduzzaman, M.; Martineau-Corcos, C.; Nouar, F.; Tissot, A.; Binet, L.; Ramsahye, N.; Devautour-Vinot, S.; Kitagawa, S.; Seki, S.; Tsutsui, Y.; Briois, V.; Steunou, N.; Maurin, G.; Uemura, T.; Serre, C. A phase transformable ultrastable titanium-carboxylate framework for photoconduction. *Nat. Commun.* **2018**, *9*, 1660.
(126) Jiang, J.; Gándara, F.; Zhang, Y.-B.; Na, K.; Yaghi, O. M.; Klemperer, W. G. Superacidity in sulfated metal−organic framework-808. *J. Am. Chem. Soc.* **2014**, *136*, 12844−12847.
(127) Sun, Q.; He, H.; Gao, W.-Y.; Aguila, B.; Wojtas, L.; Dai, Z.; Li, J.; Chen, Y.-S.; Xiao, F.-S.; Ma, S. Imparting amphiphobicity on single-crystalline porous materials. *Nat. Commun.* **2016**, *7*, 13300.
(128) Wu, H.; Yang, F.; Lv, X.-L.; Wang, B.; Zhang, Y.-Z.; Zhao, M.-J.; Li, J.-R. A stable porphyrinic metal−organic framework pore-functionalized by high-density carboxylic groups for proton conduction. *J. Mater. Chem. A* **2017**, *5*, 14525−14529.
(129) Zheng, T.; Yang, Z.; Gui, D.; Liu, Z.; Wang, X.; Dai, X.; Liu, S.; Zhang, L.; Gao, Y.; Chen, L.; Sheng, D.; Wang, Y.; Diwu, J.; Wang, J.; Zhou, R.; Chai, Z.; Albrecht-Schmitt, T. E.; Wang, S. Overcoming the crystallization and designability issues in the ultrastable zirconium phosphonate framework system. *Nat. Commun.* **2017**, *8*, 15369.
(130) Duan, J.; Higuchi, M.; Horike, S.; Foo, M. L.; Rao, K. P.; Inubushi, Y.; Fukushima, T.; Kitagawa, S. High CO_2/CH_4 and C_2 hydrocarbons/CH_4 selectivity in a chemically robust porous coordination polymer. *Adv. Funct. Mater.* **2013**, *23*, 3525−3530.
(131) Zhang, Z.; Wang, Y.; Jia, X.; Yang, J.; Li, J. The synergistic effect of oxygen and water on the stability of the isostructural family of metal−organic frameworks $[Cr_3(BTC)_2]$ and $[Cu_3(BTC)_2]$. *Dalton Trans* **2017**, *46*, 15573−15581.
(132) Park, J.; Feng, D.; Zhou, H.-C. Dual exchange in PCN-333: A facile strategy to chemically robust mesoporous chromium metal−organic framework with functional groups. *J. Am. Chem. Soc.* **2015**, *137*, 11801−11809.
(133) Li, H.; Feng, X.; Ma, D.; Zhang, M.; Zhang, Y.; Liu, Y.; Zhang, J.; Wang, B. Stable aluminum metal−organic frameworks (Al-MOFs) for balanced CO_2 and water selectivity. *ACS Appl. Mater. Interfaces* **2018**, *10*, 3160−3163.
(134) Guo, Y.; Zhang, J.; Dong, L.-Z.; Xu, Y.; Han, W.; Fang, M.; Liu, H.-K.; Wu, Y.; Lan, Y.-Q. Syntheses of exceptionally stable aluminum(III) metal−organic frameworks: How to grow high-quality, large, single crystals. *Chem. - Eur. J.* **2017**, *23*, 15518−15528.
(135) Wang, Z.-W.; Chen, M.; Liu, C.-S.; Wang, X.; Zhao, H.; Du, M. A versatile Al^{III}-based metal−organic framework with high physicochemical stability. *Chem. - Eur. J.* **2015**, *21*, 17215−17219.
(136) Feng, D.; Liu, T.-F.; Su, J.; Bosch, M.; Wei, Z.; Wan, W.; Yuan, D.; Chen, Y.-P.; Wang, X.; Wang, K.; Lian, X.; Gu, Z.-Y.; Park, J.; Zou, X.; Zhou, H.-C. Stable metal-organic frameworks containing single-molecule traps for enzyme encapsulation. *Nat. Commun.* **2015**, *6*, 5979.
(137) Feng, D.; Wang, K.; Wei, Z.; Chen, Y.-P.; Simon, C. M.; Arvapally, R. K.; Martin, R. L.; Bosch, M.; Liu, T.-F.; Fordham, S.; Yuan, D.; Omary, M. A.; Haranczyk, M.; Smit, B.; Zhou, H.-C. Kinetically tuned dimensional augmentation as a versatile synthetic route towards robust metal-organic frameworks. *Nat. Commun.* **2014**, *5*, 5723.
(138) Souto, M.; Santiago-Portillo, A.; Palomino, M.; Vitórica-Yrezábal, I. J.; Vieira, B. J. C.; Waerenborgh, J. C.; Valencia, S.; Navalón, S.; Rey, F.; García, H.; Mínguez Espallargas, G. A highly stable and hierarchical tetrathiafulvalene-based metal−organic framework with improved performance as a solid catalyst. *Chem. Sci.* **2018**, *9*, 2413−2418.
(139) Zhou, J.-M.; Shi, W.; Xu, N.; Cheng, P. Highly selective luminescent sensing of fluoride and organic small-molecule pollutants based on novel lanthanide metal−organic frameworks. *Inorg. Chem.* **2013**, *52*, 8082−8090.
(140) Ye, J.; Bogale, R. F.; Shi, Y.; Chen, Y.; Liu, X.; Zhang, S.; Yang, Y.; Zhao, J.; Ning, G. A water-stable dual-channel luminescence sensor for UO_2^{2+} ions based on an anionic terbium(III) metal−organic framework. *Chem. - Eur. J.* **2017**, *23*, 7657−7662.
(141) Yao, Q.; Bermejo Gómez, A.; Su, J.; Pascanu, V.; Yun, Y.; Zheng, H.; Chen, H.; Liu, L.; Abdelhamid, H. N.; Martín-Matute, B.; Zou, X. Series of highly stable isoreticular lanthanide metal−organic frameworks with expanding pore size and tunable luminescent properties. *Chem. Mater.* **2015**, *27*, 5332−5339.
(142) Duan, J.; Higuchi, M.; Krishna, R.; Kiyonaga, T.; Tsutsumi, Y.; Sato, Y.; Kubota, Y.; Takata, M.; Kitagawa, S. High $CO_2/N_2/O_2/CO$ separation in a chemically robust porous coordination polymer with low binding energy. *Chem. Sci.* **2014**, *5*, 660−666.
(143) Xue, D.-X.; Belmabkhout, Y.; Shekhah, O.; Jiang, H.; Adil, K.; Cairns, A. J.; Eddaoudi, M. Tunable rare earth fcu-MOF platform: Access to adsorption kinetics driven gas/vapor separations via pore size contraction. *J. Am. Chem. Soc.* **2015**, *137*, 5034−5040.
(144) Kandiah, M.; Nilsen, M. H.; Usseglio, S.; Jakobsen, S.; Olsbye, U.; Tilset, M.; Larabi, C.; Quadrelli, E. A.; Bonino, F.; Lillerud, K. P. Synthesis and stability of tagged UiO-66 Zr-MOFs. *Chem. Mater.* **2010**, *22*, 6632−6640.
(145) Guan, X.; Li, H.; Ma, Y.; Xue, M.; Fang, Q.; Yan, Y.; Valtchev, V.; Qiu, S. Chemically stable polyarylether-based covalent organic frameworks. *Nat. Chem.* **2019**, *11*, 587−594.

https://dx.doi.org/10.1021/acs.chemrev.9b00746
Chem. Rev. XXXX, XXX, XXX−XXX

(146) Sun, Y.; Sun, Q.; Huang, H.; Aguila, B.; Niu, Z.; Perman, J. A.; Ma, S. A molecular-level superhydrophobic external surface to improve the stability of metal−organic frameworks. *J. Mater. Chem. A* **2017**, *5*, 18770−18776.
(147) DeCoste, J. B.; Peterson, G. W.; Jasuja, H.; Glover, T. G.; Huang, Y.-g.; Walton, K. S. Stability and degradation mechanisms of metal−organic frameworks containing the $Zr_6O_4(OH)_4$ secondary building unit. *J. Mater. Chem. A* **2013**, *1*, 5642−5650.
(148) Joshi, J. N.; Garcia-Gutierrez, E. Y.; Moran, C. M.; Deneff, J. I.; Walton, K. S. Engineering copper carboxylate functionalities on water stable metal−organic frameworks for enhancement of ammonia removal capacities. *J. Phys. Chem. C* **2017**, *121*, 3310−3319.
(149) Huang, Y.; Qin, W.; Li, Z.; Li, Y. Enhanced stability and CO_2 affinity of a UiO-66 type metal−organic framework decorated with dimethyl groups. *Dalton Trans* **2012**, *41*, 9283−9285.
(150) Hu, Z.; Wang, Y.; Farooq, S.; Zhao, D. A highly stable metal-organic framework with optimum aperture size for CO_2 capture. *AIChE J.* **2017**, *63*, 4103−4114.
(151) Øien-Ødegaard, S.; Bouchevreau, B.; Hylland, K.; Wu, L.; Blom, R.; Grande, C.; Olsbye, U.; Tilset, M.; Lillerud, K. P. UiO-67-type metal−organic frameworks with enhanced water stability and methane adsorption capacity. *Inorg. Chem.* **2016**, *55*, 1986−1991.
(152) Yuan, S.; Qin, J.-S.; Li, J.; Huang, L.; Feng, L.; Fang, Y.; Lollar, C.; Pang, J.; Zhang, L.; Sun, D.; Alsalme, A.; Cagin, T.; Zhou, H.-C. Retrosynthesis of multi-component metal−organic frameworks. *Nat. Commun.* **2018**, *9*, 808.
(153) Feng, L.; Wang, Y.; Yuan, S.; Wang, K.-Y.; Li, J.; Day, G. S.; Qiu, D.; Cheng, L.; Chen, W.-M.; Madrahimov, S.; Zhou, H.-C. Porphyrinic metal-organic frameworks installed with brønsted acid sites for efficient tandem semisynthesis of artemisinin. *ACS Catal.* **2019**, *9*, 5111−5118.
(154) Feng, D.; Gu, Z.-Y.; Chen, Y.-P.; Park, J.; Wei, Z.; Sun, Y.; Bosch, M.; Yuan, S.; Zhou, H.-C. A highly stable porphyrinic zirconium metal−organic framework with shp-a topology. *J. Am. Chem. Soc.* **2014**, *136*, 17714−17717.
(155) Jiang, H.-L.; Feng, D.; Wang, K.; Gu, Z.-Y.; Wei, Z.; Chen, Y.-P.; Zhou, H.-C. An exceptionally stable, porphyrinic Zr metal−organic framework exhibiting pH-dependent fluorescence. *J. Am. Chem. Soc.* **2013**, *135*, 13934−13938.
(156) Liu, T.-F.; Feng, D.; Chen, Y.-P.; Zou, L.; Bosch, M.; Yuan, S.; Wei, Z.; Fordham, S.; Wang, K.; Zhou, H.-C. Topology-guided design and syntheses of highly stable mesoporous porphyrinic zirconium metal−organic frameworks with high surface area. *J. Am. Chem. Soc.* **2015**, *137*, 413−419.
(157) Feng, D.; Wang, K.; Su, J.; Liu, T.-F.; Park, J.; Wei, Z.; Bosch, M.; Yakovenko, A.; Zou, X.; Zhou, H.-C. A highly stable zeotype mesoporous zirconium metal-organic framework with ultralarge pores. *Angew. Chem., Int. Ed.* **2015**, *54*, 149−54.
(158) He, T.; Zhang, Y.-Z.; Kong, X.-J.; Yu, J.; Lv, X.-L.; Wu, Y.; Guo, Z.-J.; Li, J.-R. Zr(IV)-based metal-organic framework with T-shaped ligand: Unique structure, high stability, selective detection, and rapid adsorption of $Cr_2O_7^{2-}$ in water. *ACS Appl. Mater. Interfaces* **2018**, *10*, 16650−16659.
(159) Hu, Z.; Peng, Y.; Gao, Y.; Qian, Y.; Ying, S.; Yuan, D.; Horike, S.; Ogiwara, N.; Babarao, R.; Wang, Y.; Yan, N.; Zhao, D. Direct synthesis of hierarchically porous metal−organic frameworks with high stability and strong brønsted acidity: The decisive role of hafnium in efficient and selective fructose dehydration. *Chem. Mater.* **2016**, *28*, 2659−2667.
(160) Zheng, J.; Wu, M.; Jiang, F.; Su, W.; Hong, M. Stable porphyrin Zr and Hf metal−organic frameworks featuring 2.5 nm cages: High surface areas, SCSC transformations and catalyses. *Chem. Sci.* **2015**, *6*, 3466−3470.
(161) Logan, M. W.; Adamson, J. D.; Le, D.; Uribe-Romo, F. J. Structural stability of n-alkyl-functionalized titanium metal−organic frameworks in aqueous and humid environments. *ACS Appl. Mater. Interfaces* **2017**, *9*, 44529−44533.
(162) Ma, H.-F.; Liu, Q.-Y.; Wang, Y.-L.; Yin, S.-G. A water-stable anionic metal−organic framework constructed from columnar zinc-adeninate units for highly selective light hydrocarbon separation and efficient separation of organic dyes. *Inorg. Chem.* **2017**, *56*, 2919−2925.
(163) Xie, W.; Zhang, S.-R.; Du, D.-Y.; Qin, J.-S.; Bao, S.-J.; Li, J.; Su, Z.-M.; He, W.-W.; Fu, Q.; Lan, Y.-Q. Stable luminescent metal−organic frameworks as dual-functional materials to encapsulate Ln^{3+} ions for white-light emission and to detect nitroaromatic explosives. *Inorg. Chem.* **2015**, *54*, 3290−3296.
(164) Yu, C.; Shao, Z.; Liu, L.; Hou, H. Efficient and selective removal of copper(II) from aqueous solution by a highly stable hydrogen-bonded metal−organic framework. *Cryst. Growth Des.* **2018**, *18*, 3082−3088.
(165) Wang, Y.; He, M.; Gao, X.; Li, S.; He, Y. A metal−organic framework based on a custom-designed diisophthalate ligand exhibiting excellent hydrostability and highly selective adsorption of C_2H_2 and CO_2 over CH_4. *Dalton Trans* **2018**, *47*, 7213−7221.
(166) Wang, J.; Li, Y.; Jiang, M.; Liu, Y.; Zhang, L.; Wu, P. A highly chemically stable metal−organic framework as a luminescent probe for the regenerable ratiometric sensing of pH. *Chem. - Eur. J.* **2016**, *22*, 13023−13027.
(167) Zhang, L.; Hu, Y. H. Strong effects of higher-valent cations on the structure of the zeolitic Zn(2-methylimidazole)$_2$ framework (ZIF-8). *J. Phys. Chem. C* **2011**, *115*, 7967−7971.
(168) Mohideen, M. I. H.; Pillai, R. S.; Adil, K.; Bhatt, P. M.; Belmabkhout, Y.; Shkurenko, A.; Maurin, G.; Eddaoudi, M. A fine-tuned MOF for gas and vapor separation: A multipurpose adsorbent for acid gas removal, dehydration, and BTX sieving. *Chem* **2017**, *3*, 822−833.
(169) Lu, B.-B.; Yang, J.; Che, G.-B.; Pei, W.-Y.; Ma, J.-F. Highly stable copper(I)-based metal−organic framework assembled with resorcin[4]arene and polyoxometalate for efficient heterogeneous catalysis of azide−alkyne "click" reaction. *ACS Appl. Mater. Interfaces* **2018**, *10*, 2628−2636.
(170) Zhao, N.; Li, P.; Mu, X.; Liu, C.; Sun, F.; Zhu, G. Facile synthesis of an ultra-stable metal−organic framework with excellent acid and base resistance. *Faraday Discuss.* **2017**, *201*, 63−70.
(171) Zhou, E.-L.; Qin, C.; Huang, P.; Wang, X.-L.; Chen, W.-C.; Shao, K.-Z.; Su, Z.-M. A stable polyoxometalate-pillared metal−organic framework for proton-conducting and colorimetric biosensing. *Chem. - Eur. J.* **2015**, *21*, 11894−11898.
(172) Wang, X. R.; Du, J.; Huang, Z.; Liu, K.; Liu, Y. Y.; Huo, J. Z.; Liu, Z. Y.; Dong, X. Y.; Chen, L. L.; Ding, B. Anion directing self-assembly of 2D and 3D water-stable silver(I) cation metal organic frameworks and their applications in real-time discriminating cysteine and DNA detection. *J. Mater. Chem. B* **2018**, *6*, 4569−4574.
(173) Chen, Y.; Wang, Y.; Yang, C.; Wang, S.; Yang, J.; Li, J. Antenna-protected metal−organic squares for water/ammonia uptake with excellent stability and regenerability. *ACS Sustainable Chem. Eng.* **2017**, *5*, 5082−5089.
(174) Liang, L.; Liu, C.; Jiang, F.; Chen, Q.; Zhang, L.; Xue, H.; Jiang, H.-L.; Qian, J.; Yuan, D.; Hong, M. Carbon dioxide capture and conversion by an acid-base resistant metal-organic framework. *Nat. Commun.* **2017**, *8*, 1233.
(175) Roztocki, K.; Lupa, M.; Sławek, A.; Makowski, W.; Senkovska, I.; Kaskel, S.; Matoga, D. Water-stable metal−organic framework with three hydrogen-bond acceptors: Versatile theoretical and experimental insights into adsorption ability and thermo-hydrolytic stability. *Inorg. Chem.* **2018**, *57*, 3287−3296.
(176) Jin, W.-G.; Chen, W.; Xu, P.-H.; Lin, X.-W.; Huang, X.-C.; Chen, G.-H.; Lu, F.; Chen, X.-M. An exceptionally water stable metal−organic framework with amide-functionalized cages: Selective CO_2/CH_4 uptake and removal of antibiotics and dyes from water. *Chem. - Eur. J.* **2017**, *23*, 13058−13066.
(177) Li, X.-X.; Shen, F.-C.; Liu, J.; Li, S.-L.; Dong, L.-Z.; Fu, Q.; Su, Z.-M.; Lan, Y.-Q. A highly stable polyoxometalate-based metal−organic framework with an ABW zeolite-like structure. *Chem. Commun.* **2017**, *53*, 10054−10057.
(178) Yang, X.; Zhang, Y.; Li, F.; Guo, T.; Wu, Y.; Jin, F.; Fang, M.; Lan, Y.; Li, Y.; Zhou, Y.; Zou, Z. Theoretical and experimental studies

https://dx.doi.org/10.1021/acs.chemrev.9b00746
Chem. Rev. XXXX, XXX, XXX−XXX

on three water-stable, isostructural, paddlewheel based semiconducting metal−organic frameworks. *Dalton Trans* **2017**, *46*, 8204−8218.
(179) Xing, K.; Fan, R.; Wang, J.; Zhang, S.; Feng, K.; Du, X.; Song, Y.; Wang, P.; Yang, Y. Highly stable and regenerative metal−organic framework designed by multiwalled divider installation strategy for detection of Co(II) ions and organic aromatics in water. *ACS Appl. Mater. Interfaces* **2017**, *9*, 19881−19893.
(180) Tian, D.; Xu, J.; Xie, Z.-J.; Yao, Z.-Q.; Fu, D.-L.; Zhou, Z.; Bu, X.-H. The first example of hetero-triple-walled metal−organic frameworks with high chemical stability constructed via flexible integration of mixed molecular building blocks. *Adv. Sci.* **2016**, *3*, 1500283.
(181) Liu, X.-J.; Zhang, Y.-H.; Chang, Z.; Li, A.-L.; Tian, D.; Yao, Z.-Q.; Jia, Y.-Y.; Bu, X.-H. A water-stable metal−organic framework with a double-helical structure for fluorescent sensing. *Inorg. Chem.* **2016**, *55*, 7326−7328.
(182) Hu, Y.; Ding, M.; Liu, X.-Q.; Sun, L.-B.; Jiang, H.-L. Rational synthesis of an exceptionally stable Zn(II) metal−organic framework for the highly selective and sensitive detection of picric acid. *Chem. Commun.* **2016**, *52*, 5734−5737.
(183) Ma, D.-Y.; Li, Z.; Xiao, J.-X.; Deng, R.; Lin, P.-F.; Chen, R.-Q.; Liang, Y.-Q.; Guo, H.-F.; Liu, B.; Liu, J.-Q. Hydrostable and nitryl/methyl-functionalized metal−organic framework for drug delivery and highly selective CO_2 adsorption. *Inorg. Chem.* **2015**, *54*, 6719−6726.
(184) Gao, W.-Y.; Cai, R.; Pham, T.; Forrest, K. A.; Hogan, A.; Nugent, P.; Williams, K.; Wojtas, L.; Luebke, R.; Weseliński, Ł. J.; Zaworotko, M. J.; Space, B.; Chen, Y.-S.; Eddaoudi, M.; Shi, X.; Ma, S. Remote stabilization of copper paddlewheel based molecular building blocks in metal−organic frameworks. *Chem. Mater.* **2015**, *27*, 2144−2151.
(185) Yao, Z.-Q.; Li, G.-Y.; Xu, J.; Hu, T.-L.; Bu, X.-H. A water-stable luminescent Zn^{II} metal-organic framework as chemosensor for high-efficiency detection of Cr^{VI}-anions ($Cr_2O_7^{2-}$ and CrO_4^{2-}) in aqueous solution. *Chem. - Eur. J.* **2018**, *24*, 3192−3198.
(186) Song, D.; Bae, J.; Ji, H.; Kim, M.-B.; Bae, Y.-S.; Park, K. S.; Moon, D.; Jeong, N. C. Coordinative reduction of metal nodes enhances the hydrolytic stability of a paddlewheel metal-organic framework. *J. Am. Chem. Soc.* **2019**, *141*, 7853−7864.
(187) Chen, X.; Peng, Y.; Han, X.; Liu, Y.; Lin, X.; Cui, Y. Sixteen isostructural phosphonate metal-organic frameworks with controlled Lewis acidity and chemical stability for asymmetric catalysis. *Nat. Commun.* **2017**, *8*, 2171.
(188) Remy, T.; Peter, S. A.; Van der Perre, S.; Valvekens, P.; De Vos, D. E.; Baron, G. V.; Denayer, J. F. M. Selective dynamic CO_2 separations on Mg-MOF-74 at low pressures: A detailed comparison with 13X. *J. Phys. Chem. C* **2013**, *117*, 9301−9310.
(189) Cai, K.; Sun, F.; Liang, X.; Liu, C.; Zhao, N.; Zou, X.; Zhu, G. An acid-stable hexaphosphate ester based metal−organic framework and its polymer composite as proton exchange membrane. *J. Mater. Chem. A* **2017**, *5*, 12943−12950.
(190) Chang, J.-S.; Kyu, H. Y.; Hwa, J. S.; Hong, D.-Y.; Seo, Y.-K. Porous organic−inorganic hybrid materials and adsorbent comprising the same. U.S. US8168813B2, May 1, 2012.
(191) Chang, J.-S.; Hwang, Y. K.; Jhung, S. H.; Hong, D.-Y.; Seo, Y.-k. A synthesis method of Fe containing porous organic inorganic hybrid materials and water adsorbent using the same. KR KR100803964B1, December 13, 2006.
(192) Hwang, Y. K.; Chang, J.-S.; Seo, Y.-K.; Hwang, D. W. Porous organic-inorganic hybrid materials with crystallinity and method for preparing thereof. U.S. US8507399B2, August 13, 2013.
(193) Hwang, Y. K.; Chang, J.-S.; Hwang, D. W.; Lee, J. S. Apparatus for treating air by using porous organic-inorganic hybrid materials as an absorbent. U.S. US9038409B2, May 26, 2015.
(194) Towsif Abtab, S. M.; Alezi, D.; Bhatt, P. M.; Shkurenko, A.; Belmabkhout, Y.; Aggarwal, H.; Weseliński, Ł. J.; Alsadun, N.; Samin, U.; Hedhili, M. N.; Eddaoudi, M. Reticular chemistry in action: A hydrolytically stable MOF capturing twice its weight in adsorbed water. *Chem* **2018**, *4*, 94−105.
(195) AbdulHalim, R. G.; Bhatt, P. M.; Belmabkhout, Y.; Shkurenko, A.; Adil, K.; Barbour, L. J.; Eddaoudi, M. A fine-tuned metal−organic framework for autonomous indoor moisture control. *J. Am. Chem. Soc.* **2017**, *139*, 10715−10722.
(196) de Lange, M. F.; Gutierrez-Sevillano, J.-J.; Hamad, S.; Vlugt, T. J. H.; Calero, S.; Gascon, J.; Kapteijn, F. Understanding adsorption of highly polar vapors on mesoporous MIL-100(Cr) and MIL-101(Cr): Experiments and molecular simulations. *J. Phys. Chem. C* **2013**, *117*, 7613−7622.
(197) Küsgens, P.; Rose, M.; Senkovska, I.; Fröde, H.; Henschel, A.; Siegle, S.; Kaskel, S. Characterization of metal-organic frameworks by water adsorption. *Microporous Mesoporous Mater.* **2009**, *120*, 325−330.
(198) Shigematsu, A.; Yamada, T.; Kitagawa, H. Wide control of proton conductivity in porous coordination polymers. *J. Am. Chem. Soc.* **2011**, *133*, 2034−2036.
(199) Jeremias, F.; Fröhlich, D.; Janiak, C.; Henninger, S. K. Advancement of sorption-based heat transformation by a metal coating of highly-stable, hydrophilic aluminium fumarate MOF. *RSC Adv.* **2014**, *4*, 24073−24082.
(200) de Lange, M. F.; Zeng, T.; Vlugt, T. J. H.; Gascon, J.; Kapteijn, F. Manufacture of dense CAU-10-H coatings for application in adsorption driven heat pumps: Optimization and characterization. *CrystEngComm* **2015**, *17*, 5911−5920.
(201) Wiersum, A. D.; Soubeyrand-Lenoir, E.; Yang, Q.; Moulin, B.; Guillerm, V.; Yahia, M. B.; Bourrelly, S.; Vimont, A.; Miller, S.; Vagner, C.; Daturi, M.; Clet, G.; Serre, C.; Maurin, G.; Llewellyn, P. L. An evaluation of UiO-66 for gas-based applications. *Chem. - Asian J.* **2011**, *6*, 3270−3280.
(202) Canivet, J.; Bonnefoy, J.; Daniel, C.; Legrand, A.; Coasne, B.; Farrusseng, D. Structure−property relationships of water adsorption in metal−organic frameworks. *New J. Chem.* **2014**, *38*, 3102−3111.
(203) Rieth, A. J.; Yang, S.; Wang, E. N.; Dincă, M. Record atmospheric fresh water capture and heat transfer with a material operating at the water uptake reversibility limit. *ACS Cent. Sci.* **2017**, *3*, 668−672.
(204) Cadiau, A.; Belmabkhout, Y.; Adil, K.; Bhatt, P. M.; Pillai, R. S.; Shkurenko, A.; Martineau-Corcos, C.; Maurin, G.; Eddaoudi, M. Hydrolytically stable fluorinated metal-organic frameworks for energy-efficient dehydration. *Science* **2017**, *356*, 731−735.
(205) Lee, J. S.; Yoon, J. W.; Mileo, P. G. M.; Cho, K. H.; Park, J.; Kim, K.; Kim, H.; de Lange, M. F.; Kapteijn, F.; Maurin, G.; Humphrey, S. M.; Chang, J.-S. Porous metal−organic framework CUK-1 for adsorption heat allocation toward green applications of natural refrigerant water. *ACS Appl. Mater. Interfaces* **2019**, *11*, 25778−25789.
(206) Thommes, M.; Kaneko, K.; Neimark, A. V.; Olivier, J. P.; Rodriguez-Reinoso, F.; Rouquerol, J.; Sing, K. S. W. Physisorption of gases, with special reference to the evaluation of surface area and pore size distribution (IUPAC Technical Report). *Pure Appl. Chem.* **2015**, *87*, 1051−1069.
(207) Valenzano, L.; Civalleri, B.; Chavan, S.; Bordiga, S.; Nilsen, M. H.; Jakobsen, S.; Lillerud, K. P.; Lamberti, C. Disclosing the complex structure of UiO-66 metal organic framework: A synergic combination of experiment and theory. *Chem. Mater.* **2011**, *23*, 1700−1718.
(208) Platero-Prats, A. E.; Mavrandonakis, A.; Gallington, L. C.; Liu, Y.; Hupp, J. T.; Farha, O. K.; Cramer, C. J.; Chapman, K. W. Structural transitions of the metal-oxide nodes within metal−organic frameworks: On the local structures of NU-1000 and UiO-66. *J. Am. Chem. Soc.* **2016**, *138*, 4178−4185.
(209) Wu, H.; Chua, Y. S.; Krungleviciute, V.; Tyagi, M.; Chen, P.; Yildirim, T.; Zhou, W. Unusual and highly tunable missing-linker defects in zirconium metal−organic framework UiO-66 and their important effects on gas adsorption. *J. Am. Chem. Soc.* **2013**, *135*, 10525−10532.
(210) Seo, Y.-K.; Yoon, J. W.; Lee, J. S.; Hwang, Y. K.; Jun, C.-H.; Chang, J.-S.; Wuttke, S.; Bazin, P.; Vimont, A.; Daturi, M.; Bourrelly, S.; Llewellyn, P. L.; Horcajada, P.; Serre, C.; Férey, G. Energy-efficient

https://dx.doi.org/10.1021/acs.chemrev.9b00746
Chem. Rev. XXXX, XXX, XXX−XXX

dehumidification over hierachically porous metal−organic frameworks as advanced water adsorbents. *Adv. Mater.* **2012**, *24*, 806−810.
(211) Wöllner, M.; Klein, N.; Kaskel, S. Measuring water adsorption processes of metal-organic frameworks for heat pump applications via optical calorimetry. *Microporous Mesoporous Mater.* **2019**, *278*, 206−211.
(212) Kim, S.-I.; Yoon, T.-U.; Kim, M.-B.; Lee, S.-J.; Hwang, Y. K.; Chang, J.-S.; Kim, H.-J.; Lee, H.-N.; Lee, U. H.; Bae, Y.-S. Metal-organic frameworks with high working capacities and cyclic hydrothermal stabilities for fresh water production. *Chem. Eng. J.* **2016**, *286*, 467−475.
(213) Akiyama, G.; Matsuda, R.; Sato, H.; Hori, A.; Takata, M.; Kitagawa, S. Effect of functional groups in MIL-101 on water sorption behavior. *Microporous Mesoporous Mater.* **2012**, *157*, 89−93.
(214) Akiyama, G.; Matsuda, R.; Kitagawa, S. Highly porous and stable coordination polymers as water sorption materials. *Chem. Lett.* **2010**, *39*, 360−361.
(215) Jeremias, F.; Khutia, A.; Henninger, S. K.; Janiak, C. MIL-100(Al, Fe) as water adsorbents for heat transformation purposes—a promising application. *J. Mater. Chem.* **2012**, *22*, 10148−10151.
(216) Mileo, P. G.; Ho Cho, K.; Park, J.; Devautour-Vinot, S.; Chang, J.-S.; Maurin, G. Unraveling the water adsorption mechanism in the mesoporous MIL-100 (Fe) metal−organic framework. *J. Phys. Chem. C* **2019**, *123*, 23014−23025.
(217) Deria, P.; Chung, Y. G.; Snurr, R. Q.; Hupp, J. T.; Farha, O. K. Water stabilization of Zr_6-based metal−organic frameworks via solvent-assisted ligand incorporation. *Chem. Sci.* **2015**, *6* (9), 5172−5176.
(218) Kiener, C.; Mueller, U.; Schubert, M. Organometallic aluminum fumarate backbone material. WO WO2007/118841A2, April 12, 2007.
(219) Fröhlich, D.; Pantatosaki, E.; Kolokathis, P. D.; Markey, K.; Reinsch, H.; Baumgartner, M.; van der Veen, M. A.; De Vos, D. E.; Stock, N.; Papadopoulos, G. K.; Henninger, S. K.; Janiak, C. Water adsorption behaviour of CAU-10-H: A thorough investigation of its structure−property relationships. *J. Mater. Chem. A* **2016**, *4*, 11859−11869.
(220) Do, D. D.; Do, H. D. A model for water adsorption in activated carbon. *Carbon* **2000**, *38*, 767−773.
(221) Soubeyrand-Lenoir, E.; Vagner, C.; Yoon, J. W.; Bazin, P.; Ragon, F.; Hwang, Y. K.; Serre, C.; Chang, J.-S.; Llewellyn, P. L. How water fosters a remarkable 5-fold increase in low-pressure CO_2 uptake within mesoporous MIL-100(Fe). *J. Am. Chem. Soc.* **2012**, *134*, 10174−10181.
(222) An, H. J.; Sarker, M.; Yoo, D. K.; Jhung, S. H. Water adsorption desorption over metal-organic frameworks with ammonium group for possible application in adsorption heat transformation. *Chem. Eng. J.* **2019**, *373*, 1064−1071.
(223) Wißmann, G.; Schaate, A.; Lilienthal, S.; Bremer, I.; Schneider, A. M.; Behrens, P. Modulated synthesis of Zr-fumarate MOF. *Microporous Mesoporous Mater.* **2012**, *152*, 64−70.
(224) Liu, Y.; Chen, Z.; Liu, G.; Belmabkhout, Y.; Adil, K.; Eddaoudi, M.; Koros, W. Conformation-controlled molecular sieving effects for membrane-based propylene/propane separation. *Adv. Mater.* **2019**, *31*, 1807513.
(225) Sohail, M.; Yun, Y.-N.; Lee, E.; Kim, S. K.; Cho, K.; Kim, J.-N.; Kim, T. W.; Moon, J.-H.; Kim, H. Synthesis of highly crystalline NH_2-MIL-125 (Ti) with S-shaped water isotherms for adsorption heat transformation. *Cryst. Growth Des.* **2017**, *17*, 1208−1213.
(226) Gordeeva, L. G.; Solovyeva, M. V.; Aristov, Y. I. NH_2-MIL-125 as a promising material for adsorptive heat transformation and storage. *Energy* **2016**, *100*, 18−24.
(227) Jeremias, F.; Lozan, V.; Henninger, S. K.; Janiak, C. Programming MOFs for water sorption: Amino-functionalized MIL-125 and UiO-66 for heat transformation and heat storage applications. *Dalton Trans* **2013**, *42*, 15967−15973.
(228) Zlotea, C.; Phanon, D.; Mazaj, M.; Heurtaux, D.; Guillerm, V.; Serre, C.; Horcajada, P.; Devic, T.; Magnier, E.; Cuevas, F.; Férey, G.; Llewellyn, P. L.; Latroche, M. Effect of NH_2 and CF_3 functionalization on the hydrogen sorption properties of MOFs. *Dalton Trans* **2011**, *40*, 4879−4881.
(229) Humphrey, S. M.; Mole, R. A.; McPartlin, M.; McInnes, E. J. L.; Wood, P. T. Isolated magnetic clusters of Co(II) and Ni(II) within 3-dimensional organic frameworks of 6-mercaptonicotinic acid: Unique structural topologies based on selectivity for hard and soft coordination environments. *Inorg. Chem.* **2005**, *44*, 5981−5983.
(230) Humphrey, S. M.; Chang, J.-S.; Jhung, S. H.; Yoon, J. W.; Wood, P. T. Porous cobalt(II)−organic frameworks with corrugated walls: Structurally robust gas-sorption materials. *Angew. Chem., Int. Ed.* **2007**, *46*, 272−275.
(231) Kalmutzki, M. J.; Diercks, C. S.; Yaghi, O. M. Metal−organic frameworks for water harvesting from air. *Adv. Mater.* **2018**, *30*, 1704304.
(232) Elsayed, E.; Al-Dadah, R.; Mahmoud, S.; Anderson, P. A.; Elsayed, A.; Youssef, P. G. CPO-27(Ni), aluminium fumarate and MIL-101(Cr) MOF materials for adsorption water desalination. *Desalination* **2017**, *406*, 25−36.
(233) Noorpoor, Z.; Pakdehi, S. G.; Rashidi, A. High capacity and energy-efficient dehydration of liquid fuel 2-dimethyl amino ethyl azide (DMAZ) over chromium terephthalic (MIL-101) nano-adsorbent. *Adsorption* **2017**, *23*, 743−752.
(234) Lv, X.-L.; Yuan, S.; Xie, L.-H.; Darke, H. F.; Chen, Y.; He, T.; Dong, C.; Wang, B.; Zhang, Y.-Z.; Li, J.-R.; Zhou, H.-C. Ligand-rigidification for enhancing the stability of metal−organic frameworks. *J. Am. Chem. Soc.* **2019**, *141*, 10283−10293.
(235) Henninger, S. K.; Jeremias, F.; Kummer, H.; Janiak, C. MOFs for use in adsorption heat pump processes. *Eur. J. Inorg. Chem.* **2012**, *2012*, 2625−2634.
(236) Ko, N.; Choi, P. G.; Hong, J.; Yeo, M.; Sung, S.; Cordova, K. E.; Park, H. J.; Yang, J. K.; Kim, J. Tailoring the water adsorption properties of MIL-101 metal−organic frameworks by partial functionalization. *J. Mater. Chem. A* **2015**, *3*, 2057−2064.
(237) Padial, N. M.; Quartapelle Procopio, E.; Montoro, C.; López, E.; Oltra, J. E.; Colombo, V.; Maspero, A.; Masciocchi, N.; Galli, S.; Senkovska, I.; Kaskel, S.; Barea, E.; Navarro, J. A. R. Highly hydrophobic isoreticular porous metal−organic frameworks for the capture of harmful volatile organic compounds. *Angew. Chem., Int. Ed.* **2013**, *52*, 8290−8294.
(238) Wright, A. M.; Rieth, A. J.; Yang, S.; Wang, E. N.; Dincă, M. Precise control of pore hydrophilicity enabled by post-synthetic cation exchange in metal−organic frameworks. *Chem. Sci.* **2018**, *9*, 3856−3859.
(239) Khutia, A.; Rammelberg, H. U.; Schmidt, T.; Henninger, S.; Janiak, C. Water sorption cycle measurements on functionalized MIL-101Cr for heat transformation application. *Chem. Mater.* **2013**, *25*, 790−798.
(240) Ehrenmann, J.; Henninger, S. K.; Janiak, C. Water adsorption characteristics of MIL-101 for heat-transformation applications of MOFs. *Eur. J. Inorg. Chem.* **2011**, *2011*, 471−474.
(241) Deria, P.; Mondloch, J. E.; Tylianakis, E.; Ghosh, P.; Bury, W.; Snurr, R. Q.; Hupp, J. T.; Farha, O. K. Perfluoroalkane functionalization of NU-1000 via solvent-assisted ligand incorporation: Synthesis and CO_2 adsorption studies. *J. Am. Chem. Soc.* **2013**, *135*, 16801−16804.
(242) Zheng, J.; Vemuri, R. S.; Estevez, L.; Koech, P. K.; Varga, T.; Camaioni, D. M.; Blake, T. A.; McGrail, B. P.; Motkuri, R. K. Pore-engineered metal-organic frameworks with excellent adsorption of water and fluorocarbon refrigerant for cooling applications. *J. Am. Chem. Soc.* **2017**, *139*, 10601−10604.
(243) Liu, J.; Wang, Y.; Benin, A. I.; Jakubczak, P.; Willis, R. R.; LeVan, M. D. CO_2/H_2O adsorption equilibrium and rates on metal−organic frameworks: HKUST-1 and Ni/DOBDC. *Langmuir* **2010**, *26*, 14301−14307.
(244) Schoenecker, P. M.; Carson, C. G.; Jasuja, H.; Flemming, C. J. J.; Walton, K. S. Effect of water adsorption on retention of structure and surface area of metal−organic frameworks. *Ind. Eng. Chem. Res.* **2012**, *51*, 6513−6519.

https://dx.doi.org/10.1021/acs.chemrev.9b00746
Chem. Rev. XXXX, XXX, XXX−XXX

(245) Rezk, A.; Al-Dadah, R.; Mahmoud, S.; Elsayed, A. Experimental investigation of metal organic frameworks characteristics for water adsorption chillers. *Proc. Inst. Mech. Eng., Part C* **2013**, *227*, 992−1005.
(246) Al-Janabi, N.; Hill, P.; Torrente-Murciano, L.; Garforth, A.; Gorgojo, P.; Siperstein, F.; Fan, X. Mapping the Cu-BTC metal−organic framework (HKUST-1) stability envelope in the presence of water vapour for CO_2 adsorption from flue gases. *Chem. Eng. J.* **2015**, *281*, 669−677.
(247) Liu, J.; Zheng, J.; Barpaga, D.; Sabale, S.; Arey, B.; Derewinski, M. A.; McGrail, B. P.; Motkuri, R. K. A tunable bimetallic MOF-74 for adsorption chiller applications. *Eur. J. Inorg. Chem.* **2018**, *2018*, 885−889.
(248) Zhao, Z.; Wang, S.; Yang, Y.; Li, X.; Li, J.; Li, Z. Competitive adsorption and selectivity of benzene and water vapor on the microporous metal organic frameworks (HKUST-1). *Chem. Eng. J.* **2015**, *259*, 79−89.
(249) Ahnfeldt, T.; Gunzelmann, D.; Wack, J.; Senker, J.; Stock, N. Controlled modification of the inorganic and organic bricks in an Al-based MOF by direct and post-synthetic synthesis routes. *CrystEngComm* **2012**, *14*, 4126−4136.
(250) Bon, V.; Senkovskyy, V.; Senkovska, I.; Kaskel, S. Zr(IV) and Hf(IV) based metal−organic frameworks with reo-topology. *Chem. Commun.* **2012**, *48*, 8407−8409.
(251) Van Assche, T. R. C.; Duerinck, T.; Gutiérrez Sevillano, J. J.; Calero, S.; Baron, G. V.; Denayer, J. F. M. High adsorption capacities and two-step adsorption of polar adsorbates on copper−benzene-1,3,5-tricarboxylate metal−organic framework. *J. Phys. Chem. C* **2013**, *117*, 18100−18111.
(252) Elsayed, E.; Al-Dadah, R.; Mahmoud, S.; Elsayed, A.; Anderson, P. A. Aluminium fumarate and CPO-27(Ni) MOFs: Characterization and thermodynamic analysis for adsorption heat pump applications. *Appl. Therm. Eng.* **2016**, *99*, 802−812.
(253) Kim, S.-N.; Kim, J.; Kim, H.-Y.; Cho, H.-Y.; Ahn, W.-S. Adsorption/catalytic properties of MIL-125 and NH_2-MIL-125. *Catal. Today* **2013**, *204*, 85−93.
(254) Reinsch, H.; Feyand, M.; Ahnfeldt, T.; Stock, N. CAU-3: A new family of porous MOFs with a novel Al-based brick: $[Al_2(OCH_3)_4(O_2C\text{-}X\text{-}CO_2)]$ (X = aryl). *Dalton Trans* **2012**, *41*, 4164−4171.
(255) Cai, Y.; Zhang, Y.; Huang, Y.; Marder, S. R.; Walton, K. S. Impact of alkyl-functionalized BTC on properties of copper-based metal−organic frameworks. *Cryst. Growth Des.* **2012**, *12*, 3709−3713.
(256) Santra, A.; Senkovska, I.; Kaskel, S.; Bharadwaj, P. K. Gas storage in a partially fluorinated highly stable three-dimensional porous metal−organic framework. *Inorg. Chem.* **2013**, *52*, 7358−7366.
(257) Kayal, S.; Chakraborty, A.; Teo, H. W. B. Green synthesis and characterization of aluminium fumarate metal-organic framework for heat transformation applications. *Mater. Lett.* **2018**, *221*, 165−167.
(258) Shi, B.; Al-Dadah, R.; Mahmoud, S.; Elsayed, A.; Elsayed, E. CPO-27(Ni) metal−organic framework based adsorption system for automotive air conditioning. *Appl. Therm. Eng.* **2016**, *106*, 325−333.
(259) Cmarik, G. E.; Kim, M.; Cohen, S. M.; Walton, K. S. Tuning the adsorption properties of UiO-66 via ligand functionalization. *Langmuir* **2012**, *28*, 15606−15613.
(260) Goesten, M. G.; Juan-Alcañiz, J.; Ramos-Fernandez, E. V.; Sai Sankar Gupta, K. B.; Stavitski, E.; van Bekkum, H.; Gascon, J.; Kapteijn, F. Sulfation of metal−organic frameworks: Opportunities for acid catalysis and proton conductivity. *J. Catal.* **2011**, *281*, 177−187.
(261) Wade, C. R.; Corrales-Sanchez, T.; Narayan, T. C.; Dincă, M. Postsynthetic tuning of hydrophilicity in pyrazolate MOFs to modulate water adsorption properties. *Energy Environ. Sci.* **2013**, *6*, 2172−2177.
(262) Montoro, C.; Linares, F.; Quartapelle Procopio, E.; Senkovska, I.; Kaskel, S.; Galli, S.; Masciocchi, N.; Barea, E.; Navarro, J. A. R. Capture of nerve agents and mustard gas analogues by hydrophobic robust MOF-5 type metal−organic frameworks. *J. Am. Chem. Soc.* **2011**, *133*, 11888−11891.
(263) Tannert, N.; Ernst, S.-J.; Jansen, C.; Bart, H.-J.; Henninger, S.; Janiak, C. Evaluation of the highly stable metal-organic framework MIL 53(Al) TDC (TDC = 2,5 thiophenedicarboxylate) as a new and promising adsorbent for heat transformation applications. *J. Mater. Chem. A* **2018**, *6*, 17706−17712.
(264) Rieth, A. J.; Wright, A. M.; Rao, S.; Kim, H.; LaPotin, A. D.; Wang, E. N.; Dincă, M. Tunable metal−organic frameworks enable high-efficiency cascaded adsorption heat pumps. *J. Am. Chem. Soc.* **2018**, *140*, 17591−17596.
(265) Teo, H. W. B.; Chakraborty, A.; Kayal, S. Formic acid modulated (fam) aluminium fumarate MOF for improved isotherms and kinetics with water adsorption: Cooling/heat pump applications. *Microporous Mesoporous Mater.* **2018**, *272*, 109−116.
(266) Jasuja, H.; Burtch, N. C.; Huang, Y.-g.; Cai, Y.; Walton, K. S. Kinetic water stability of an isostructural family of zinc-based pillared metal−organic frameworks. *Langmuir* **2013**, *29*, 633−642.
(267) Zhang, J.-P.; Zhu, A.-X.; Lin, R.-B.; Qi, X.-L.; Chen, X.-M. Pore surface tailored SOD-type metal-organic zeolites. *Adv. Mater.* **2011**, *23*, 1268−1271.
(268) Peng, L.; Yang, S.; Sun, D. T.; Asgari, M.; Queen, W. L. MOF/polymer composite synthesized using a double solvent method offers enhanced water and CO_2 adsorption properties. *Chem. Commun.* **2018**, *54*, 10602−10605.
(269) Wittmann, T.; Siegel, R.; Reimer, N.; Milius, W.; Stock, N.; Senker, J. Enhancing the water stability of Al-MIL-101-NH_2 via postsynthetic modification. *Chem. - Eur. J.* **2015**, *21*, 314−323.
(270) Wickenheisser, M.; Jeremias, F.; Henninger, S. K.; Janiak, C. Grafting of hydrophilic ethylene glycols or ethylenediamine on coordinatively unsaturated metal sites in MIL-100(Cr) for improved water adsorption characteristics. *Inorg. Chim. Acta* **2013**, *407*, 145−152.
(271) Yu, C.; Bourrelly, S.; Martineau, C.; Saidi, F.; Bloch, E.; Lavrard, H.; Taulelle, F.; Horcajada, P.; Serre, C.; Llewellyn, P. L.; Magnier, E.; Devic, T. Functionalization of Zr-based MOFs with alkyl and perfluoroalkyl groups: The effect on the water sorption behavior. *Dalton Trans* **2015**, *44*, 19687−19692.
(272) Jasuja, H.; Jiao, Y.; Burtch, N. C.; Huang, Y.-g.; Walton, K. S. Synthesis of cobalt-, nickel-, copper-, and zinc-based, water-stable, pillared metal−organic frameworks. *Langmuir* **2014**, *30*, 14300−14307.
(273) Biswas, S.; Ahnfeldt, T.; Stock, N. New functionalized flexible Al-MIL-53-X (X = -Cl, -Br, -CH_3, -NO_2, -$(OH)_2$) solids: Syntheses, characterization, sorption, and breathing behavior. *Inorg. Chem.* **2011**, *50*, 9518−9526.
(274) Kim, H.; Cho, H. J.; Narayanan, S.; Yang, S.; Furukawa, H.; Schiffres, S.; Li, X.; Zhang, Y.-B.; Jiang, J.; Yaghi, O. M.; Wang, E. N. Characterization of adsorption enthalpy of novel water-stable zeolites and metal-organic frameworks. *Sci. Rep.* **2016**, *6*, 19097.
(275) Reinsch, H.; Marszałek, B.; Wack, J.; Senker, J.; Gil, B.; Stock, N. A new Al-MOF based on a unique column-shaped inorganic building unit exhibiting strongly hydrophilic sorption behaviour. *Chem. Commun.* **2012**, *48*, 9486−9488.
(276) Biswas, S.; Grzywa, M.; Nayek, H. P.; Dehnen, S.; Senkovska, I.; Kaskel, S.; Volkmer, D. A cubic coordination framework constructed from benzobistriazolate ligands and zinc ions having selective gas sorption properties. *Dalton Trans* **2009**, 6487−6495.
(277) Aríñez-Soriano, J.; Albalad, J.; Vila-Parrondo, C.; Pérez-Carvajal, J.; Rodríguez-Hermida, S.; Cabeza, A.; Juanhuix, J.; Imaz, I.; Maspoch, D. Single-crystal and humidity-controlled powder diffraction study of the breathing effect in a metal−organic framework upon water adsorption/desorption. *Chem. Commun.* **2016**, *52*, 7229−7232.
(278) de Lange, M. F.; Ottevanger, C. P.; Wiegman, M.; Vlugt, T. J. H.; Gascon, J.; Kapteijn, F. Crystals for sustainability − structuring Al-based MOFs for the allocation of heat and cold. *CrystEngComm* **2015**, *17*, 281−285.
(279) Kundu, T.; Sahoo, S. C.; Banerjee, R. Variable water adsorption in amino acid derivative based homochiral metal organic frameworks. *Cryst. Growth Des.* **2012**, *12*, 4633−4640.

https://dx.doi.org/10.1021/acs.chemrev.9b00746
Chem. Rev. XXXX, XXX, XXX−XXX

(280) Lenzen, D.; Bendix, P.; Reinsch, H.; Fröhlich, D.; Kummer, H.; Möllers, M.; Hügenell, P. P. C.; Gläser, R.; Henninger, S.; Stock, N. Scalable green synthesis and full-scale test of the metal-organic framework CAU-10-H for use in adsorption-driven chillers. *Adv. Mater.* **2018**, *30*, 1705869.
(281) Chen, Z.; Wang, X.; Islamoglu, T.; Farha, O. K. Green synthesis of a functionalized zirconium-based metal−organic framework for water and ethanol adsorption. *Inorganics* **2019**, *7*, 56.
(282) Jasuja, H.; Zang, J.; Sholl, D. S.; Walton, K. S. Rational tuning of water vapor and CO_2 adsorption in highly stable Zr-based MOFs. *J. Phys. Chem. C* **2012**, *116*, 23526−23532.
(283) Yamada, T.; Shirai, Y.; Kitagawa, H. Synthesis, water adsorption, and proton conductivity of solid-solution-type metal−organic frameworks $Al(OH)(bdc\text{-}OH)_x(bdc\text{-}NH_2)_{1-x}$. *Chem. - Asian J.* **2014**, *9*, 1316−1320.
(284) Fröhlich, D.; Henninger, S. K.; Janiak, C. Multicycle water vapour stability of microporous breathing MOF aluminium isophthalate CAU-10-H. *Dalton Trans* **2014**, *43*, 15300−15304.
(285) Permyakova, A.; Skrylnyk, O.; Courbon, E.; Affram, M.; Wang, S.; Lee, U.-H.; Valekar, A. H.; Nouar, F.; Mouchaham, G.; Devic, T.; De Weireld, G.; Chang, J.-S.; Steunou, N.; Frère, M.; Serre, C. Synthesis optimization, shaping, and heat reallocation evaluation of the hydrophilic metal−organic framework MIL-160(Al). *ChemSusChem* **2017**, *10*, 1419−1426.
(286) Zhang, K.; Lively, R. P.; Dose, M. E.; Brown, A. J.; Zhang, C.; Chung, J.; Nair, S.; Koros, W. J.; Chance, R. R. Alcohol and water adsorption in zeolitic imidazolate frameworks. *Chem. Commun.* **2013**, *49*, 3245−3247.
(287) Begum, S.; Horike, S.; Kitagawa, S.; Krautscheid, H. Water stable triazolyl phosphonate MOFs: Steep water uptake and facile regeneration. *Dalton Trans* **2015**, *44*, 18727−18730.
(288) Kondo, A.; Daimaru, T.; Noguchi, H.; Ohba, T.; Kaneko, K.; Kanoh, H. Adsorption of water on three-dimensional pillared-layer metal organic frameworks. *J. Colloid Interface Sci.* **2007**, *314*, 422−426.
(289) Henninger, S. K.; Habib, H. A.; Janiak, C. MOFs as adsorbents for low temperature heating and cooling applications. *J. Am. Chem. Soc.* **2009**, *131*, 2776−2777.
(290) Yang, Q.; Vaesen, S.; Ragon, F.; Wiersum, A. D.; Wu, D.; Lago, A.; Devic, T.; Martineau, C.; Taulelle, F.; Llewellyn, P. L.; Jobic, H.; Zhong, C.; Serre, C.; De Weireld, G.; Maurin, G. A water stable metal−organic framework with optimal features for CO_2 capture. *Angew. Chem., Int. Ed.* **2013**, *52*, 10316−10320.
(291) Jasuja, H.; Huang, Y.-g.; Walton, K. S. Adjusting the stability of metal−organic frameworks under humid conditions by ligand functionalization. *Langmuir* **2012**, *28*, 16874−16880.
(292) Karra, J. R.; Jasuja, H.; Huang, Y.-G.; Walton, K. S. Structural stability of BTTB-based metal−organic frameworks under humid conditions. *J. Mater. Chem. A* **2015**, *3*, 1624−1631.
(293) O'Nolan, D.; Kumar, A.; Zaworotko, M. J. Water vapor sorption in hybrid pillared square grid materials. *J. Am. Chem. Soc.* **2017**, *139*, 8508−8513.
(294) Sun, J.-K.; Ji, M.; Chen, C.; Wang, W.-G.; Wang, P.; Chen, R.-P.; Zhang, J. A charge-polarized porous metal−organic framework for gas chromatographic separation of alcohols from water. *Chem. Commun.* **2013**, *49*, 1624−1626.
(295) Kundu, T.; Sahoo, S. C.; Banerjee, R. Relating pore hydrophilicity with vapour adsorption capacity in a series of amino acid based metal organic frameworks. *CrystEngComm* **2013**, *15*, 9634−9640.
(296) Liu, L.; Telfer, S. G. Systematic ligand modulation enhances the moisture stability and gas sorption characteristics of quaternary metal−organic frameworks. *J. Am. Chem. Soc.* **2015**, *137*, 3901−3909.
(297) Bon, V.; Senkovska, I.; Weiss, M. S.; Kaskel, S. Tailoring of network dimensionality and porosity adjustment in Zr- and Hf-based MOFs. *CrystEngComm* **2013**, *15*, 9572−9577.
(298) Lin, X.-M.; Li, T.-T.; Chen, L.-F.; Zhang, L.; Su, C.-Y. Two ligand-functionalized Pb(II) metal−organic frameworks: Structures and catalytic performances. *Dalton Trans* **2012**, *41*, 10422−10429.
(299) Sadakiyo, M.; Yamada, T.; Kitagawa, H. Hydroxyl group recognition by hydrogen-bonding donor and acceptor sites embedded in a layered metal−organic framework. *J. Am. Chem. Soc.* **2011**, *133*, 11050−11053.
(300) Benoit, V.; Pillai, R. S.; Orsi, A.; Normand, P.; Jobic, H.; Nouar, F.; Billemont, P.; Bloch, E.; Bourrelly, S.; Devic, T.; Wright, P. A.; de Weireld, G.; Serre, C.; Maurin, G.; Llewellyn, P. L. MIL-91(Ti), a small pore metal−organic framework which fulfils several criteria: An upscaled green synthesis, excellent water stability, high CO_2 selectivity and fast CO_2 transport. *J. Mater. Chem. A* **2016**, *4*, 1383−1389.
(301) Jasuja, H.; Walton, K. S. Experimental study of CO_2, CH_4, and water vapor adsorption on a dimethyl-functionalized UiO-66 framework. *J. Phys. Chem. C* **2013**, *117*, 7062−7068.
(302) Biswas, S.; Couck, S.; Denysenko, D.; Bhunia, A.; Grzywa, M.; Denayer, J. F. M.; Volkmer, D.; Janiak, C.; Van Der Voort, P. Sorption and breathing properties of difluorinated MIL-47 and Al-MIL-53 frameworks. *Microporous Mesoporous Mater.* **2013**, *181*, 175−181.
(303) Quartapelle Procopio, E.; Fukushima, T.; Barea, E.; Navarro, J. A. R.; Horike, S.; Kitagawa, S. A soft copper(II) porous coordination polymer with unprecedented aqua bridge and selective adsorption properties. *Chem. - Eur. J.* **2012**, *18*, 13117−13125.
(304) Han, L.; Yan, Y.; Sun, F.; Cai, K.; Borjigin, T.; Zhao, X.; Qu, F.; Zhu, G. Single- and double-layer structures and sorption properties of two microporous metal−organic frameworks with flexible tritopic ligand. *Cryst. Growth Des.* **2013**, *13*, 1458−1463.
(305) Birsa Čelič, T.; Mazaj, M.; Guillou, N.; Elkaim, E.; El Roz, M.; Thibault-Starzyk, F.; Mali, G.; Rangus, M.; Čendak, T.; Kaučič, V.; Zabukovec Logar, N. Study of hydrothermal stability and water sorption characteristics of 3-dimensional Zn-based trimesate. *J. Phys. Chem. C* **2013**, *117*, 14608−14617.
(306) Li, G.-B.; Li, L.; Liu, J.-M.; Yang, T.; Su, C.-Y. A $CdSO_4$-type 3D metal−organic framework showing coordination dynamics on Cu^{2+} axial sites: Vapochromic response and guest sorption selectivity. *Cryst. Growth Des.* **2013**, *13*, 1518−1525.
(307) Hou, C.; Liu, Q.; Okamura, T.-a.; Wang, P.; Sun, W.-Y. Dynamic porous metal−organic frameworks: Synthesis, structure and sorption property. *CrystEngComm* **2012**, *14*, 8569−8576.
(308) Biswas, S.; Rémy, T.; Couck, S.; Denysenko, D.; Rampelberg, G.; Denayer, J. F. M.; Volkmer, D.; Detavernier, C.; Van Der Voort, P. Partially fluorinated MIL-47 and Al-MIL-53 frameworks: Influence of functionalization on sorption and breathing properties. *Phys. Chem. Chem. Phys.* **2013**, *15*, 3552−3561.
(309) McHugh, L. N.; McPherson, M. J.; McCormick, L. J.; Morris, S. A.; Wheatley, P. S.; Teat, S. J.; McKay, D.; Dawson, D. M.; Sansome, C. E. F.; Ashbrook, S. E.; Stone, C. A.; Smith, M. W.; Morris, R. E. Hydrolytic stability in hemilabile metal-organic frameworks. *Nat. Chem.* **2018**, *10*, 1096−1102.
(310) Lin, X.; Blake, A. J.; Wilson, C.; Sun, X. Z.; Champness, N. R.; George, M. W.; Hubberstey, P.; Mokaya, R.; Schröder, M. A porous framework polymer based on a Zinc(II) 4,4'-bipyridine-2,6,2',6'-tetracarboxylate: Synthesis, structure, and "zeolite-like" behaviors. *J. Am. Chem. Soc.* **2006**, *128*, 10745−10753.
(311) Niekiel, F.; Lannoeye, J.; Reinsch, H.; Munn, A. S.; Heerwig, A.; Zizak, I.; Kaskel, S.; Walton, R. I.; de Vos, D.; Llewellyn, P.; Lieb, A.; Maurin, G.; Stock, N. Conformation-controlled sorption properties and breathing of the aliphatic Al-MOF [Al(OH)(CDC)]. *Inorg. Chem.* **2014**, *53*, 4610−4620.
(312) Comotti, A.; Bracco, S.; Sozzani, P.; Horike, S.; Matsuda, R.; Chen, J.; Takata, M.; Kubota, Y.; Kitagawa, S. Nanochannels of two distinct cross-sections in a porous Al-based coordination polymer. *J. Am. Chem. Soc.* **2008**, *130*, 13664−13672.
(313) Kundu, T.; Sahoo, S. C.; Saha, S.; Banerjee, R. Salt metathesis in three dimensional metal−organic frameworks (MOFs) with unprecedented hydrolytic regenerability. *Chem. Commun.* **2013**, *49*, 5262−5264.
(314) Biswal, B. P.; Panda, T.; Banerjee, R. Solution mediated phase transformation (RHO to SOD) in porous Co-imidazolate based

https://dx.doi.org/10.1021/acs.chemrev.9b00746
Chem. Rev. XXXX, XXX, XXX−XXX

zeolitic frameworks with high water stability. *Chem. Commun.* **2012**, *48*, 11868−11870.
(315) Huang, Y.; Zheng, X.; Duan, J.; Liu, W.; Zhou, L.; Wang, C.; Wen, L.; Zhao, J.; Li, D. A highly stable multifunctional three-dimensional microporous framework: Excellent selective sorption and visible photoluminescence. *Dalton Trans* **2014**, *43*, 6811−6818.
(316) Hou, C.; Liu, Q.; Wang, P.; Sun, W.-Y. Porous metal−organic frameworks with high stability and selective sorption for CO_2 over N_2. *Microporous Mesoporous Mater.* **2013**, *172*, 61−66.
(317) Borjigin, T.; Sun, F.; Zhang, J.; Cai, K.; Ren, H.; Zhu, G. A microporous metal−organic framework with high stability for GC separation of alcohols from water. *Chem. Commun.* **2012**, *48*, 7613−7615.
(318) Bourrelly, S.; Moulin, B.; Rivera, A.; Maurin, G.; Devautour-Vinot, S.; Serre, C.; Devic, T.; Horcajada, P.; Vimont, A.; Clet, G.; Daturi, M.; Lavalley, J.-C.; Loera-Serna, S.; Denoyel, R.; Llewellyn, P. L.; Férey, G. Explanation of the adsorption of polar vapors in the highly flexible metal organic framework MIL-53(Cr). *J. Am. Chem. Soc.* **2010**, *132*, 9488−9498.
(319) Wang, C.; Luo, Y.-H.; He, X.-T.; Hong, D.-L.; Wang, J.-Y.; Chen, F.-H.; Chen, C.; Sun, B.-W. Porous high-valence metal−organic framework featuring open coordination sites for effective water adsorption. *Inorg. Chem.* **2019**, *58*, 3058−3064.
(320) Sanda, S.; Parshamoni, S.; Konar, S. Third-generation breathing metal−organic framework with selective, stepwise, reversible, and hysteretic adsorption properties. *Inorg. Chem.* **2013**, *52*, 12866−12868.
(321) Liu, J.; Zhang, F.; Zou, X.; Yu, G.; Zhao, N.; Fan, S.; Zhu, G. Environmentally friendly synthesis of highly hydrophobic and stable MIL-53 MOF nanomaterials. *Chem. Commun.* **2013**, *49*, 7430−7432.
(322) Weber, G.; Bezverkhyy, I.; Bellat, J.-P.; Ballandras, A.; Ortiz, G.; Chaplais, G.; Patarin, J.; Coudert, F.-X.; Fuchs, A. H.; Boutin, A. Mechanism of water adsorption in the large pore form of the gallium-based MIL-53 metal-organic framework. *Microporous Mesoporous Mater.* **2016**, *222*, 145−152.
(323) Zhang, K.; Xie, X.; Li, H.; Gao, J.; Nie, L.; Pan, Y.; Xie, J.; Tian, D.; Liu, W.; Fan, Q.; Su, H.; Huang, L.; Huang, W. Highly water-stable lanthanide-oxalate MOFs with remarkable proton conductivity and tunable luminescence. *Adv. Mater.* **2017**, *29*, 1701804.
(324) Zhang, S.-Y.; Jensen, S.; Tan, K.; Wojtas, L.; Roveto, M.; Cure, J.; Thonhauser, T.; Chabal, Y. J.; Zaworotko, M. J. Modulation of water vapor sorption by a fourth-generation metal-organic material with a rigid framework and self-switching pores. *J. Am. Chem. Soc.* **2018**, *140*, 12545−12552.
(325) Shigematsu, A.; Yamada, T.; Kitagawa, H. Selective separation of water, methanol, and ethanol by a porous coordination polymer built with a flexible tetrahedral ligand. *J. Am. Chem. Soc.* **2012**, *134*, 13145−13147.
(326) Plessius, R.; Kromhout, R.; Dantas Ramos , A. L.; Ferbinteanu, M.; Mittelmeijer-Hazeleger, M. C.; Krishna, R.; Rothenberg, G.; Tanase, S. Highly selective water adsorption in a lanthanum metal−organic framework. *Chem. - Eur. J.* **2014**, *20*, 7922−7925.
(327) Guo, P.; Wong-Foy, A. G.; Matzger, A. J. Microporous coordination polymers as efficient sorbents for air dehumidification. *Langmuir* **2014**, *30*, 1921−1925.
(328) Ciahotný, K.; Hlinčík, T.; Vagenknechtová, A.; Prokeš, O. Adsorbents for the natural gas drying at CNG stations. *Acta Montanistica Slovaca* **2015**, *21*, 306−313.
(329) Xue, D.-X.; Cairns, A. J.; Belmabkhout, Y.; Wojtas, L.; Liu, Y.; Alkordi, M. H.; Eddaoudi, M. Tunable rare-earth fcu-MOFs: A platform for systematic enhancement of CO_2 adsorption energetics and uptake. *J. Am. Chem. Soc.* **2013**, *135*, 7660−7667.
(330) Rozyyev, V.; Yavuz, C. T. An all-purpose porous cleaner for acid gas removal and dehydration of natural gas. *Chem* **2017**, *3*, 719−721.
(331) Gonçalves, D. V.; Snurr, R. Q.; Lucena, S. M. P. Impact of H_2O and CO_2 on methane storage in metal−organic frameworks. *Adsorption* **2019**, *25*, 1633−1642.
(332) Chen, Y.; Qiao, Z.; Huang, J.; Wu, H.; Xiao, J.; Xia, Q.; Xi, H.; Hu, J.; Zhou, J.; Li, Z. Unusual moisture-enhanced CO_2 capture within microporous PCN-250 frameworks. *ACS Appl. Mater. Interfaces* **2018**, *10*, 38638−38647.
(333) Aristov, Y. Concept of adsorbent optimal for adsorptive cooling/heating. *Appl. Therm. Eng.* **2014**, *72*, 166−175.
(334) Solovyeva, M. V.; Gordeeva, L. G.; Krieger, T. A.; Aristov, Y. I. MOF-801 as a promising material for adsorption cooling: Equilibrium and dynamics of water adsorption. *Energy Convers. Manage.* **2018**, *174*, 356−363.
(335) Chaemchuen, S.; Xiao, X.; Klomkliang, N.; Yusubov, M. S.; Verpoort, F. Tunable metal−organic frameworks for heat transformation applications. *Nanomaterials* **2018**, *8*, 661.
(336) Graf, S.; Redder, F.; Bau, U.; de Lange, M.; Kapteijn, F.; Bardow, A. Toward optimal metal-organic frameworks for adsorption chillers: Insights from the scale-up of MIL-101(Cr) and NH_2-MIL-125. *Energy Technol.* **2020**, *8*, 1900617.
(337) Tannert, N.; Jansen, C.; Nießing, S.; Janiak, C. Robust synthesis routes and porosity of the Al-based metal−organic frameworks Al-fumarate, CAU-10-H and MIL-160. *Dalton Trans* **2019**, *48*, 2967−2976.
(338) Krajnc, A.; Varlec, J.; Mazaj, M.; Ristić, A.; Logar, N. Z.; Mali, G. Superior performance of microporous aluminophosphate with LTA topology in solar-energy storage and heat reallocation. *Adv. Energy Mater.* **2017**, *7*, 1601815.
(339) Henninger, S. K.; Schicktanz, M.; Hügenell, P. P. C.; Sievers, H.; Henning, H. M. Evaluation of methanol adsorption on activated carbons for thermally driven chillers part I: Thermophysical characterisation. *Int. J. Refrig.* **2012**, *35*, 543−553.
(340) de Lange, M. F.; van Velzen, B. L.; Ottevanger, C. P.; Verouden, K. J. F. M.; Lin, L.-C.; Vlugt, T. J. H.; Gascon, J.; Kapteijn, F. Metal−organic frameworks in adsorption-driven heat pumps: The potential of alcohols as working fluids. *Langmuir* **2015**, *31*, 12783−12796.
(341) Iacomi, P.; Lee, U. H.; Valekar, A. H.; Chang, J.-S.; Llewellyn, P. L. Investigating the effect of alumina shaping on the sorption properties of promising metal−organic frameworks. *RSC Adv.* **2019**, *9*, 7128−7135.
(342) Jeremias, F.; Fröhlich, D.; Janiak, C.; Henninger, S. K. Water and methanol adsorption on MOFs for cycling heat transformation processes. *New J. Chem.* **2014**, *38*, 1846−1852.
(343) Britt, D.; Tranchemontagne, D.; Yaghi, O. M. Metal-organic frameworks with high capacity and selectivity for harmful gases. *Proc. Natl. Acad. Sci. U. S. A.* **2008**, *105*, 11623−11627.
(344) Morris, W.; Doonan, C. J.; Yaghi, O. M. Postsynthetic modification of a metal−organic framework for stabilization of a hemiaminal and ammonia uptake. *Inorg. Chem.* **2011**, *50*, 6853−6855.
(345) Dakkama, H. J.; Youssef, P. G.; Al-Dadah, R. K.; Mahmoud, S. Adsorption ice making and water desalination system using metal organic frameworks/water pair. *Energy Convers. Manage.* **2017**, *142*, 53−61.
(346) Mo, Z.-W.; Zhou, H.-L.; Zhou, D.-D.; Lin, R.-B.; Liao, P.-Q.; He, C.-T.; Zhang, W.-X.; Chen, X.-M.; Zhang, J.-P. Mesoporous metal-organic frameworks with exceptionally high working capacities for adsorption heat transformation. *Adv. Mater.* **2018**, *30*, 1704350.
(347) Santori, G.; Di Santis, C. Optimal fluids for adsorptive cooling and heating. *Sustainable Mater. Technol.* **2017**, *12*, 52−61.
(348) Teo, H. W. B.; Chakraborty, A.; Kitagawa, Y.; Kayal, S. Experimental study of isotherms and kinetics for adsorption of water on aluminium fumarate. *Int. J. Heat Mass Transfer* **2017**, *114*, 621−627.
(349) Betke, U.; Klaus, M.; Eggebrecht, J. G.; Scheffler, M.; Lieb, A. MOFs meet macropores: Dynamic direct crystallization of the microporous aluminum isophthalate CAU-10 on reticulated open-cellular alumina foams. *Microporous Mesoporous Mater.* **2018**, *265*, 43−56.
(350) Tatlier, M. Performances of MOF vs. zeolite coatings in adsorption cooling applications. *Appl. Therm. Eng.* **2017**, *113*, 290−297.

https://dx.doi.org/10.1021/acs.chemrev.9b00746
Chem. Rev. XXXX, XXX, XXX−XXX

(351) Henninger, S. K.; Ernst, S.-J.; Gordeeva, L.; Bendix, P.; Fröhlich, D.; Grekova, A. D.; Bonaccorsi, L.; Aristov, Y.; Jaenchen, J. New materials for adsorption heat transformation and storage. *Renewable Energy* **2017**, *110*, 59−68.
(352) Kummer, H.; Baumgartner, M.; Hügenell, P.; Fröhlich, D.; Henninger, S. K.; Gläser, R. Thermally driven refrigeration by methanol adsorption on coatings of HKUST-1 and MIL-101(Cr). *Appl. Therm. Eng.* **2017**, *117*, 689−697.
(353) Solovyeva, M. V.; Aristov, Y. I.; Gordeeva, L. G. NH_2-MIL-125 as promising adsorbent for adsorptive cooling: Water adsorption dynamics. *Appl. Therm. Eng.* **2017**, *116*, 541−548.
(354) Wilde, T.; Ott, M.; Auweter, A.; Meijer, I.; Ruch, P.; Hilger, M.; Kühnert, S.; Huber, H. In CooLMUC-2: A supercomputing cluster with heat recovery for adsorption cooling, *33rd Thermal Measurement, Modeling & Management Symposium (SEMI-THERM), 13−17 March 2017, San Jose, CA*, 2017; pp 115−121.
(355) Graf, S.; Lanzerath, F.; Bardow, A. The IR-large-temperature-jump method: Determining heat and mass transfer coefficients for adsorptive heat transformers. *Appl. Therm. Eng.* **2017**, *126*, 630−642.
(356) Wu, H.; Salles, F.; Zajac, J. A critical review of solid materials for low-temperature thermochemical storage of solar energy based on solid-vapour adsorption in view of space heating uses. *Molecules* **2019**, *24*, 945.
(357) Li, W.; Xia, X.; Li, S. Large-scale evaluation of cascaded adsorption heat pumps based on metal/covalent-organic frameworks. *J. Mater. Chem. A* **2019**, *7*, 25010−25019.
(358) Karak, S.; Kandambeth, S.; Biswal, B. P.; Sasmal, H. S.; Kumar, S.; Pachfule, P.; Banerjee, R. Constructing ultraporous covalent organic frameworks in seconds via an organic terracotta process. *J. Am. Chem. Soc.* **2017**, *139*, 1856−1862.
(359) Stegbauer, L.; Hahn, M. W.; Jentys, A.; Savasci, G.; Ochsenfeld, C.; Lercher, J. A.; Lotsch, B. V. Tunable water and CO_2 sorption properties in isostructural azine-based covalent organic frameworks through polarity engineering. *Chem. Mater.* **2015**, *27*, 7874−7881.
(360) Schlüsener, C.; Xhinovci, M.; Ernst, S.-J.; Schmitz, A.; Tannert, N.; Janiak, C. Solid-solution mixed-linker synthesis of isoreticular Al-based MOFs for an easy hydrophilicity tuning in water-sorption heat transformations. *Chem. Mater.* **2019**, *31*, 4051−4062.
(361) Tschense, C. B. L.; Reimer, N.; Hsu, C.-W.; Reinsch, H.; Siegel, R.; Chen, W.-J.; Lin, C.-H.; Cadiau, A.; Serre, C.; Senker, J.; Stock, N. New group 13 MIL-53 derivates based on 2,5-thiophenedicarboxylic acid. *Z. Anorg. Allg. Chem.* **2017**, *643*, 1600−1608.
(362) Horcajada, P.; Surblé, S.; Serre, C.; Hong, D.-Y.; Seo, Y.-K.; Chang, J.-S.; Grenèche, J.-M.; Margiolaki, I.; Férey, G. Synthesis and catalytic properties of MIL-100(Fe), an iron(III) carboxylate with large pores. *Chem. Commun.* **2007**, 2820−2822.
(363) Wahiduzzaman, M.; Lenzen, D.; Maurin, G.; Stock, N.; Wharmby, M. T. Rietveld refinement of MIL-160 and its structural flexibility upon H_2O and N_2 adsorption. *Eur. J. Inorg. Chem.* **2018**, *2018*, 3626−3632.
(364) Bon, V.; Senkovska, I.; Evans, J. D.; Wöllner, M.; Hölzel, M.; Kaskel, S. Insights into the water adsorption mechanism in the chemically stable zirconium-based MOF DUT-67 − A prospective material for adsorption-driven heat transformations. *J. Mater. Chem. A* **2019**, *7*, 12681−12690.
(365) Lee, J. Y.; Olson, D. H.; Pan, L.; Emge, T. J.; Li, J. Microporous metal−organic frameworks with high gas sorption and separation capacity. *Adv. Funct. Mater.* **2007**, *17*, 1255−1262.
(366) Dybtsev, D. N.; Chun, H.; Kim, K. Rigid and flexible: A highly porous metal−organic framework with unusual guest-dependent dynamic behavior. *Angew. Chem., Int. Ed.* **2004**, *43*, 5033−5036.
(367) *Database of Zeolite Structures*; International Zeolite Association. 2017; http://www.iza-structure.org/databases/ (accessed 2020-03-07).
(368) Mora, A. J.; Fitch, A. N.; Cole, M.; Goyal, R.; Jones, R. H.; Jobic, H.; Carr, S. W. The structure of the calcined aluminophosphate $ALPO_4$-5 determined by high-resolution X-ray and neutron powder diffraction. *J. Mater. Chem.* **1996**, *6*, 1831−1835.
(369) Wragg, D. S.; Johnsen, R. E.; Norby, P.; Fjellvåg, H. The adsorption of methanol and water on SAPO-34: *in situ* and *ex situ* X-ray diffraction studies. *Microporous Mesoporous Mater.* **2010**, *134*, 210−215.
(370) Yeh, R. L.; Ghosh, T. K.; Hines, A. L. Effects of regeneration conditions on the characteristics of water vapor adsorption on silica gel. *J. Chem. Eng. Data* **1992**, *37*, 259−261.
(371) Schicktanz, M.; Hügenell, P.; Henninger, S. K. Evaluation of methanol/activated carbons for thermally driven chillers, part II: The energy balance model. *Int. J. Refrig.* **2012**, *35*, 554−561.
(372) ul Qadir, N.; Said, S. A. M.; Mansour, R. B. Modeling the performance of a two-bed solar adsorption chiller using a multi-walled carbon nanotube/MIL-100(Fe) composite adsorbent. *Renewable Energy* **2017**, *109*, 602−612.
(373) Freni, A.; Bonaccorsi, L.; Calabrese, L.; Caprì, A.; Frazzica, A.; Sapienza, A. SAPO-34 coated adsorbent heat exchanger for adsorption chillers. *Appl. Therm. Eng.* **2015**, *82*, 1−7.
(374) Tu, Y.; Wang, R.; Zhang, Y.; Wang, J. Progress and expectation of atmospheric water harvesting. *Joule* **2018**, *2*, 1452−1475.
(375) Wahlgren, R. V. Atmospheric water vapour processor designs for potable water production: A review. *Water Res.* **2001**, *35*, 1−22.
(376) LaPotin, A.; Kim, H.; Rao, S. R.; Wang, E. N. Adsorption-based atmospheric water harvesting: Impact of material and component properties on system-level performance. *Acc. Chem. Res.* **2019**, *52*, 1588−1597.
(377) Trapani, F.; Polyzoidis, A.; Loebbecke, S.; Piscopo, C. G. On the general water harvesting capability of metal-organic frameworks under well-defined climatic conditions. *Microporous Mesoporous Mater.* **2016**, *230*, 20−24.
(378) *Drinking Water Eegulations*; United States EPA, 2017; https://www.epa.gov/dwreginfo/drinking-water-regulations (accessed 2020-03-07).
(379) Wang, H.; Lustig, W. P.; Li, J. Sensing and capture of toxic and hazardous gases and vapors by metal−organic frameworks. *Chem. Soc. Rev.* **2018**, *47*, 4729−4756.
(380) Bobbitt, N. S.; Mendonca, M. L.; Howarth, A. J.; Islamoglu, T.; Hupp, J. T.; Farha, O. K.; Snurr, R. Q. Metal-organic frameworks for the removal of toxic industrial chemicals and chemical warfare agents. *Chem. Soc. Rev.* **2017**, *46*, 3357−3385.
(381) Llabrés i Xamena, F. X.; Gascon, J., *Metal Organic Frameworks As Heterogeneous Catalysts*; The Royal Society of Chemistry: Cambridge, UK, 2013.
(382) Bavykina, A.; Kolobov, N.; Khan, I. S.; Bau, J. A.; Ramirez, A.; Gascon, J., Metal−organic frameworks in heterogeneous catalysis: recent progress, new trends and future perspectives. *Chem. Rev.* **2020**, DOI: 10.1021/acs.chemrev.9b00685
(383) Cranston, J.; Askalany, A.; Santori, G. Efficient drying in washer dryers by combining sorption and heat pumping. *Energy* **2019**, *183*, 683−692.
(384) *Dishwasher with Zeolith Drying Technology*; Siemens-BSH, 2020; https://www.siemens-home.bsh-group.com/nl/inspiratie/highlights/zeolith (accessed 2020-03-06).
(385) Hauer, A.; Fischer, F. Open adsorption system for an energy efficient dishwasher. *Chem. Ing. Tech.* **2011**, *83*, 61−66.
(386) Santori, G.; Frazzica, A.; Freni, A.; Galieni, M.; Bonaccorsi, L.; Polonara, F.; Restuccia, G. Optimization and testing on an adsorption dishwasher. *Energy* **2013**, *50*, 170−176.
(387) Li, C.; Goswami, Y.; Stefanakos, E. Solar assisted sea water desalination: A review. *Renewable Sustainable Energy Rev.* **2013**, *19*, 136−163.
(388) Sharon, H.; Reddy, K. S. A review of solar energy driven desalination technologies. *Renewable Sustainable Energy Rev.* **2015**, *41*, 1080−1118.
(389) Ng, K. C.; Wang, X.-L.; Gao, L.; Chakraborty, A.; Saha, B. N.; Koyama, S.; Akisawa, A.; Kashiwagi, T. *Apparatus and method for desalination*. WO WO2006121414A1, May 11, 2006.

https://dx.doi.org/10.1021/acs.chemrev.9b00746
Chem. Rev. XXXX, XXX, XXX−XXX

(390) Wu, J. W.; Hu, E. J.; Biggs, M. J. Thermodynamic cycles of adsorption desalination system. *Appl. Energy* **2012**, *90*, 316−322.
(391) Olkis, C.; Brandani, S.; Santori, G. Design and experimental study of a small scale adsorption desalinator. *Appl. Energy* **2019**, *253*, 113584.
(392) Ng, K. C.; Thu, K.; Kim, Y.; Chakraborty, A.; Amy, G. Adsorption desalination: An emerging low-cost thermal desalination method. *Desalination* **2013**, *308*, 161−179.
(393) Ng, K. C.; Thu, K.; Saha, B. B.; Chakraborty, A. Study on a waste heat-driven adsorption cooling cum desalination cycle. *Int. J. Refrig.* **2012**, *35*, 685−693.
(394) Youssef, P. G.; Dakkama, H.; Mahmoud, S. M.; Al-Dadah, R. K. Experimental investigation of adsorption water desalination/cooling system using CPO-27Ni MOF. *Desalination* **2017**, *404*, 192−199.
(395) Elsayed, E.; Al-Dadah, R.; Mahmoud, S.; Anderson, P.; Elsayed, A. Experimental testing of aluminium fumarate MOF for adsorption desalination. *Desalination* **2020**, *475*, 114170.
(396) Freitas, S. K. S.; Borges, R. S.; Merlini, C.; Barra, G. M. O.; Esteves, P. M. Thermal conductivity of covalent organic frameworks as a function of their pore size. *J. Phys. Chem. C* **2017**, *121*, 27247−27252.
(397) Huang, J.; Xia, X.; Hu, X.; Li, S.; Liu, K. A general method for measuring the thermal conductivity of MOF crystals. *Int. J. Heat Mass Transfer* **2019**, *138*, 11−16.
(398) Gascon, J.; van Ommen, J. R.; Moulijn, J. A.; Kapteijn, F. Structuring catalyst and reactor − An inviting avenue to process intensification. *Catal. Sci. Technol.* **2015**, *5*, 807−817.
(399) Kapteijn, F.; Heiszwolf, J. J.; Nijhuis, T. A.; Moulijn, J. A. Monoliths in Multiphase Catalytic Processes—Aspects and Prospects. *CatTech* **1999**, *3*, 24−41.
(400) Halevi, O.; Tan, J. M. R.; Lee, P. S.; Magdassi, S. Hydrolytically stable MOF in 3D-printed structures. *Adv. Sustainable Syst.* **2018**, *2*, 1700150.
(401) Silva, P.; Vilela, S. M. F.; Tome, J. P. C.; Almeida Paz, F. A. Multifunctional metal−organic frameworks: from academia to industrial applications. *Chem. Soc. Rev.* **2015**, *44*, 6774−6803.
(402) Giordano, L.; Gubis, J.; Bierman, G.; Kapteijn, F. Conceptual design of membrane-based pre-combustion CO_2 capture process: Role of permeance and selectivity on performance and costs. *J. Membr. Sci.* **2019**, *575*, 229−241.
(403) *REACH Regulations (Registration, Evaluation, Authorisation and Restriction of Chemicals)*; European Union, 2019; https://ec.europa.eu/environment/chemicals/reach/reach_en.htm (accessed 2020-03-07).

https://dx.doi.org/10.1021/acs.chemrev.9b00746
Chem. Rev. XXXX, XXX, XXX−XXX